Avdelning, institution
Division, Department

LINKÖPINGS UNIVERSITET

Department of Physics, Chemistry and Biology
Linköping University

Datum
Date

2019-02-15

Språk
Language

☐ Svenska/Swedish
☒ Engelska/English

☐ _____

Rapporttyp
Report category

☐ Licentiatavhandling
☒ Examensarbete
☐ C-uppsats
☐ D-uppsats
☐ Övrig rapport

☐ _____

ISBN

ISRN: LITH-IFM-A-EX--19/3601--SE

Serietitel och serienummer **ISSN**
Title of series, numbering _____

URL för elektronisk version

Titel
Title

Optimization of gas flow uniformity in enhancement of Metal Organic Chemical Vapor Deposition growth for III-nitrides

Författare
Author

Kevin Olsson

Sammanfattning
Abstract

The thesis focuses on the gas flow profile optimization of a non-conventional injector in a hot-wall MOCVD system. The injector's gas flow profile is simulated with CFD and demonstrates a well-behaved laminar flow with a parabolic profile. To ensure the theory is in coherence with the reality, a qualitative study with five thermocouples in a test graphite piece of the was performed.
First the thesis will take you through an introduction of the semiconductor field to arrive in a problem formulation. Then you will read about the principles of MOCVD systems, fluid dynamics principles and thermocouple theory. The experiment's way of approach is then described through all steps from blue print to results. A discussion about the result and the conclusion will be read before the proposals of future work based on the thesis work.
The laminar flow is confirmed according to the resulting data and the limitations of the system is set to two different cases depending on background temperature.
At 1000 °C a laminar flow is strongly indicated to be obtained at position 3A, closest to the growth area, within the gas flow range of 25 SLM regardless of background pressure, except for 700 mBar indicating turbulent flow for 15 SLM an up. At 20 and 200 mBar the laminar flow limit is suggested by data to be even higher and reaching a value of 35 SLM.
At 450 °C the data indicate a laminar flow up to 20 SLM at position 3A regardless of background pressure condition, except for 700 mBar where the data indicate a laminar flow at 35 and 40 SLM. 50 mBar strongly indicates a laminar flow profile up to a gas flow of 35 SLM. With a background pressure of 20 mBar, the data suggests a laminar flow profile up to at least 25 SLM. At 100 mBar the data indicates a laminar flow within the range of 30 SLM.

Nyckelord
Keyword

III-nitrides, hot-wall MOCVD system, GaN-on-SiC, gas flow profile, laminar flow

Optimization of gas flow uniformity in enhancement of Metal Organic Chemical Vapor Deposition growth for III-nitrides

Kevin Olsson

Tutors, Dr. Martin Eriksson, Prof. Olof Kordina, Dr. Jr-Tai Chen

Examiner, Prof. Vanya Darakchieva

IFM
Linköping University
SE-581 83 Linköping, Sweden
+46 (0)13-28 10 00, www.liu.se

LINKÖPING UNIVERSITY

Abstract

The thesis focuses on the gas flow profile optimization of a non-conventional injector in a hot-wall MOCVD system. The injector's gas flow profile is simulated with CFD and demonstrates a well-behaved laminar flow with a parabolic profile. To ensure the theory is in coherence with the reality, a qualitative study with five thermocouples in a test graphite piece of the was performed.

First the thesis will take you through an introduction of the semiconductor field to arrive in a problem formulation. Then you will read about the principles of MOCVD systems, fluid dynamics principles and thermocouple theory. The experiment's way of approach is then described through all steps from blue print to results. A discussion about the result and the conclusion will be read before the proposals of future work based on the thesis work.

The laminar flow is confirmed according to the resulting data and the limitations of the system is set to two different cases depending on background temperature.

At 1000 °C a laminar flow is strongly indicated to be obtained at position 3A, closest to the growth area, within the gas flow range of 25 SLM regardless of background pressure, except for 700 mBar indicating turbulent flow for 15 SLM an up. At 20 and 200 mBar the laminar flow limit is suggested by data to be even higher and reaching a value of 35 SLM.

At 450 °C the data indicate a laminar flow up to 20 SLM at position 3A regardless of background pressure condition, except for 700 mBar where the data indicate a laminar flow at 35 and 40 SLM. 50 mBar strongly indicates a laminar flow profile up to a gas flow of 35 SLM. With a background pressure of 20 mBar, the data suggests a laminar flow profile up to at least 25 SLM. At 100 mBar the data indicates a laminar flow within the range of 30 SLM.

Acknowledgement

I would like to thank many of you for the help with my thesis writing. If it had not been for you, I would not have had a thesis work to present.

First, I would like to thank my examiner Prof. Vanya Darakchieva, for helping me with accomplishing the chapter of my engineer studies at LiU. It has been fantastic to have you correcting my thesis, calming me with coffee and chocolate in the stressful times, and for the future career discussions. Thank you, Vanya.

Second, I would like to thank you Martin Eriksson for being the most amazing colleague, Jr-Tai Chen for being my mentor, boss and friend through this journey and Olof Kordina for giving me the opportunity of starting my carrier with you as my tutor and being my expert through the thesis and last but not least the rest of SweGaN for being part of the start line of my carrier running track. You have helped me developed who I am and who I would like to become in the future.

I also want to thank Roger Nilsson and Jonas Rosberg at Epiluvac for being my tutors throughout the master thesis. I've gained a lot of knowledge about the MOCVD systems and how to become a good engineer.

I would like to thank Dan Loyd for being my expert through the thesis work. The pedagogically explanations and theoretical assignments of heat transfer and fluid dynamics have been highly valued.

Last, I would from the bottom of my heart like to thank my family and friends for being my supporters through the lows and sharing the joy through the highs at LiU. I am blessed for having you all in my life.

Linköping in February 2019

Kevin Olsson

Table of Contents

Figures

Nomenclatures

Nomenclature	*Definition*
MOCVD	Metal Organic Chemical Vapor Deposition
CVD	Chemical Vapor Deposition
MFC	Mass Flow Controller
EPC	Electronic Pressure Controller
HEMT	High Electron Mobility Transistor
TMIn	Trimethylindium
TMAl	Trimethylaluminum
TMGa	Trimethylgallium
GaN	Gallium Nitride
NH_3	Ammonia
H_2	Hydrogen
SiC	Silicon Carbide
CV	Capacitance-Voltage measurement
XRD	X-ray Diffraction
AFM	Atomic Force Microscopy
SLM	Standard Liters per Minute

SCCM	Standard Cubic Centimeters per Minute
A/D Converter	Analog to digital signal converter
CPU	Central Processing Unit
mBar	Millibar (1 atm = 1013.25 mBar = 101.325 kPa)

1 Introduction

The semiconductor industry is one of the largest industries in the world. Reaching 412.22 billion U.S. dollars by the end of 2017 in sales, the market is targeting 483.72 billion U.S. dollars by the end of year 2019, according to WSTS. (World Semiconductor Trade Statistics, 2018)

In this market a variety of semiconductors aiming for different segments in terms of applications, product need and regions can be found. The III-nitrides are one of the specialties delivered in this business and in certainty the global Gallium Nitride (GaN) semiconductor device market. The market is extremely competitive and the most advancements were made, more easily, in between 2010 to 2016. After 2016 it has been a few players competing through partnerships and other strategic collaborations. It is a hot topic for the scientists and researchers are trying to achieve a name among the pioneers. (Grand View Research, Inc, 2017)

1.1 Background

Since the device market is strongly competitive it creates demands on the material to be produced for the GaN devices. The clientele for the devices requires higher power and lower energy consumption in their devices. Simultaneously, the customers need devices with smaller surface areas which requires a different growth technique in addition to the conventional lateral GaN high-electron mobility transistors (HEMTs), which is the vertical HEMT. The vertical HEMT is fulfilling the clienteles demand on the product, but results in a material which is still in research phase. (Chen, 2015)

The GaN could be demonstrated as the younger sibling challenging its older sibling silicon (Si) and more likely will the Si have a changed focus compared as of today. The GaN has wider bandgap, higher breakdown voltage, larger power density and its favorable heat dissipation is a result of its high thermal conductivity. (Kordina, 1994) (Chen, 2015)

The GaN application areas are in LEDs, IC electronics, power devices, RF devices and other application areas for conventional transistors. Since the power field for GaN is a relative new research area for the material and as told before it set new demands on the material which further put pressure on the growth equipment. In particular, the growth equipment is of highest importance from a material perspective since a high-quality material needs to be manufactured. The growth equipment must be able to precisely control the Si, C and O impurities since the GaN is more favorable of being grown on top of silicon carbide (SiC) and not Si. One of these reasons are that the SiC lattice parameter has a lower in-plane lattice mismatch with GaN of only 3.4 % compared to with Si which is of 17 %. It is important to note that for GaN-on-SiC epitaxy the growth must be assisted by an aluminum nitride (AlN) nucleation layer. (Amano, et al., 1986) (M. Asif Khan, 1992) (J. M. Redwing, 1996) (Chen, 2015) (Grand View Research, Inc, 2017)

A spin-off company from Linköping University is focusing on the novelty of GaN-on-SiC HEMT structures. The GaN-on-SiC is grown in a newly built hot-wall MOCVD reactor at Linköping University, which is a reactor equally owned by the two parties.

MOCVD growth for the semiconductor industry has been the leading growth technique since the late 1990s because of its accurate growth precision and especially for the III-nitrides. The MOCVD system used at Linköping University is a horizontal hot-wall MOCVD system which distinguishes from the cold-wall MOCVD system. In the cold-wall MOCVD system, the substrate is heated from underneath when in the hot-wall MOCVD system it is heated from all around. In this new reactor, the substrate is heated from underneath and from the top creating as good as systems using coils wrapping around the substrate. The hot-wall MOCVD system is manufactured by Epiluvac which plays a major role in the optimization of the reactor injector. (Chen, 2015)

The injector introduces the metal organics such as *trimethylgallium*, *trimethylaluminum* and *trimethylindium* simultaneously with their carrier (H_2 and N_2) and hydride (NH_3) gas into the chamber. Since the injector is non-conventional compared to any MOCVD system, qualitative methods to optimize and measure the gas flow profile are demanded.

1.2 Purpose

An industrial project has been established to further develop the hot-wall MOCVD growth equipment and this thesis is focused on the non-conventional injector.

The focus in this thesis is on the optimization of the injector in the reactor which in turn consists of eleven independent outlets that are patent pending. Through qualitative measurements, the profile of the gas flow can be extracted and other important parameters as well. Together with internally theoretical calculations and externally performed CFD, *Computational Fluid Dynamics*, simulations – the measured data can be compared with these references. This is then used to extract information on how to proceed the injector optimization.

Since in this writing moment there are not any papers to be found online or in dissertations regarding gas flow profile optimization in a MOCVD reactor of III-nitrides with CFD simulations and qualitative thermocouple studies. The optimization of the gas flow profile in terms of obtaining a planar and laminar flow with such large number of thermocouples according to earlier simulations performed on the hot-wall MOCVD system are one of its kind. The aim is to find a state-of-the-art solution to this optimization which could be applicable on new development of GaN-on-SiC hot-wall MOCVD systems. The purpose of the thesis is also to reveal a completely novel injector design which is in writing moment patent pending and how it should be optimized is strived to be solved within this thesis.

1.3 Problem formulation

To what degree can a laminar gas flow profile be obtained in the hot-wall MOCVD system?

To what degree is the gas flow profile in accordance with the computational fluid dynamics simulations?

What system limitations have been discovered and concluded?

To what degree can the laminar velocity profile be controlled i.e. can a concave velocity profile be obtained?

1.4 Limitations

A strict limitation is time since this thesis is an industrial project with strict deadlines and the planned commissioning of the new reactor is the spring 2019.

The thermoelements to be used in the reactor are limited to a maximum operating temperature of 1000 °C which limits the process and test growth temperature. It could also come to affect the results if the hot-wall MOCVD system is only optimized for up to 1000 °C, but an investigation regarding this question mark is performed during the result analysis.

Gas to be used in the thesis is N_2 due to it is an unharmful gas since the measurements sometimes requires quick openings of the lid to the reactor to change measure spots of the thermocouples. The system demands to use a temperature above 450 °C because of pyrometer limitations and it also requires using a background pressure lower than 700 mBar because of system pump capacity.

2 Theory and principles

2.1 Metal Organic Chemical Vapor Deposition (MOCVD)

CVD is a growth technique that stands for Chemical Vapor Deposition and is a commonly used growth technique in the industry as in the research. The initiation of the CVD process can be described with significant key steps. It shall be noticed that MOCVD growth is a special case of the CVD growth technique and it distinguishes at the introduction of the precursors into the growth process. In a MOCVD process, the precursor gas is a Metal Organic, hence the abbreviation MOCVD. See Figure 1, Figure 2 and Figure 3 for the atomic models of the organometals and Figure 4 for the hot-wall MOCVD system used in this thesis.

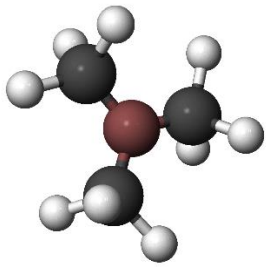

Figure 1 Trimethylgallium (above). By Epop [Public domain], from Wikimedia Commons

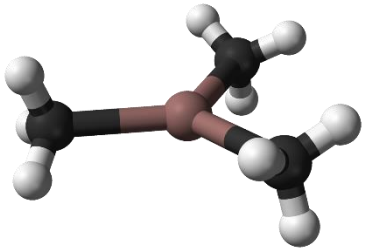

Figure 2 Trimethylindium (above). By Ben Mills [Public domain], from Wikimedia Commons

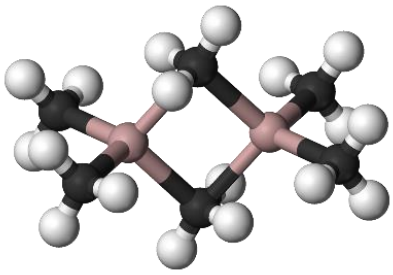

Figure 3 Trimethylaluminum (above). By Benjah-bmm27 [Public domain], from Wikimedia Commons

Figure 4 Hot-wall MOCVD system used in thesis. Copyright Epiluvac AB and SweGaN AB.

The substrate where the growth will take place on is placed inside of a square-shaped part called the susceptor of the reactor. In this susceptor a plate called satellite will be containing a rotatable disc in it on which the substrate will be placed.

The reactor is then pumped down to a vacuum of approximately $1x10^{-3}$ mBar and then backfilled and controlled at a constant pressure which could be in between a few millibars up to 700 mBar, depending of growth conditions. When the correct pressure is obtained, heating of the susceptor is started. (Chen, 2015) The susceptor is heated by resistive heating which is created by conducting a high current through serpentine formed state-of-the-art graphite. The electrons flowing through the graphite will travel from a high potential to a lower potential resulting in a performed work by the electrons. The work performed by the electrons is then equal to the power equation from Ohm's law and is also the resulted heat created. With a known resistance of the material, the current can be adjusted in such way that the created heat is controlled, that is the heating temperature of the system. (Csanyi, 2017)

The significant key steps of the actual growth process after the initiation is described in pedagogic manner according to Dr. Chen in REF (Chen, 2015).

1. Transport of precursors to the growth zone;
2. Gas-phase reactions of precursors in the growth zone producing reactive intermediates and by-products;
3. Mass transport of reactants to the substrate surface;
4. Adsorption of reactants to the substrate surface;
5. Surface diffusion to growth sites;
6. Nucleation, and surface reactions leading to solid formation;
7. Desorption and mass transport of decomposed fragments away from the growth zone;
8. Exhaust to the pumping system.

In Figure 5 all process steps are seen.

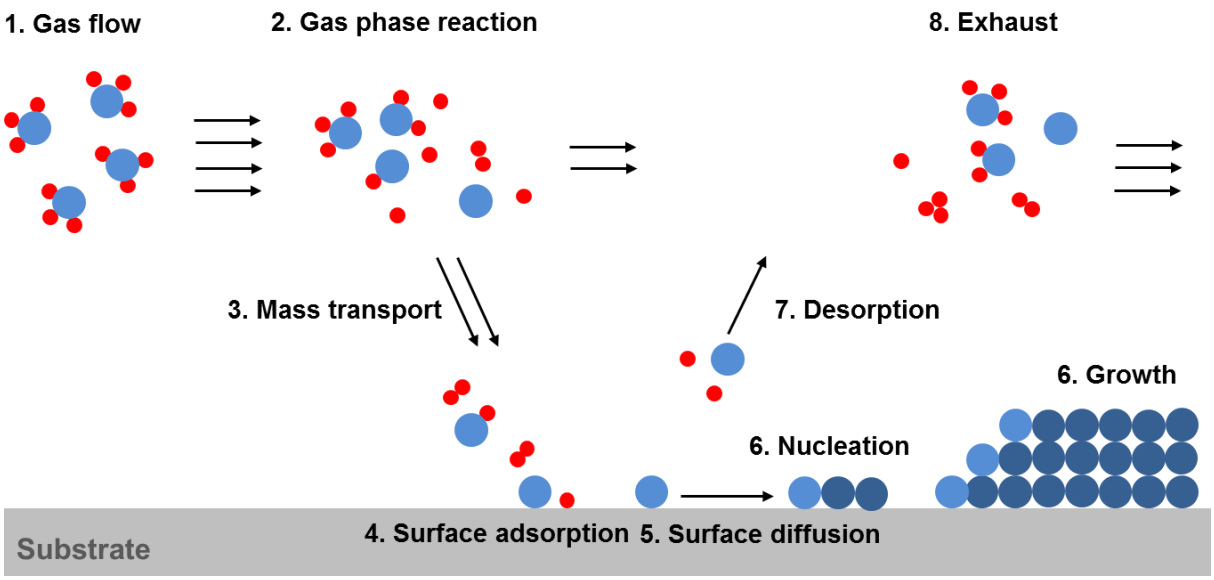

Figure 5 MOCVD process steps. Copyright Jr-Tai Chen, 2015.

In the first step, the precursors will be let in through the injector consisting of eleven outlets. The outlets will each carry a certain gas and there will be five outlets for the organometal plus its carrier gas and the remaining six will carry the hydride gas – ammonia. The middle pipe will carry the organometal and starting from the right outlet it will carry ammonia.

Each outlet is controlled by a *mass flow controller, MFC,* which in their turn are connected to the external piping.

To not perturb the gases in the outlets more than desired, the wedges of the injector are shaped with a small angle (tapered) to cautiously let the gases pass by. Immediately outside of the outlet area, where the wedges end, the gases will start intermixing, and gas-phase reactions are triggered. Now step two is reached in Figure 5Figure 5 MOCVD process steps. Copyright Jr-Tai Chen, 2015.. The idea is not to trigger the intermixing before reaching the deposition area, but it is also as important to have the gas intermixed right before the growth area.

Step five is one of the most critical steps for the deposition since if the gases react or do not react will determine the cluster composition and composition uniformity of the epilayers. The precursor molecules and the ammonia will *crack* under controlled reforms because of the heat and then they will form new molecules with each other which will be the formation of the III-nitrides. E.g. the precursor TMGa together with NH_3 form GaN. Depending on the injected gas flow rate and the background pressure, the deposition rate and the impurity incorporation will be controlled. The lack of mixing the gases will result in cluster formation on the epiwafer which is certainly not a desired behavior in the epitaxial growth of HEMT structures.

When the temperature is increased in the process the gas molecules which have been dependent of the temperature is transiting from temperature dependence and is now more dependent by the gas flow rate. This process step is called mass transport and is when the molecules are approaching the surface. This is what step three significantly means.

In step four and five, the gas molecules are adsorbed to the surface or the substrate where desired growth location is. The molecules, in this case of the III-N growth, of the organometals will adsorb to the surface if the gas pressure and temperature are favorable. If the temperature is too high or the pressure too low, the organometals or reactants will desorb from the surface instead of being adsorbed. In all cases, some part of the reactants will however be desorbed.

After the reactants have been adsorbed, they will then transit the stage of surface diffusion which will place the molecules in vacant positions at the substrate. This is how the epilayers will grow atom layer by atom layer during controlled conditions.

The molecules will then transit from gas phase to solid state where the nucleation of the material is taking place. The material which was not adsorbed to the surface will be pumped out through the exhaust of the reactor, which explains the last steps of the MOCVD process. (Hitchman, 2009) (Chen, 2015)

2.2 Fluid dynamic principles

A gas flow can generally be described as turbulent or laminar. In a MOCVD process, the laminar flow is the desired type to achieve.

The reasons why a laminar flow is desired is mainly that the intermixing of the gas molecules in the gas phase should be kept low. Intermixing is only desired to occur in the depletion area where the growth takes place. If the flow is laminar, the molecules will be kept in their straight lanes from the injector outlet to the depletion area. An additional reason to keep the gas flow laminar is due to the heat exchange of the gas molecules kinetic energy and its surrounding. This is also a phenomenon that is desired to eliminate since the heat transport in laminar flow is primarily dominated by the heat conduction and convection and is easier to control and predict.

The laminar gas flow is layers of the fluid or gas on top of each other as in Figure 6 where the layers have different velocities and temperatures compared to the adjacent layers. In this way the temperature and velocity of each layer compounds can be controlled with the limitations of the gas injector outlet diameter.

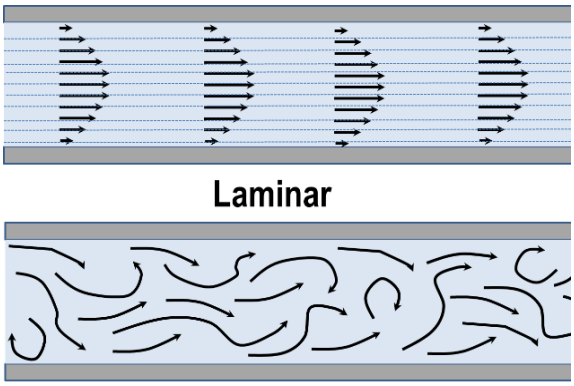

Figure 6 Laminar and turbulent flow. By Joseasorrentino – Own work and translated to English by Kevin Olsson, CC BY-SA 3.0

In stark contrast to the laminar flow with its parallel and straight gas flow layers, the turbulent flow does not contain this layer-by-layer structure. Instead, it behaves like gas flow streams with different origins and moves in much more complex patterns. The heat transfer is substantially more rapid since the molecules in the middle of the stream could in the next second be at the wall. This leads to a more uniform heat distribution of the gas; same of the wall temperatures. (Kordina, 1994)

By calculating *Reynold's number,* a hint of the gas behavior can be seen. Reynold's number is seen in Equation 1,

$$Re = \frac{\rho u L}{\mu} = \frac{uL}{\nu} \qquad \text{Equation 1}$$

where *Re* is the dimensionless Reynold's number, ρ is the fluid density, u is the fluid's mean velocity, L the characteristic linear dimension, ν the kinematic viscosity of the fluid and μ is the dynamic viscosity of the fluid.

The characteristic linear dimension is depending on the fluid dynamic case which in this case is a non-cylindrical tube so the characteristic linear dimension, L, is equal to the hydraulic dimension d_h which can be seen in Equation 2,

$$d_h = \frac{4A}{O} \qquad \text{Equation 2}$$

where, A is the non-circular tube's cross-section area and O its circumference.

A value of < 2300 shows a gas behavior of *laminar* type and a higher number of about > 2300 demonstrates a developed *turbulent* flow behavior in a circular tube.

Although this is only valid for infinitely large surfaces it leads to a difficult confirmation regarding laminar or turbulent flow with only the Reynold's number as reference. (Storck, et al., 2016)

The fluid's mean velocity can then be calculated by the root-mean-square velocity of the gas in combination of the kinetic energy of gas molecules. This leads to Equation 3,

$$pV = nRT \qquad \text{Equation 3}$$

where p is the gas pressure, V the volume of the molecules, n the number of moles in gas particles, R the ideal gas constant and T is the temperature. The kinetic energy is defined in Equation 4 where k_B is Boltzmann's constant, v the molecule velocity, m the mass of the molecule and T the temperature.

$$E_{kinetic} = \frac{1}{2}mv^2 = \frac{3}{2}k_B T \qquad \text{Equation 4}$$

Equation 3 inserted in Equation 4, gives the relationship of kinetic energy expressed in Boltzmann's constant and temperature, Equation 5.

$$v_{rms} = \sqrt{\frac{3RT}{M}} \qquad \text{Equation 5}$$

v_{rms} is the root-mean-square velocity, *R* the ideal gas constant, *T* the temperature and *M* the molar mass [grams/mole]. (Vincent Summers, Sciencing, 2018)

The laminar flow gives great advantages when the gas flow profile is to be calculated and visualized. In Figure 7, the flow profile of a laminar gas flow between two plates can be seen.

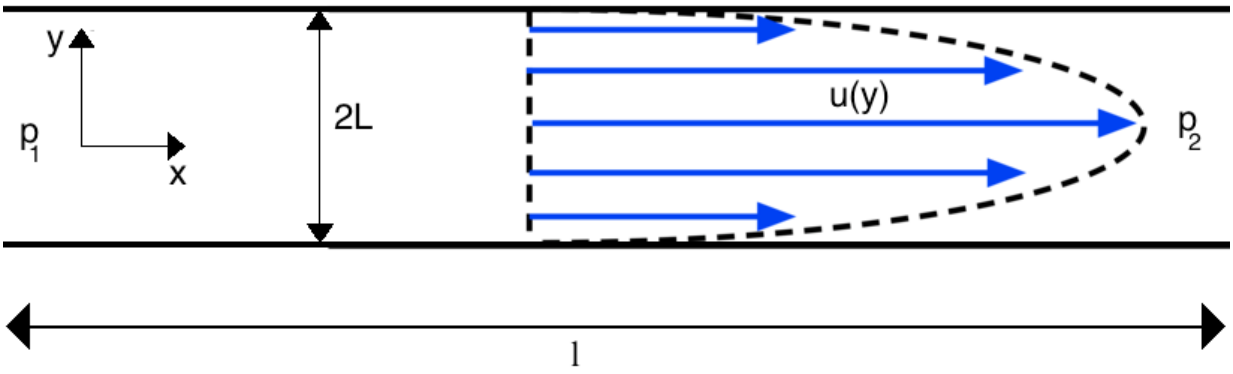

Figure 7 Flow profile in parallel plates. By Ryan Toomey, University of South Florida - Own work and edited by Kevin Olsson, CC BY-SA 4.0

Where *2L* is the distance between the two plates, p_1-p_2 gives the constant pressure difference over the length *l* and *u(y)* is the velocity at distance *y* from the walls. The velocity profile can be calculated which can be seen in greater details in REF (Kordina, 1994) and the result is expressed in Equation 6.

$$u(y) = \frac{p_1 - p_2}{2\mu}(L^2 - y^2) \qquad \text{Equation 6}$$

If the laminar flow is fully developed, it will look the same along the x-axis in Figure 7 which will induce that the molecules will be at the same distance *y* from the walls along its distance *x*.

The reason why the symmetry used to calculate the gas flow profile is a result from the ratio of the injectors dimensions, its width and height. Since it usually is much wider than it is high, the symmetry could be approximated to two parallel plates which gives a fully usable expression as Equation 6. (Kordina, 1994) (Storck, et al., 2016)

Since this reactor is a hot-wall MOCVD system it will also heat the gas along the rectangular shaped liner which will change the characteristics in the gas traveling along the liner. The gas will be heated and thus the density will decrease, and its dynamic viscosity increase which is applicable if the temperature is increasing, which is a desired result for the laminar flow.

So, what happens along the reactor walls? At first, the gas along the walls is layers as explained earlier in the thesis. The layers that are closest to the walls will have zero velocity and how thick these layers are together can be described by the Blasius profile which can be seen in Figure 8.

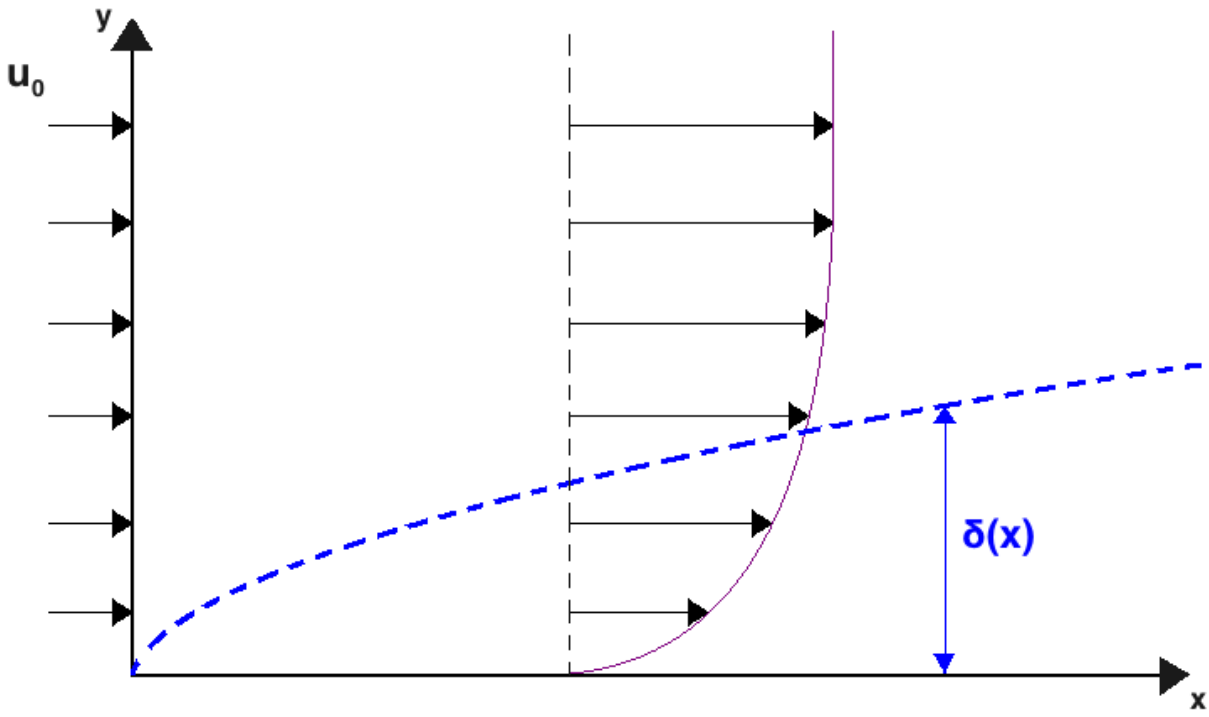

Figure 8 The Blasius profile of the gas velocity over one plate.

δ(x) sets the level to up where the velocity of the gas is almost equal to zero and is called the *boundary layer* which is the blue dashed lines and in fact the velocity is less than $0.99u_0$ below this line. Blasius profile is described by Equation 7.

$$\delta(x) = 4.99\sqrt{\frac{\nu x}{u_0}} \qquad \text{Equation 7}$$

where, *v* is the kinematic viscosity, *x* the thickness of the boundary layer and u_0 the gas velocity.

2.3 Mass Flow Controller, MFC

A mass flow controller, MFC, can be set to sustain a specific flow rate of a gas or liquid. In this thesis the agent to control will be various gases. The MFC will then automatically ensure the set gas flow rate will be the actual output gas flow rate and will not act upon fluctuations or changes in the gas pressure. The structure of a standard MFC can be seen in Figure 9 and is explained below.

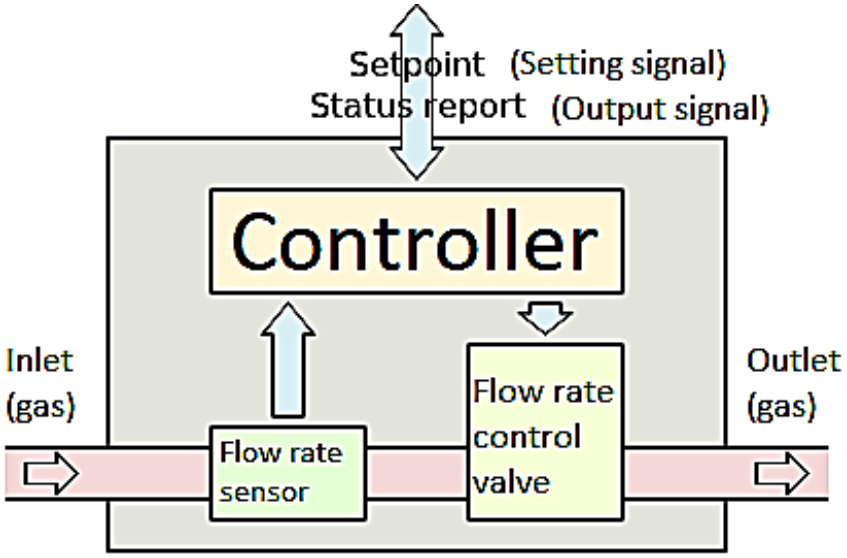

Figure 9 Principles of a mass flow controller.

First the gas is directed into the inlet of the MFC which leads to a two-crossing to the *bypass* and the *flow rate sensor* as the latter is where the gas is heated up by two coils (according to the MFC model used in this thesis, Appendix A). The sensor will detect the temperature of the gas as proportional to the mass flow rate. The controller which then consists of a CPU, a transceiver, *A/D converters* and a *valve driver circuit* will use the A/D converter to convert the temperature change response to an electrical signal. The sensor signal will then be amplified and passed through some noise reduction to create a more stable signal which is the systems output signal in a voltage of 0 to 5 V. The detected flow rate of the sensor is then sent to the *comparison circuit* where it is compared to the *set-point signal*. The difference is then calculated and directed to the *flow rate control valve* which compensates the gas outlet so that the difference reaches as close to zero as possible, within its fault tolerance. The output signal, *outlet flow rate*, will then be as the desired set flow rate. (© 1996-2018 HORIBA, 2018)

In this thesis, MFCs of brand *Horiba* and model number *SEC-N124MGM* are used to control the mass flow rate of the injector outlets. According to the specification of selected *model SEC-N124 MGMR-07 N2 10SLM 4CR*, the MFC is from the fabric designed to fit on a ¼ VCR male type fitting at the outlet and inlet connection.

It is also designed to handle a certain range of gas flows for certain gases which is specified in table *"Gas and full-scale flow rate table (e.g.)"* on p. 4 in Appendix A. The full-scale flow rate is set to 10 SLM in N_2 which together with a conversion factor will show the actual flow of the used gas.

The valve type is of normally closed and has a good control of the gas flow rate at fully closed control valve below 2.0 % of the full-scale flow rate. The MFC can sustain a well-controlled flow rate in between 2 to 100 % of the full-scale flow rate which is in the range of 0.2 to 10 SLM.

There is a small error in the actual flow rate compared to the set flow rate which is ± 1.0 % of the set-point value. This can be seen on p. 3 in Appendix A.

2.4 Thermocouples

The thermocouple consists of two wires which are of different materials to sustain a potential difference in the voltmeter of the two wires. The wires are called thermoelements and when in junction they form a thermocouple. If the wires would have been of the same material, the potential difference between the wires would have been equal to zero. This due to that they will experience the same temperature change and hence the wires will not conduct a current which will give rise to the potential difference.

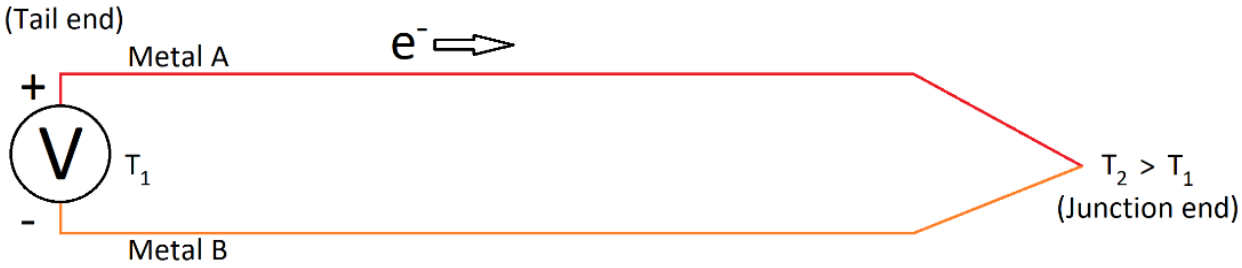

Figure 10 Thermocouple circuit of two different metals with seen current flow.

In Figure 10 thermocouple measuring circuit can be shown. The principles of a thermocouple are to measure the temperature of an ambient, in this thesis the introduced gases in the hot-wall MOCVD system's injector and see how the temperature changes over time. The temperature change of the introduced gas in the chamber can then be related to the velocity of the gas as in Equation 1 in subsection 2.2.

The relation between the temperature and the potential difference is explained by Equation 8. When a temperature difference arises, and the wires are of different materials, an electro motoric force will be present in the circuit. This is called the *Seebeck effect*.

$$V_{emf} = \int_{T_1}^{T_2} (S_1(T) - S_2(T))dT \qquad \text{Equation 8}$$

V_{emf} is the induced electromotive force by the circuit, T_1 and T_2 the temperature at the tail end and the junction end respectively, and $S_1(T)$ and $S_2(T)$ is the Seebeck coefficients of respectively metal A and B which is to be found online at *NIST ITS-90 Thermocouple Database*. (Scervini, 2009) (U.S. Secretary of Commerce on behalf of the United States of America, 1995/2018)

The junction end of the thermocouple will be located where the environment's temperature is to be measured, that is junction end in Figure 10. The other end of the wires will be the tail end where the reference temperature will be measured. Since the measurement with two thermoelements, a thermocouple, is a differential measurement it has been natural to keep the tail end at 0 °C and conventionally in an ice bath with prolonged wires of Cu. It is unambiguously not convenient today in an industrial standard process where thermoelements are widely used to measure different operating and process temperatures where small-sized measurement systems are demanded.

The solution to this problem has been to use an IC, integrated circuit, called *cold junction compensator*. The tail end is now allowed to fluctuate at ambient temperature since the cold junction compensator will compensate by producing a voltage that corresponds to the difference from 0 °C to the ambient temperature. This difference can later be added to the thermocouple to sustain the temperature and voltage relationship. Since this is an additional

measurement to be done with not exact numbers in the ambient temperature difference, a small error is introduced. (Scervini, 2009) (Lee, 2016)

Different types of thermoelements are available in the market and in this thesis the focus will be of the N type which has a maximum operating temperature of 1000 °C and consists of a NiCrSi composition as wire material. The tolerance for the output is ± 1.5 °C and ± 0.4 % of measured value in the range of -40 °C to +375 °C respectively +375 °C to +1000 °C which applies to the European standard IEC 60584-1, see Appendix D (INOR Process AB, 2014). See Appendix E for the data sheet of the thermoelements. The N type's voltage output is described by the ten-degree polynomial in Equation 9,

$$V_{emf} = \sum_{i=0}^{10} c_i \, (t)^i \qquad \text{Equation 9}$$

where *t* is the temperature in degree Celsius and c_i are the Seebeck coefficients in the table for N type thermoelements in NIST ITS-90 Thermocouple Database. (U.S. Secretary of Commerce on behalf of the United States of America, 1995/2018) (Scervini, 2009)

3 Approach

3.1 Remodeling of graphite in injector

The graphite inside of the injector needed to be exchanged during the test measurements of the gas flow profile and the gas flow temperature measurements. This was due to the thermocouples to measure the gas temperature in the different flow areas; upstream (vicinity of growth area), downstream or in between these critical areas. The thermocouples needed to be inserted through the graphite and therefore drilling in the graphite was needed. These drilled holes in the graphite would have affected the current graphite roof piece in the reactor since it needs to be symmetric and to contain no errors or misalignments. The graphite piece with its drilled holes is seen as a CAD model in Figure 11.

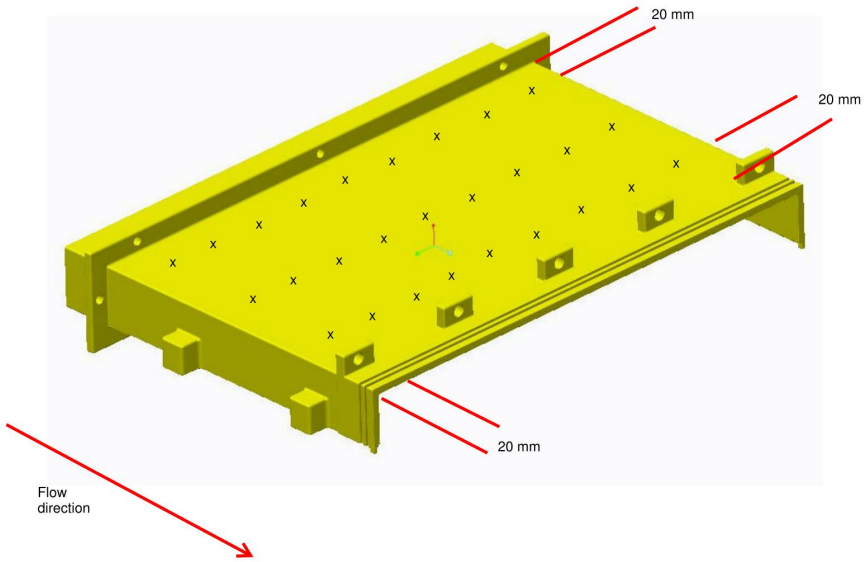

Figure 11 Hand drawn positions for drilled holes in graphite test piece. Copyright Epiluvac.

The new test piece of graphite was designed by Epiluvac and installed by the thesis author in cooperation with Epiluvac.

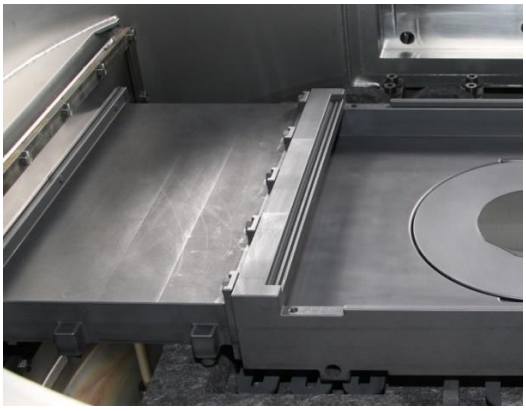

Figure 12 Injector to the left, wafer to the right and graphite liner in between. Copyright Epiluvac.

The graphite piece can also be seen in Figure 12 where the injector and the wafer in its satellite can be seen in the same figure.

3.2 Calculating reference gas velocity

An estimation of the gas mean velocity in the liner was also calculated with following equations and assumptions. The volume flow of the gas was set to F_v SLM which is equal to $F_v/60$ L/s or $F_v/60{,}000$ m^3/s. The gas pressure upstream the liner was set to p_{gas} bar which is equal to $p_{gas}/10$ MPa. The pressure in the liner is set to p_{liner} bar which is equal to $p_{liner}/10$ MPa. The ideal gas law according to Equation 3 can be solved for p and expressed with the gas density ρ in Equation 10.

$$p = \rho RT \qquad \text{Equation 10}$$

If the gas pressure in the liner would be reduced to $p_{gas}/100$ MPa, the gas density would also be reduced to 1/10 of the original gas density, upstream the liner. The continuity equation can be written as in Equation 11.

$$\frac{dm}{dt} = \rho A w \qquad \text{Equation 11}$$

Where dm/dt is the mass flow, A the cross-section area of the liner and w the mean gas velocity. Inserting values results in Equation 12, Equation 13, Equation 14, Equation 15 and Equation 16. The volume flow, Aw, upstream the liner is set to 0.0005 m^3/s and the mass flow, ρAw, is the same regardless of position in the liner. If the gas density in the upstream liner is reduced to 1/10, the volume flow in the liner increases to 0.005 m^3/s.

$$p_{gas} = 1\ bar = 0.1\ MPa \qquad \text{Equation 12}$$

$$p_{liner} = 50\ mBar = 0.005\ MPa \qquad \text{Equation 13}$$

The volume flow is given by Equation 14.

$$F_V = Aw = 30\ SLM = \frac{30}{60} L/s\ = 0.0005\, m^3/s \qquad \text{Equation 14}$$

The cross-section area is given by Equation 15.

$$A = 0.3 * 0.023\ m^2 = 0.0069\ m^2 \qquad \text{Equation 15}$$

Solving for the mean velocity results in Equation 16.

$$w \text{ via } Aw = \frac{dV}{dt} \Rightarrow w = \frac{0.0005}{0.0069}\frac{m}{s} = 0.072\frac{m}{s} \qquad \text{Equation 16}$$

These calculations are made on the assumptions that the temperature is the same upstream as downstream the liner. If the liner temperature instead is higher than the gas temperature, the gas will be heated on its passage through the liner until reaching the liner temperature, downstream the liner. The latter is the case in this MOCVD reactor. When the gas temperature is increased, the gas density will decrease. This will result in an increasing gas velocity when it

flows through the liner. The gas velocity can be roughly estimated through the continuity equation in Equation 17.

$$\frac{dm}{dt} = \rho_1 A_1 w_1 = \rho_2 A_2 w_2 \quad \text{Equation 17}$$

Where ρ is the gas density, A the cross-section area and w the gas mean velocity. Index *1* is in the vicinity of the injector in the liner and index *2* is located at the outlet of the liner, upstream of the susceptor. Index 2 can be placed anywhere inside of the liner since the mass flow is constant. Solving Equation 17 for w_2 results in Equation 18.

$$w_2 = (A_1 w_1)(\rho_1/\rho_2)(1/A_2) \quad \text{Equation 18}$$

A_1w_1 is seen in Equation 14 and A_2 is known from Equation 15. The density ratio (ρ_1/ρ_2) is expressed with the ideal gas law in Equation 10 in Equation 19.

$$(\rho_1/\rho_2) = (p_1/p_2)(T_2/T_1) \quad \text{Equation 19}$$

The pressure relation is described in Equation 20.

$$(p_1/p_2) = \left(p_{gas}/p_{liner}\right) = \frac{0.1}{0.005} = 20 \quad \text{Equation 20}$$

The gas temperature upstream the liner, T_1, is assumed to be 20 °C and the gas temperature downstream the liner, T_2 in the vicinity of the susceptor, is assumed to be 1000 °C. Inserting the known and assumed values into Equation 18 results in Equation 21.

$$w_2 = (A_1 w_1)(\rho_1/\rho_2)(1/A_2) = 0.0005 * \left(20 * \frac{1000+273}{20+273}\right) * \left(\frac{1}{0.0069}\right) \approx 6.297 \frac{m}{s} \quad \text{Equation 21}$$

The roughly estimation of the mean gas velocity is then assumed to be 6.297 m/s at these conditions. The velocity, density and the temperature are in these calculations assumed to be independent of the coordinates *x*, *y* and *z* and the time *t*, but they are all functions of these parameters.

3.3 Measurements with thermoelements

The thermoelements used in the measurements are of N type which is studied to be suitable for the temperature measurements, see Figure 13. When measuring with thermoelements it is of high importance to make sure they are all calibrated. This is to ensure the accuracy of the data sampled from the thermoelements. Since these thermoelements are acquired new from the producer, they are all calibrated.

Figure 13 Thermocouple of type N used in measurements.

The flange on the reactor of where the thermoelements should be placed are specially designed with five holes for the five thermoelements. See Figure 14 below.

Figure 14 Thermoelements connected to reactor chamber. Copyright Epiluvac AB.

In the gas system of the hot-wall MOCVD system, two EPCs can be found which are controlling the pressure in the run lines of the injector, which are the pipes connecting the EPC and the injector outlets. There are two run lines carrying the precursors, its hydride gases and carrier gases in this hot-wall MOCVD system, RL1 and RL2, which are connected to six respectively five MFCs. The MFCs are then connected to the injector outlets. How the total flow ratio over the run lines was set, can be seen in section 3.4.

The EPCs for the run line MFCs needed adjustments for each different flow rate measurement, since the MFCs demands a higher pressure in their inlets compared to their outlets. When

changing flows, the EPCs therefore needed to be adjusted accordingly to sustain the pressure difference over the MFC.

The thermocouples were used at three different positions; 1, 2 and 3. These numbers represents the row, counted from the injector, see Figure 15. In addition to different positions, the thermoelements were used at three different height positions in the liner, the graphite piece next to the injector.

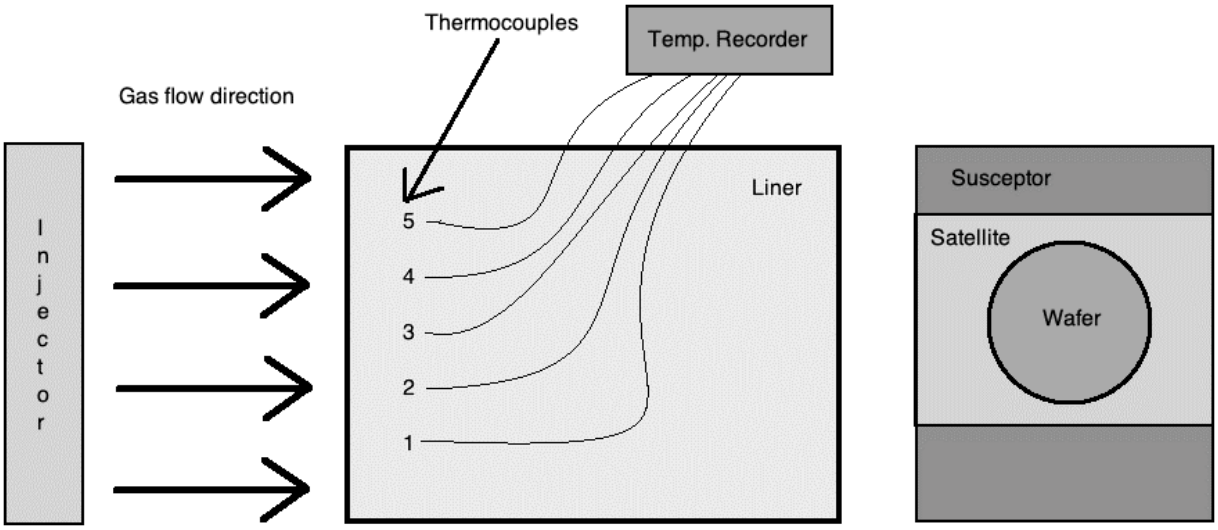

Figure 15 Measurement setup with thermocouples.

To make sure the thermoelements were fixed at correct heights accordingly with the test schedule, two extra graphite pieces were manufactured which are seen in Figure 16. The distance between the thermoelements and the inner bottom of the liner was measured to 2.05 mm which represented position A. Then the cable of the thermoelement was bent 90° so it could rest in its drilled hole on top of the test graphite piece when the thermoelements were placed in the holes. For position B and C, the new manufactured graphite pieces were placed on top of the graphite liner, creating an extra distance for the thermoelement inside of the liner. Position B and C is 8.05 mm respectively 14.05 mm above the inner liner bottom.

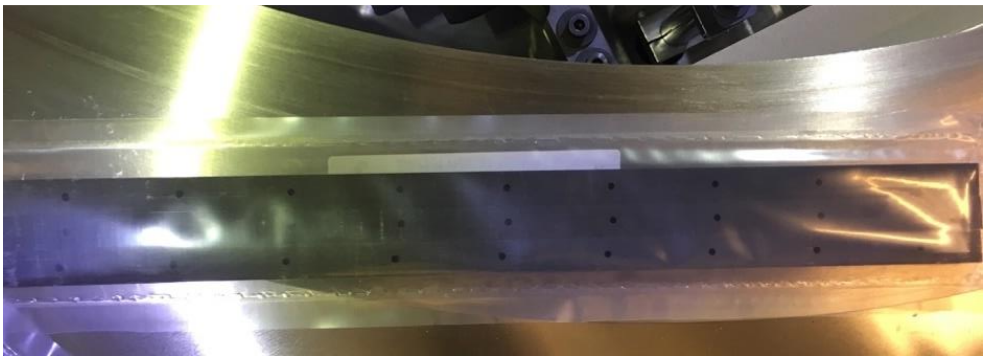

Figure 16 Graphite piece for measurements at height positions B and C.

To not accidentally move the thermoelement cables, they were fixed inside the reactor drum and to distinguish them from one another they were marked with numbers ranging from one to five. In Figure 17 thermocouples can be seen in position B, in the middle of the injector outlet and upstream. In Figure 18 the thermocouple can be seen from the outlet of the liner. It can also be seen that the thermoelements have been labeled with number tags to distinguish them from each other.

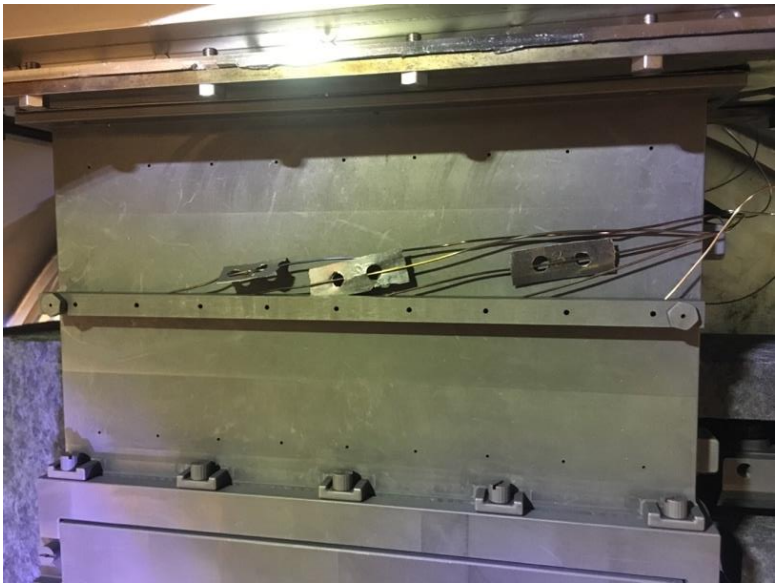

Figure 17 Thermocouples in position B, seen from above.

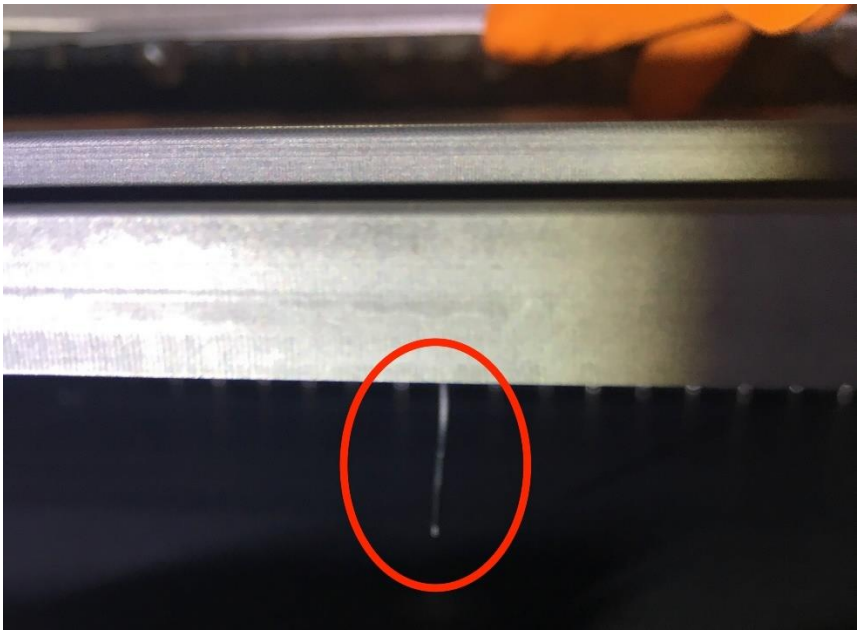

Figure 18 Thermocouple in position A, outside injector outlet seen from upstream the liner.

The software used to extract the raw data from the thermocouples is called MadgeTech and works as it logs the thermocouples output data which is a temperature in degree Celsius in the hot-wall MOCVD system and the software is then used to extract the data from the hot-wall MOCVD system. It then saves it in a database which can be exported to an Excel spreadsheet for data manipulation. In Figure 19 example data of some of the first tests with the

thermocouples can be seen saved in an Excel spreadsheet with seven columns, five for the recorded temperatures and two for the time and the date.

Device Name:		OctTemp	OctTemp	OctTemp	OctTemp	OctTemp
Device Description:		Eight Channel Thermocouple Temperature Data Logger	Eight Channel Thermocouple Temperature Data Logger	Eight Channel Thermocouple Temperature Data Logger	Eight Channel Thermocouple Temperature Data Logger	Eight Channel Thermocouple Temperature Data Logger
Serial Number:		Q81890	Q81890	Q81890	Q81890	Q81890
Device ID:		MultiChannel	MultiChannel	MultiChannel	MultiChannel	MultiChannel
		Channel 2	Channel 4	Channel 6	Channel 8	Channel 10
Date	Time	Thermocouple 1 (°C)	Thermocouple 2 (°C)	Thermocouple 3 (°C)	Thermocouple 4 (°C)	Thermocouple 5 (°C)
2018-12-10	10:37:07	17,2	17,8	17,2	17,2	17,1
2018-12-10	10:37:12	17	17,9	17,1	17,3	16,9
2018-12-10	10:37:17	17,1	17,7	17,1	17,1	17
2018-12-10	10:37:22	16,9	17,7	17,2	17,3	16,7
2018-12-10	10:37:27	17	18,1	17,1	17,4	16,9
2018-12-10	10:37:32	17,3	17,6	17,1	17,2	16,8
2018-12-10	10:37:37	17	17,8	17,1	17,1	17
2018-12-10	10:37:42	17,3	17,8	17,3	17,2	16,7
2018-12-10	10:37:47	17,2	17,9	17,1	17,1	16,9

Figure 19 Example data extracted from MadgeTech software and saved in Excel spreadsheet.

The software also saves it in a graph where all the thermocouples can be seen with trend lines, see Figure 20. All the thermocouples have a significant color which is described in the figure as well.

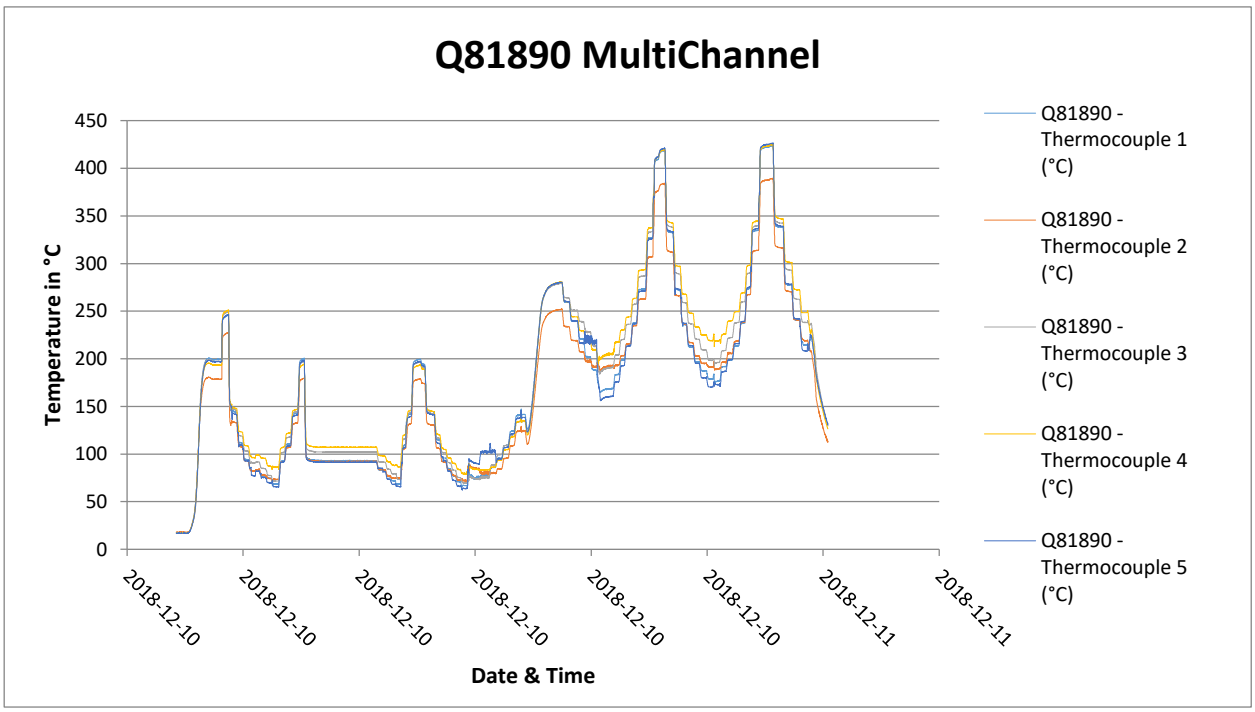

Figure 20 Trend lines created by MadgeTech software.

The hardware located in the reactor which connects the thermocouples with the reactor is seen in Figure 21. The hardware is manufactured by MadgeTech and is of model OctTemp which by is name has eight channels to record thermocouple temperatures with.

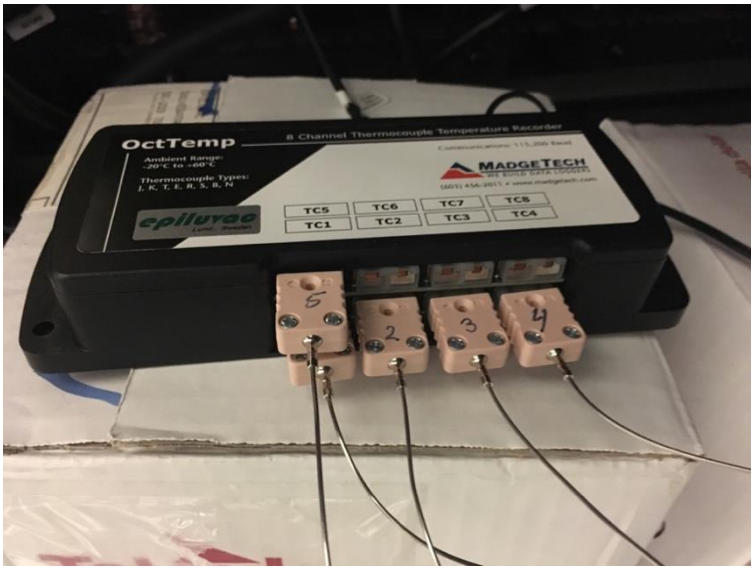

Figure 21 Temperature recorder of five thermocouples used in measurements.

The recorded data was then seen in the accompanied software, Figure 20 and the data could be extracted for each thermocouple.

To ensure the thermocouples were measuring the same temperature under the same condition in the same spot, they were all placed together and bonded by a graphite thread in one of the bolt holes in the interface of the liner and susceptor, see Figure 22.

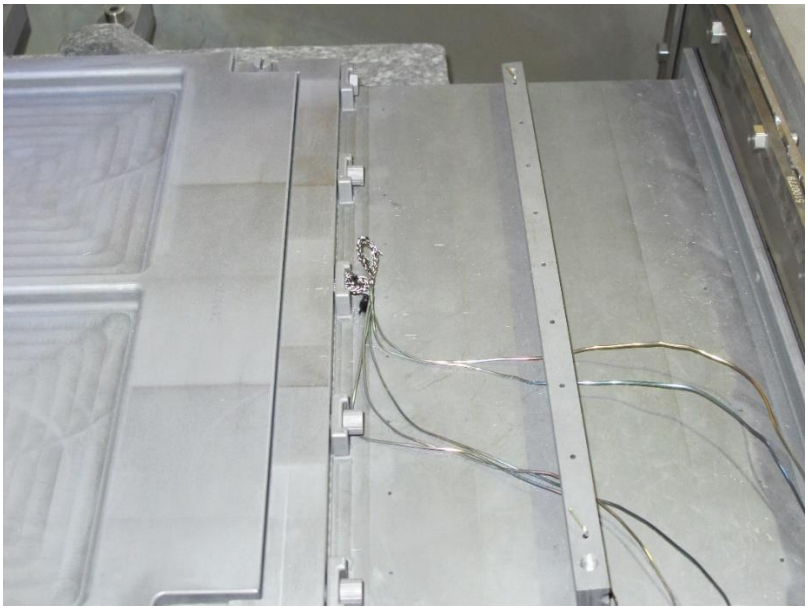

Figure 22 Setup of thermocouple temperature verification at the end of measurements. Copyright Epiluvac AB.

3.4 Test schedule

The test schedule includes all the tests performed on the hot-wall MOCVD system to extract a result of the gas flow uniformity. The schedule is divided into eight columns which are A containing the test number, B containing the background pressure in mBar, C containing the temperature of the heating elements in degree Celsius, D containing the total gas flow of the injector in Standard Liters per Minute, H containing thermocouple number, I containing the measured data value of the thermoelements, same as I but in Kelvin and K a time stamp. In the columns containing three positions, 1, 2 and 3, is a table located which shows the position of the thermocouples in the test graphite piece.

The table is divided into three columns and nine rows where each table position represents a hole position in the test graphite piece seen in Figure 11. Depth of thermocouples have 3 positions (depths) which are; 2.05 mm above the injector bottom (A), 8.05 mm above the injector bottom (B) and 14.05 mm above the injector bottom (C). The positions of the thermocouples are furthermore divided into three columns where the very left column is closest to the injector outlets and each 'A/B/C' represents the placement of each thermocouple and at which height. Each row in the table represents a side position in the flow direction where the flow is directed from left to the right in the table. See, Figure 23 where each of the columns are displayed for test 395.

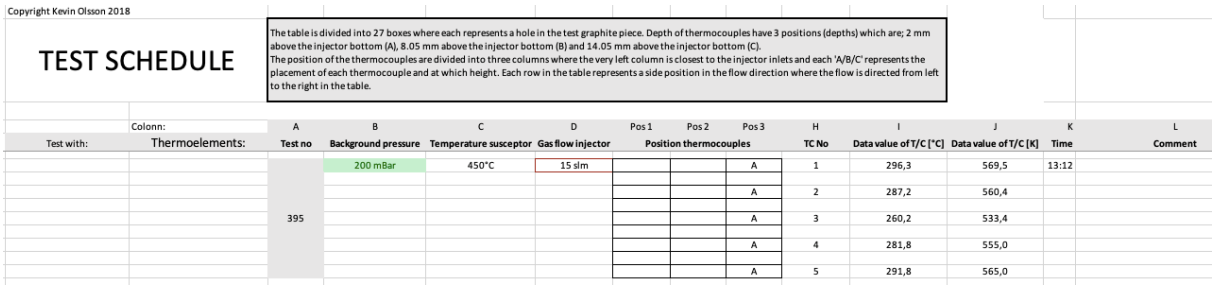

Copyright Kevin Olsson 2018

TEST SCHEDULE

The table is divided into 27 boxes where each represents a hole in the test graphite piece. Depth of thermocouples have 3 positions (depths) which are; 2 mm above the injector bottom (A), 8.05 mm above the injector bottom (B) and 14.05 mm above the injector bottom (C).
The position of the thermocouples are divided into three columns where the very left column is closest to the injector inlets and each 'A/B/C' represents the placement of each thermocouple and at which height. Each row in the table represents a side position in the flow direction where the flow is directed from left to the right in the table.

	Colonn:	A	B	C	D	Pos 1	Pos 2	Pos 3	H	I	J	K	L
Test with:	Thermoelements:	Test no	Background pressure	Temperature susceptor	Gas flow injector	Position thermocouples			TC No	Data value of T/C [°C]	Data value of T/C [K]	Time	Comment
			200 mBar	450°C	15 slm			A	1	296,3	569,5	13:12	
								A	2	287,2	560,4		
		395						A	3	260,2	533,4		
								A	4	281,8	555,0		
								A	5	291,8	565,0		

Figure 23 Test schedule showing data of test 395.

How the data was divided over the two run lines during the measurements can be seen in Table 3 Total flow rate over run line 1 and run line 2., where also the total flow in SLM can be seen.

The full test schedule can be found in Appendix C.

4 Results

The measurements were carried out at five different positions inside of the graphite liner. The tests have been done with variating flows of 0 to 40 SLM at fixed pressures of 20, 50, 100, 200 and 700 mBar. These tests have then been performed at a low temperature of 450°C and an elevated temperature of 1000°C. The result is presented in subsections of relevant positions. For each data point corresponding to a temperature, the system has been allowed to stabilize for five to ten minutes until reaching stable temperature. The raw data with additional diagrams of the measurement data are to be found in Appendix F.

Whether laminar flow is established or not has been defined according to the profile symmetry such as Figure 7 and Equation 6 in addition to fluid dynamic theory in subsection 2.2 *Fluid dynamic principles*. If the profile of the gas flow is deviating from expected symmetry of a parabolic function. It is considered to what extend the relative measured temperature differ from position TC1 to TC5. A symmetry is established as the temperature is decreasing or increasing towards TC3, which should be the local minimum respectively maximum. As pairs, TC5 with TC1 and TC4 with TC2 will pairwise need to have the same temperature, in the thermocouple's tolerance which is ± 0.4 % of measured value in the range of +375 °C to +1000 °C, found in subsection 2.4. TC1 is located to the far left and TC5 to the far right when facing the injector. The result gives indications which can be stronger, weaker or non-conclusive regarding the gas behavior in the different cases. The referred graphs not displayed in sections 4.1 and 4.2 are found in Appendix H.

4.1 Temperature over flows at fixed pressures

Following sections 4.1.1 through 4.1.5 contain raw data plotted in 3D at variating flows at fixed pressures. The results are 3D plots with temperature dependency of the flow for each thermocouple.

4.1.1 Position 1B

The first measurements were at position 1B which corresponds to the measurement point closest the injector and at 8 mm above the liner bottom. This was the only measurement performed at position 1. See Appendix H for the result in section 9.8.1.1.

4.1.2 Position 2A

The measurements at position 2A which corresponds to the measurement point equally close to the injector as the liner outlet and at 2 mm above the liner bottom. This was one of the three measurements performed at position 2. In addition to position A, the height positions B at 8 mm and C, at 14 mm above the liner bottom were carried out. See Appendix H for the result in section 9.8.1.2.

4.1.3 Position 2B

See Appendix H for the additional diagrams in section 9.8.1.3.

The equations for the trendlines of the thermocouples in Figure 24 and Figure 26 are used to plot Figure 25 respectively Figure 27. It can be seen that the flow profile is planar up to 30 SLM and the temperatures of the thermocouples indicates the same behavior as explained in section 4.1.5 for position 3A in Figure 32. The delta T is decreasing for the thermocouples with increased flows and delta T for TC4 is starting to decrease less rapid compared to the others.

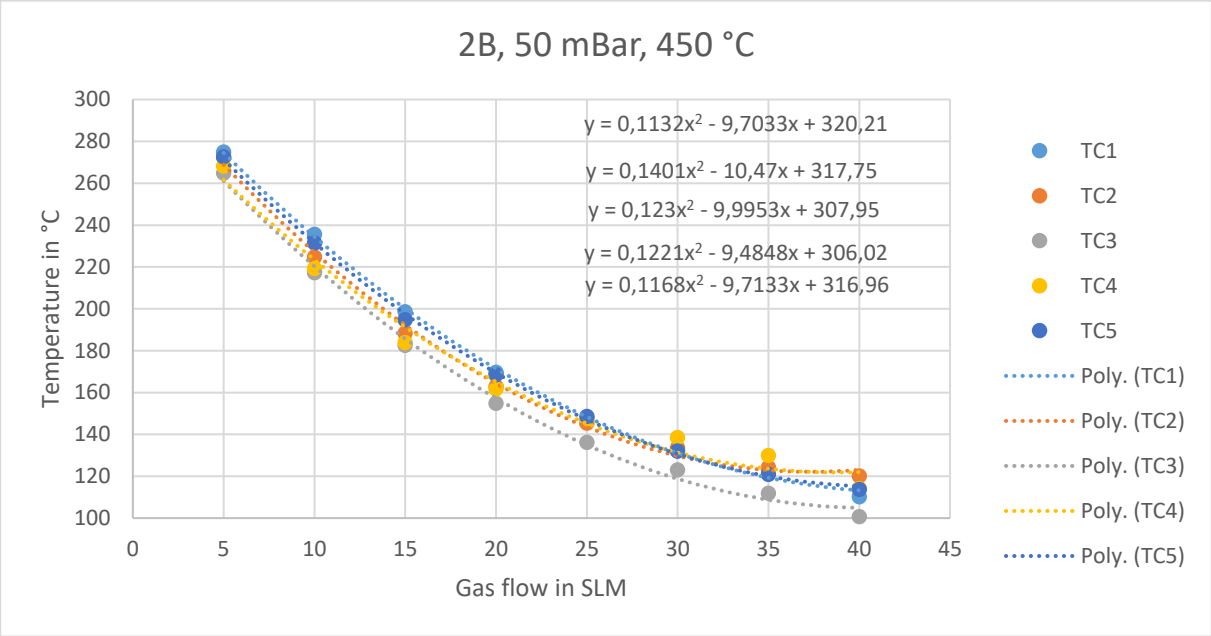

Figure 24 Position 2B with T over flow at 50 mBar background pressure and at a susceptor temperature of 450°C.

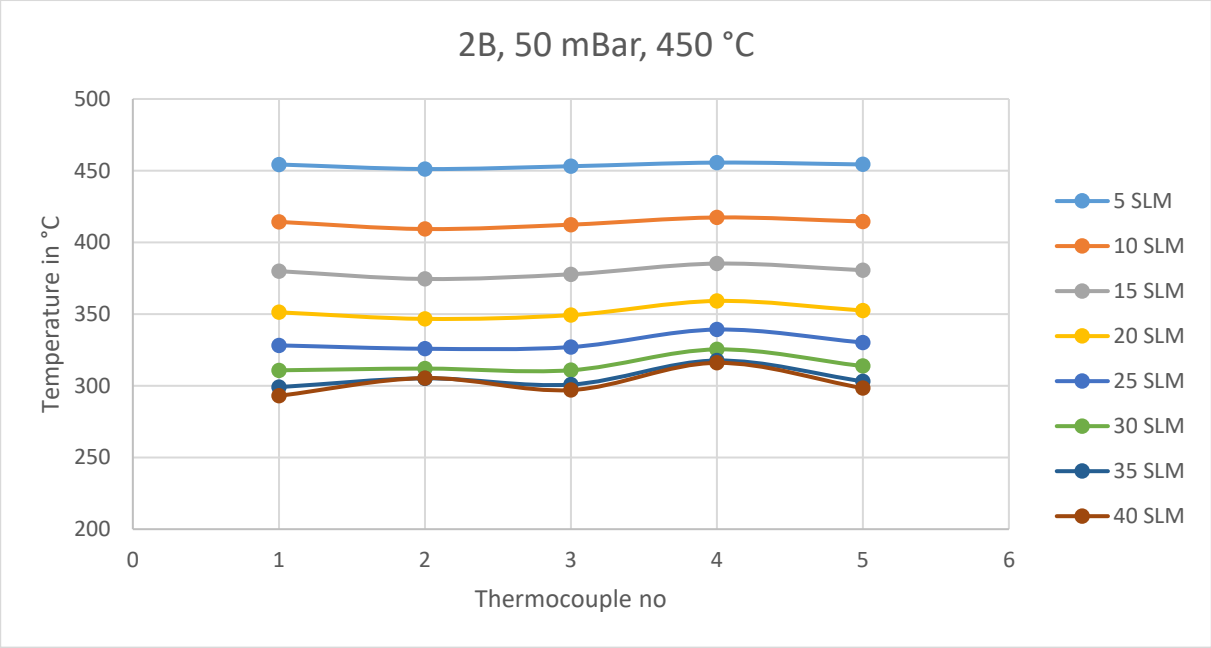

Figure 25 Position 2B normalized gas flow profile with T over TC at 50 mBar background pressure and at a susceptor temperature of 450°C.

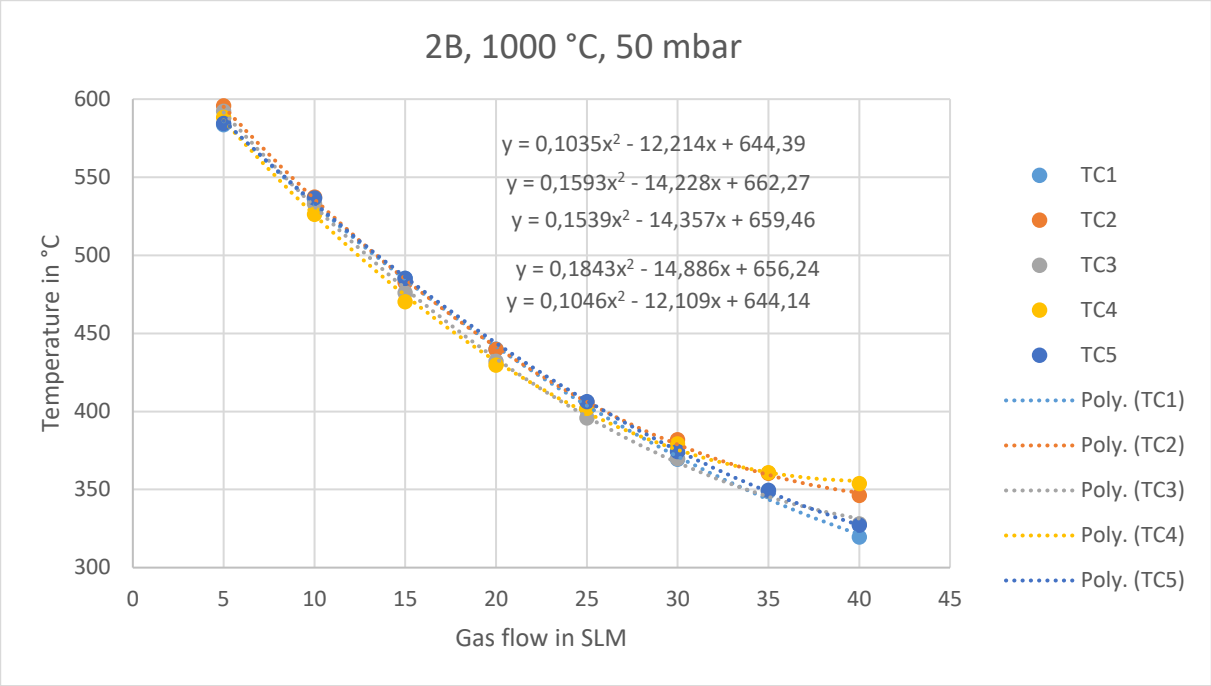

Figure 26 Position 2B with T over flow at 50 mBar background pressure and at a susceptor temperature of 1000 °C.

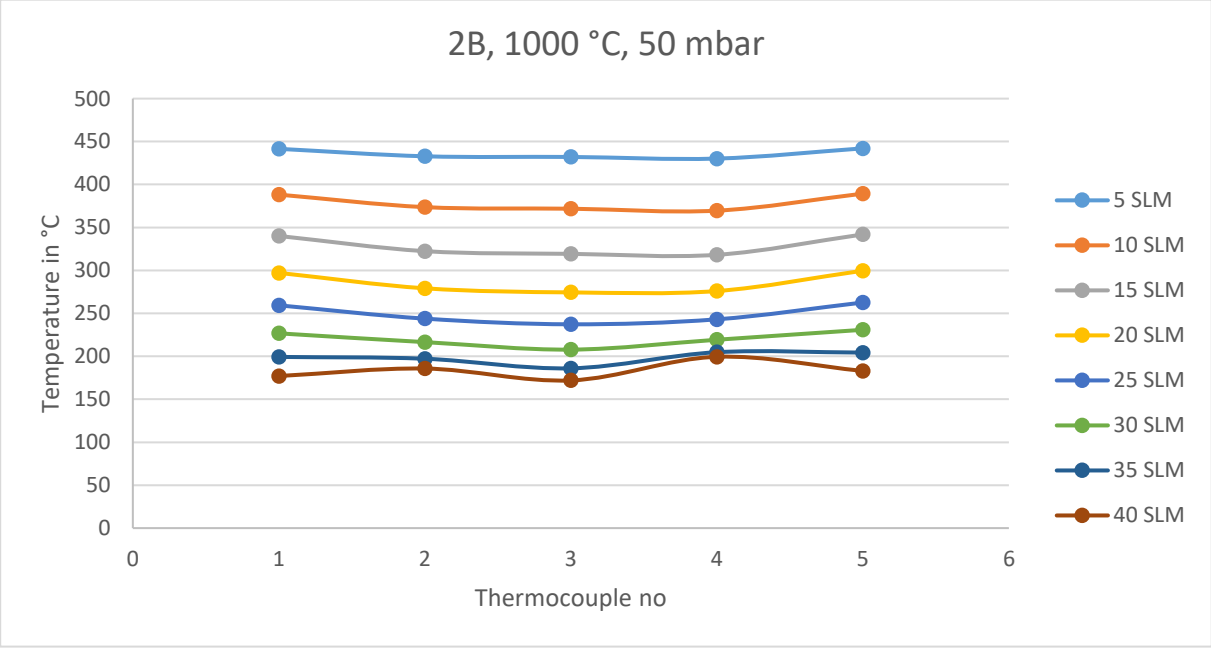

Figure 27 Position 2B normalized gas flow profile with T over TC at 50 mBar background pressure and at a susceptor temperature of 1000°C.

4.1.4 Position 2C

See Appendix H for the result in section 9.8.1.4.

4.1.5 Position 3A

The measurements at position 3A which corresponds to the measurement point closest the susceptor and at 2 mm above the liner bottom. This was the only measurement performed at position 3. Additional diagrams are seen in Appendix H in section 9.8.1.5. A second-degree polynomial can fit the trend for TC3 in Figure 28 very good and it can show the trends of the temperature decrease for all the thermocouples. For gas flows up to 25 SLM at 50 mBar a strong indication for laminar flow is seen with a minimal deviation of TC2 and TC4 at flows higher than 25 SLM. The same result is seen for 100 mbar in Figure 30. At 20 and 200 mBar, see section 9.8.1.5 for figures, the same result is seen, but an improvement of obtaining a laminar flow up to 35 SLM. For 700 mBar in section 9.8.1.5 no laminar flow is indicated regardless of flow.

In Figure 29 and Figure 76 the measured temperature is plotted against the TC and a trend can be seen when increasing the flow. Approximately a temperature reduction of roughly 20 to 25^{o}C is seen for the decreasing flows which indicate a good response of the thermocouples. The trend lines have been positioned at the same initial value since the interesting part of the response is the change in the temperature. Since the change of temperature over increased flows is almost constant, the profile can be assumed to be linear. Calculating the mean velocity of all the thermocouples is then performed according to Equation 16. At 5 SLM the mean velocity is calculated to 5SLM/0.69 dm^2 = 7.25 dm/min which is about 1.21 cm/s at 1 atm and at 50 mBar the velocity is 24.2 cm/s. What can be seen is that the quadratic term in the polynomials are lower against the walls and higher towards the center which indicates that for higher flows there are smaller temperature changes for the thermocouples which makes the temperature relation non-linear for the higher flows. Along the walls it takes longer time to reach a non-linear behavior compared to for TC2 to TC4 which all have a more dominating quadratic term.

In Figure 29 the gas flow profile can be seen and is the closest to be expected. The data shows a more planar profile for lower flows and when increasing the flow, it is seen that the temperature reduction is decreasing. For 5 SLM a straight profile can be seen. Increasing the gas flow along the interval of 10 to 25 SLM gives rise to larger horns at TC2 and TC4 and increasing to 35 and 40 SLM indicates a weak parabolic shape of the gas flow profile.

TC1 and TC5 behaves well and decreases with approximately 20 ^{o}C when increasing the gas flow by 5 SLM and slightly less delta T at high flows.

TC2 and TC4 are more dynamic and have large temperature reduction when increasing the lower flows and smaller delta T reductions at higher flows. The behavior is like TC1 and TC5, but with slightly larger amplification.

TC3 begins to behave like TC1 and TC5, but the temperature reduction is not as large towards the higher flows.

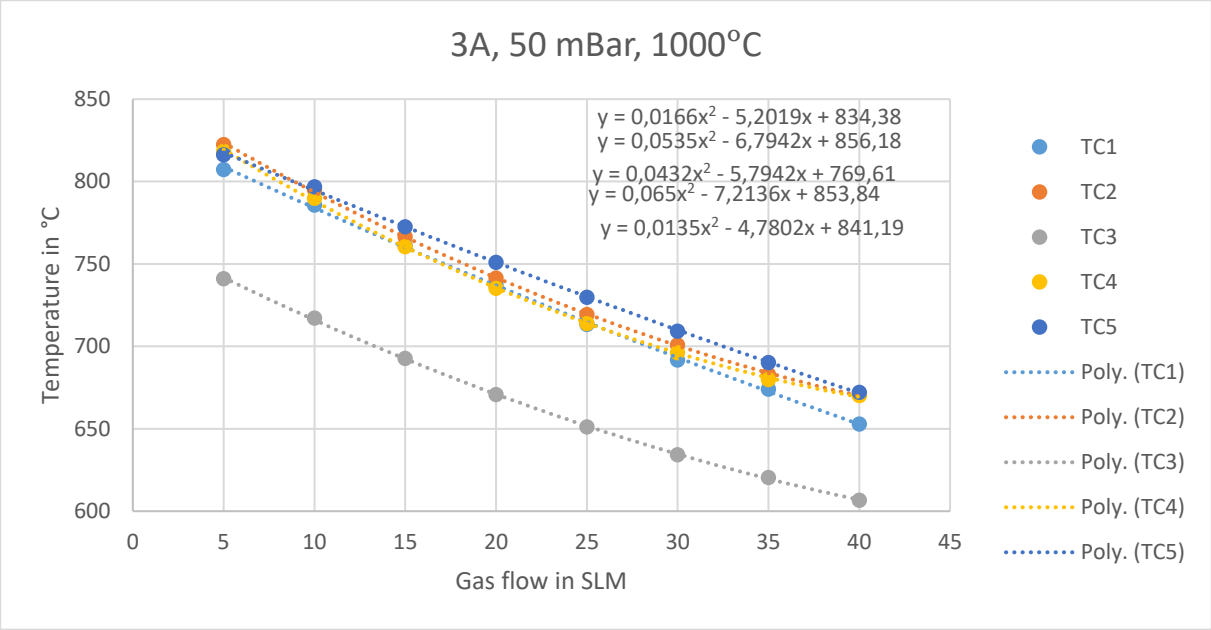

Figure 28 Position 3A with T over flow at 50 mBar background pressure and at a susceptor temperature of 1000°C.

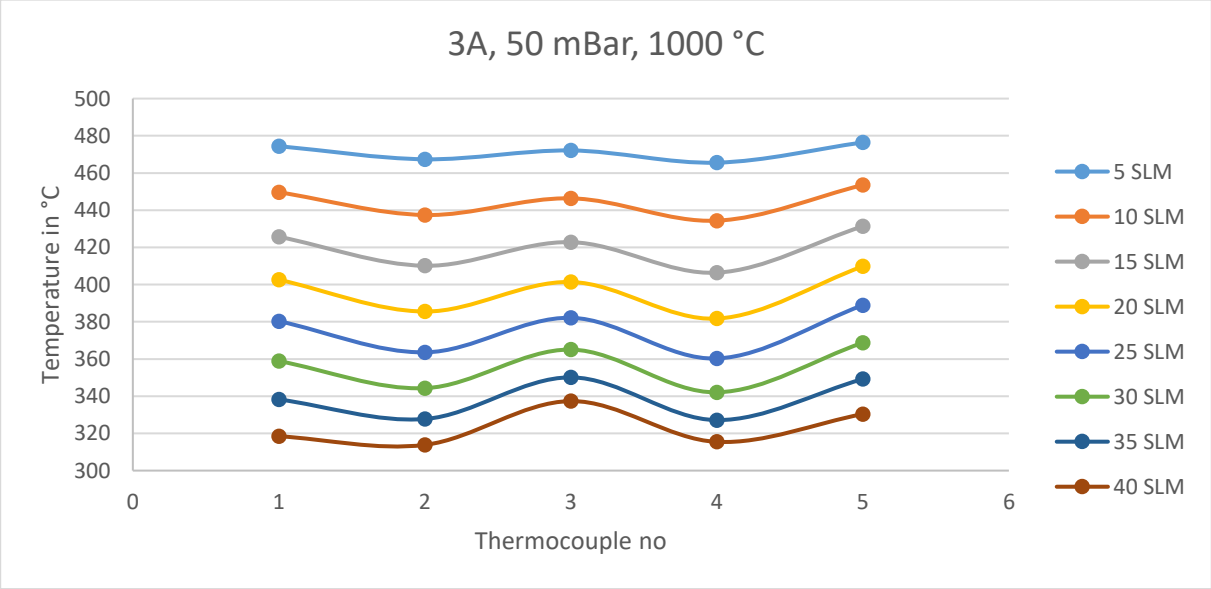

Figure 29 Position 3A normalized gas flow profile with T over TC at 50 mBar background pressure and at a susceptor temperature of 1000°C.

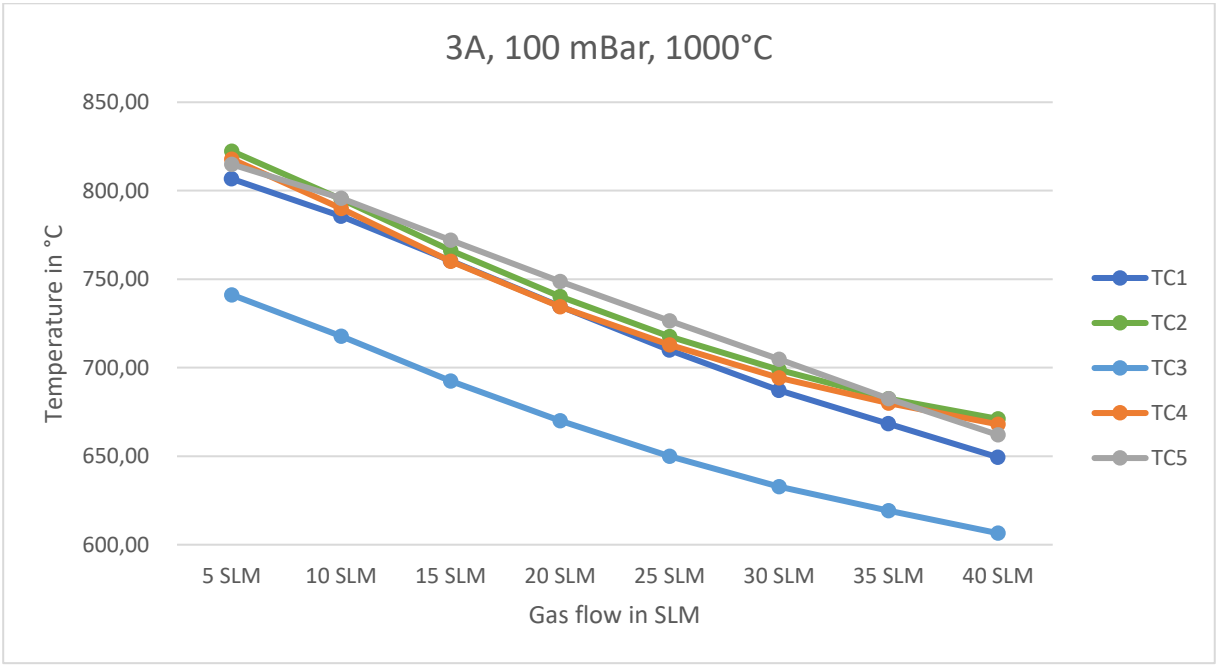

Figure 30 Position 3A with T over flow at 100 mBar background pressure and at a susceptor temperature of 1000°C.

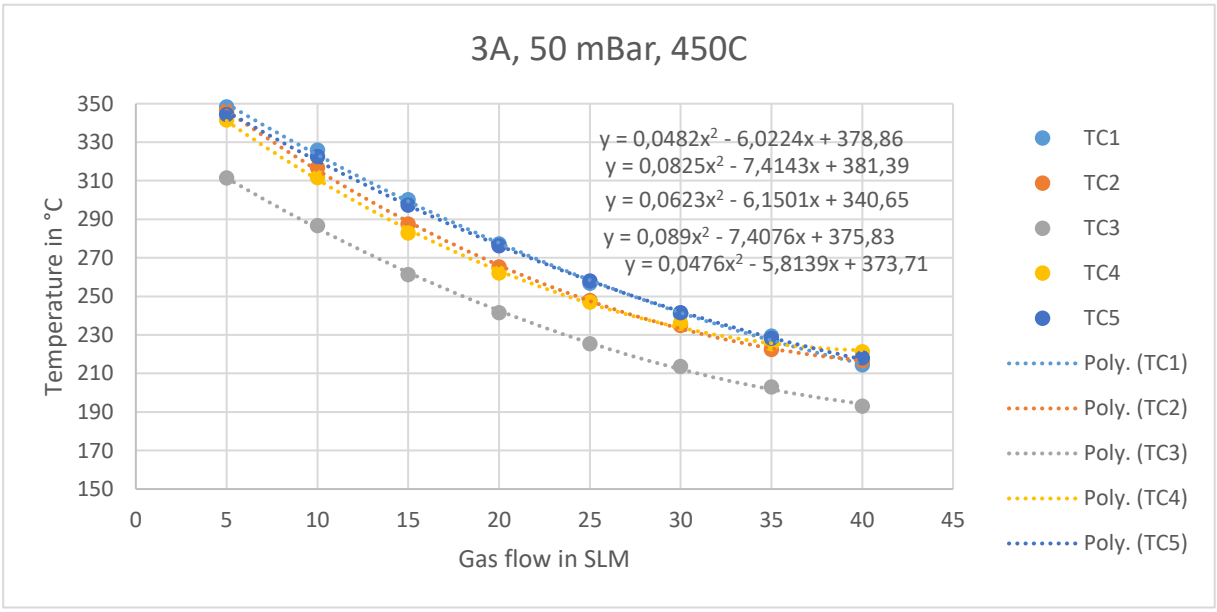

Figure 31 Position 3A with T over flow at 50 mBar background pressure and at a susceptor temperature of 450°C.

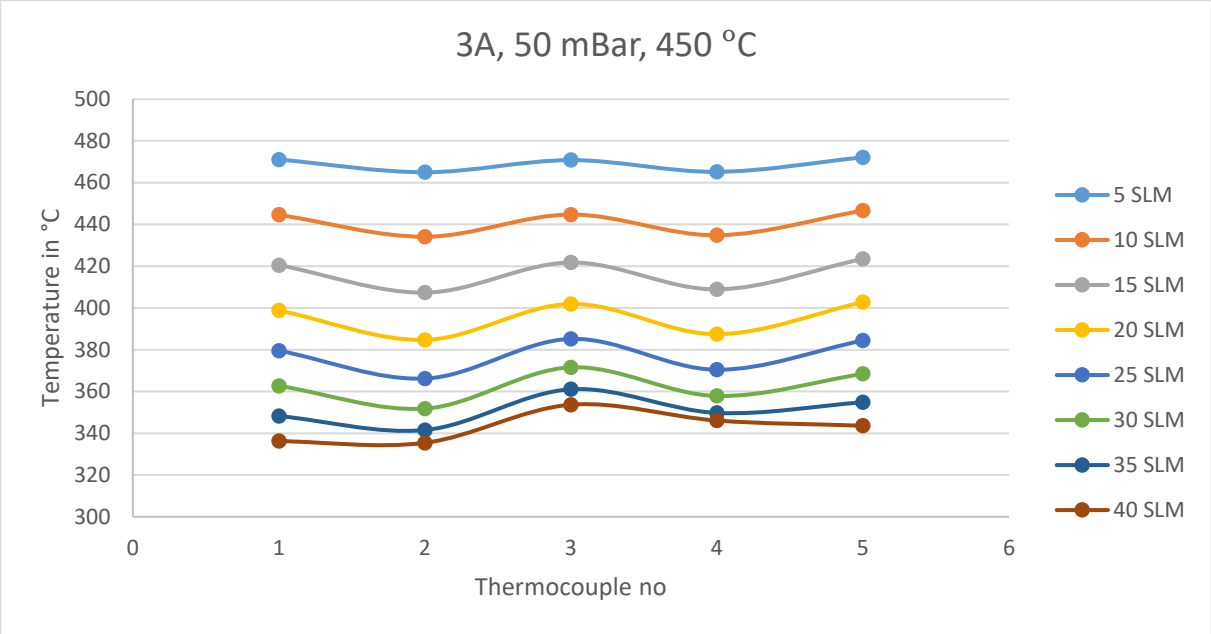

Figure 32 Position 3A normalized gas flow profile with T over TC at 50 mBar background pressure and at a susceptor temperature of 450°C.

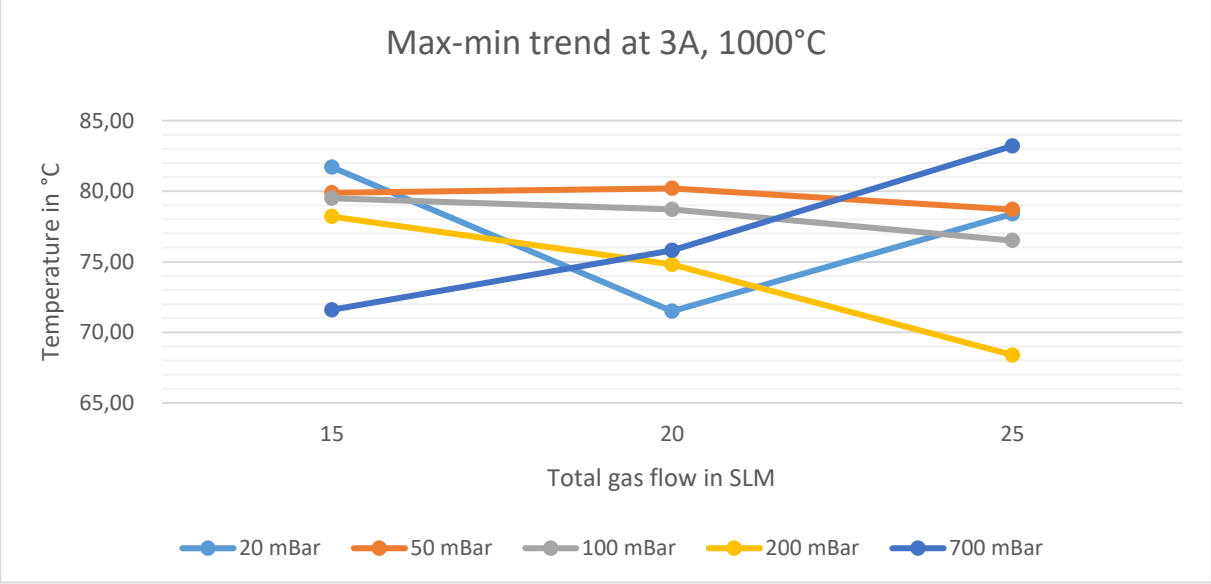

Figure 33 Max-min trendline at position 3A at susceptor temperature of 1000 °C at total gas flows 15, 20 and 25 SLM.

In Figure 33 a trendline of ΔT is shown, where ΔT is the temperature difference between the maximum and minimum of the measured temperature at 15, 20 and 25 SLM. The result indicates that the temperature difference between the maximum and minimum is almost constant throughout the measurements independent of the background pressure with a spread of maximum 12 °C at 700 mBar. A planar trend line indicates more accurate measurements with the thermocouples.

4.2 Temperature over pressures at fixed flows

Following sections 4.2.1 through 4.2.5 contain raw data plotted in 3D at variating background pressures at fixed gas flows. The results are 3D plots with temperature dependent of the pressure for each thermocouple.

4.2.1 Position 1B

The measurements at position 1B which corresponds to the measurement point closest the susceptor and at 8 mm above the liner bottom. This was the only measurement performed at position 3. See result in Appendix H in section 9.8.2.1.

4.2.2 Position 2A

The measurements at position 2A which corresponds to the measurement point equally close to the injector as the liner outlet and at 2 mm above the liner bottom. This was one of the three measurements performed at position 2. In addition to position A, the height positions B at 8 mm and C, at 14 mm above the liner bottom were carried out. See result in Appendix H in section 9.8.2.2.

4.2.3 Position 2B

See result in Appendix H in section 9.8.2.3.

4.2.4 Position 2C

See result in Appendix H in section 9.8.2.4.

4.2.5 Position 3A

See results of measurements in Appendix H in section 9.8.2.4.

At 450^{o}C the trend lines in Figure 34 at 15 SLM are constant up to 100 mBar with a small temperature reduction for 200 mBar and above 200 mBar the trend lines are decreasing for all thermocouples except for TC4 which is increasing. This indicates an event of a transition from laminar to turbulent. In Figure 35 at 25 SLM the trend lines are constant up to 100 mBar (TC3 up to 700 mBar) and above 100 mBar TC1 and TC2 increase in temperature and TC4 and TC5 decrease in temperature which could indicate a transit to turbulence.

At 1000^{o}C in Figure 36 and Figure 37 the trend lines are almost constant up to 200 mBar and temperature reduction for all thermocouples are seen for higher pressures except for TC1, TC2 and TC4 in Figure 37 which remain at almost the same temperature. A small temperature reduction can though also be seen at TC1, TC2 and TC4. In Figure 38, Figure 39, Figure 40 and Figure 41 the temperature can be seen plotted over the thermocouples instead for the different background pressures.

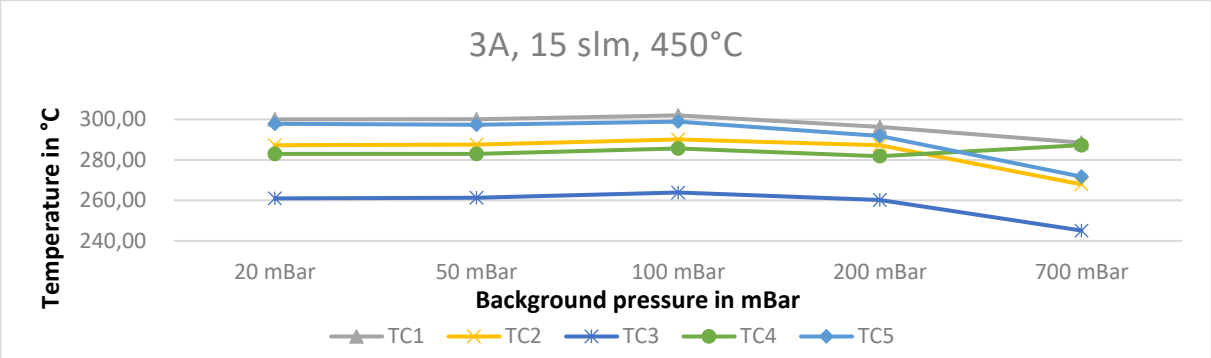

Figure 34 Position 3A with T over background pressure at 15 SLM and at a susceptor temperature of 450°C.

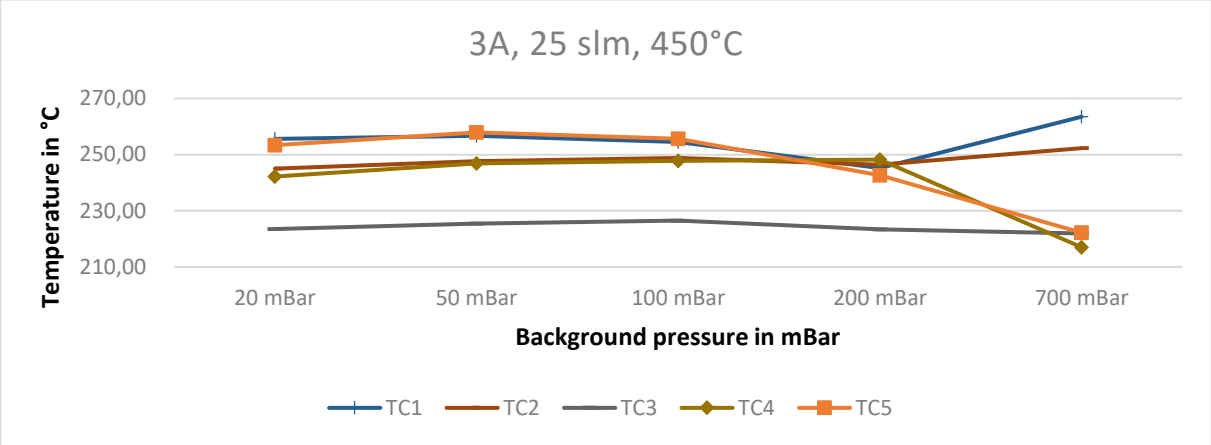

Figure 35 Position 3A with T over background pressure at 25 SLM and at a susceptor temperature of 450°C.

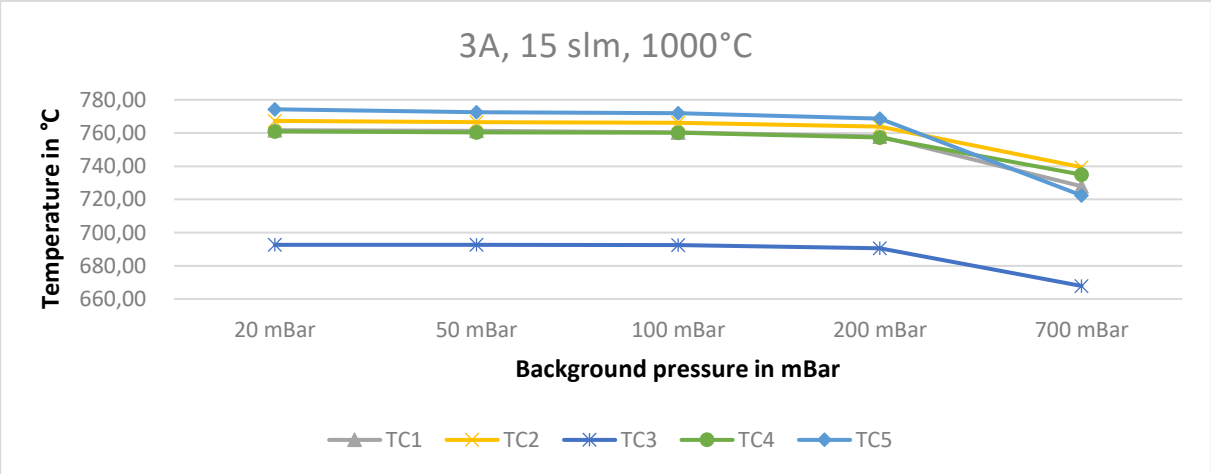

Figure 36 Position 3A with T over background pressure at 15 SLM and at a susceptor temperature of 1000°C.

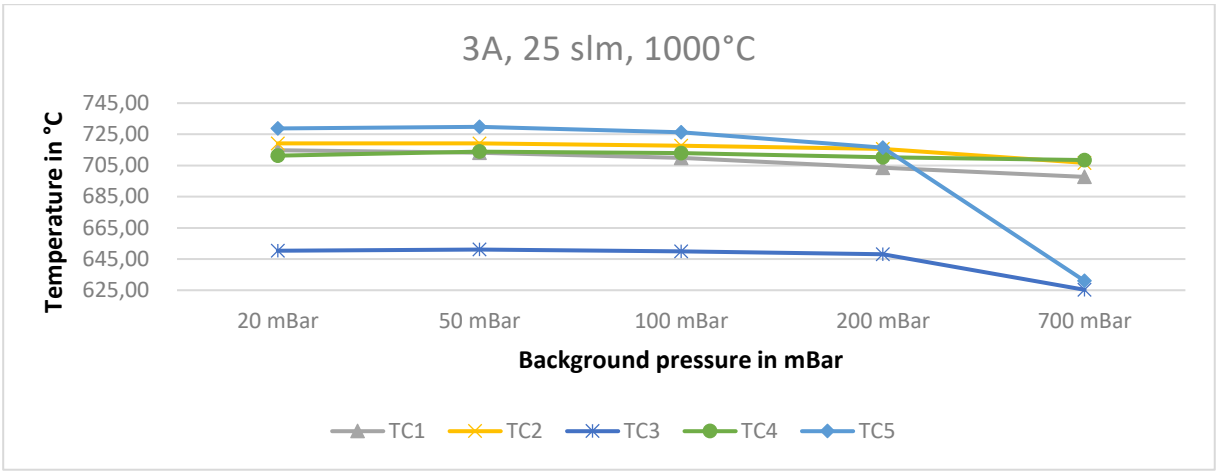

Figure 37 Position 3A with T over background pressure at 25 SLM and at a susceptor temperature of 1000°C.

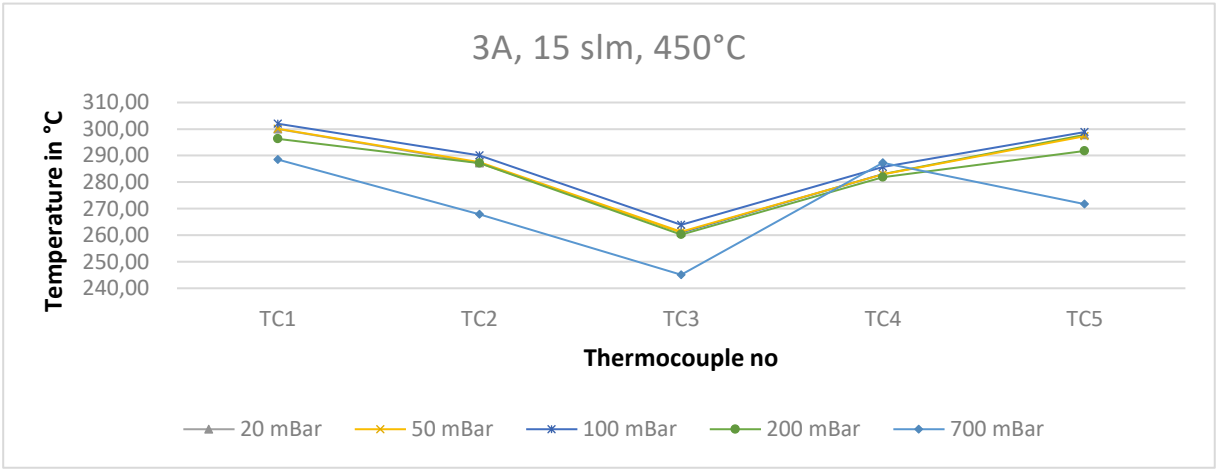

Figure 38 Position 3A with T over TC at 15 SLM and at a susceptor temperature of 450°C.

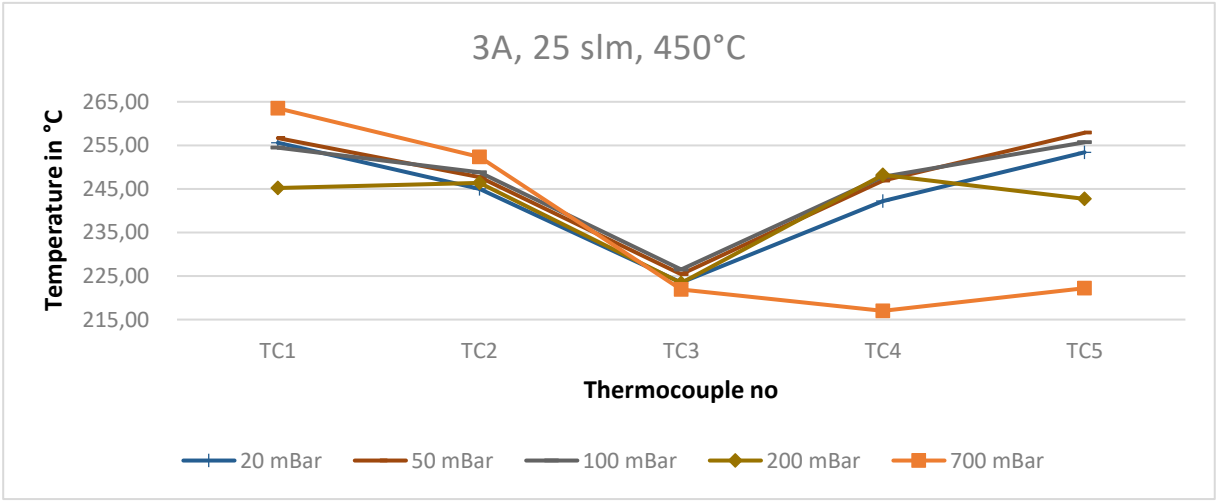

Figure 39 Position 3A with T over TC at 25 SLM and at a susceptor temperature of 450°C.

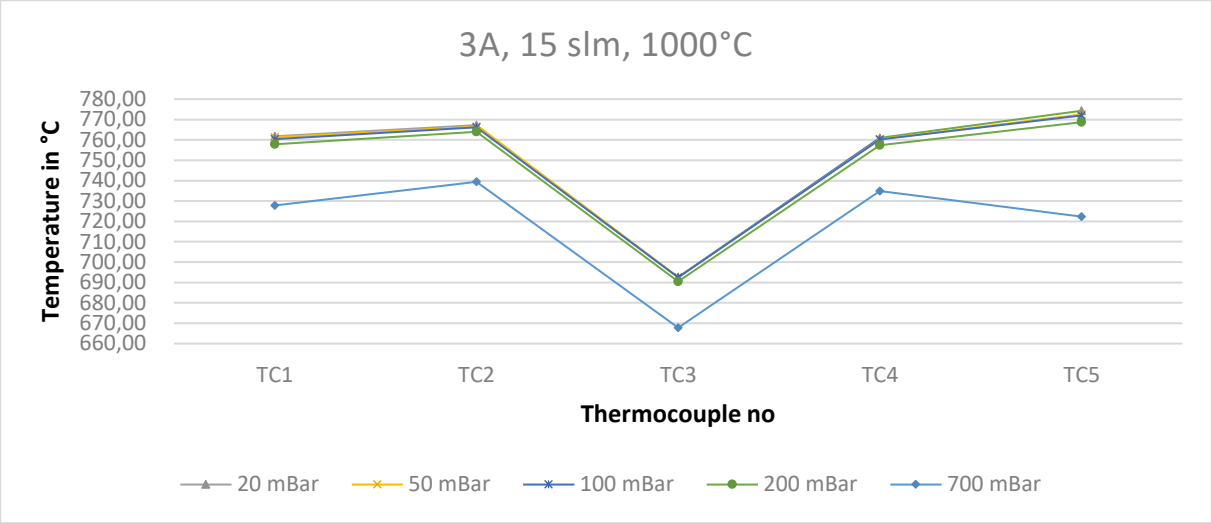

Figure 40 Position 3A with T over TC at 15 SLM and at a susceptor temperature of 1000°C.

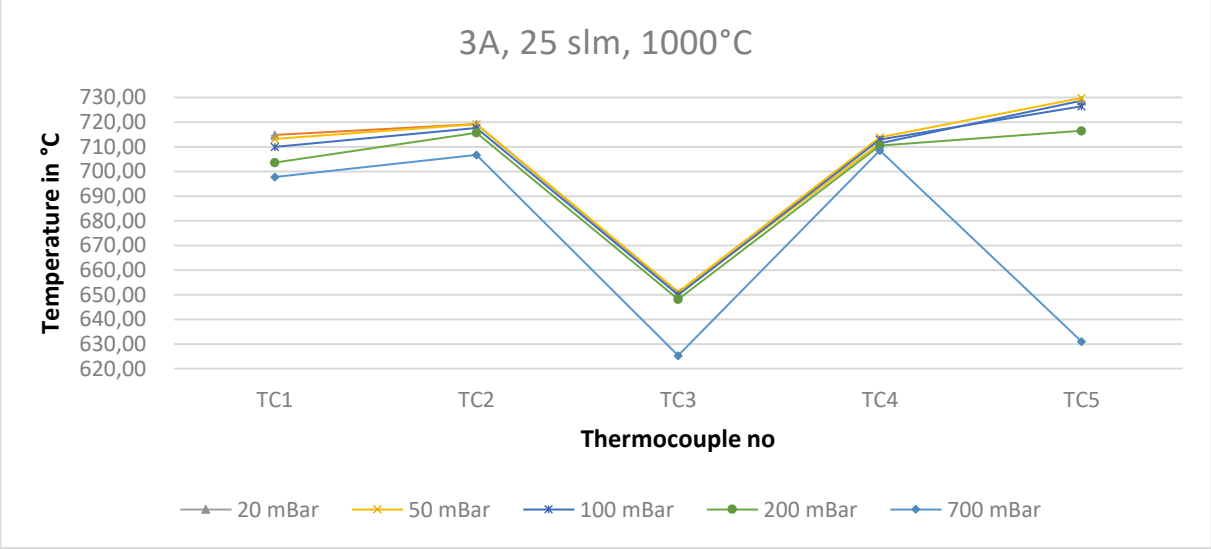

Figure 41 Position 3A with T over TC at 25 SLM and at a susceptor temperature of 1000°C.

4.3 Controllability of flow profile

To see how well controlled the flow profile is, two tests at position 3A at temperature 450°C and 1000°C under the conditions with 20 SLM and 100 mBar were conducted. See Figure 42 and Figure 43. The flow profile shows a good accuracy at TC1, TC2 and TC5 for both tests with a delta T less than 1.5 °C. TC3 and TC4 deviates and could not be set to the same temperatures as for the other thermocouples. With an adjustment of the input gas flow an effect of approximately 5 % could be seen in the temperature change which contributes to that the change in the injector response is smaller than the performed adjustment.

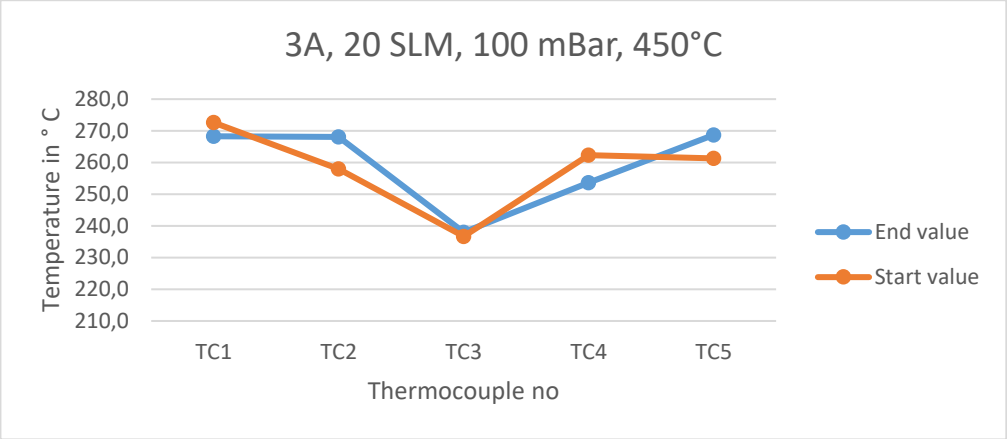

Figure 42 Flow profile experiment at position 3A with 20 SLM flow, background pressure of 100 mBar and at 450°C.

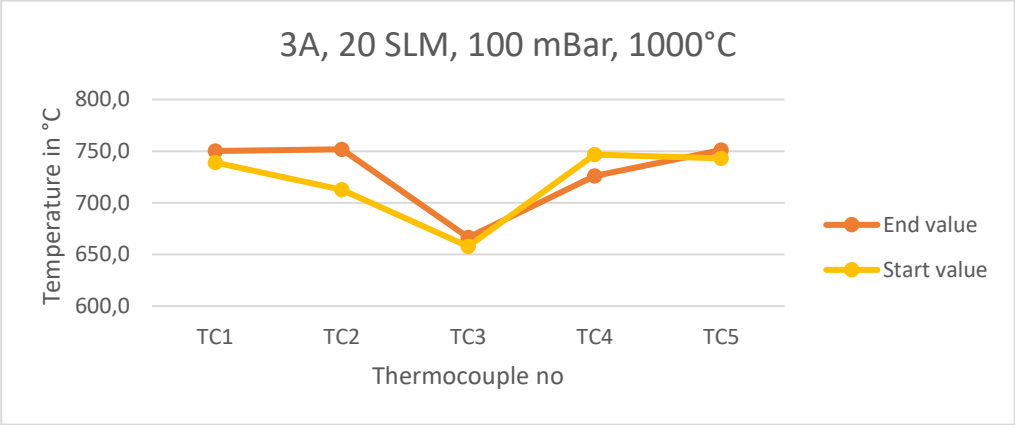

Figure 43 Flow profile experiment at position 3A with 20 SLM flow, background pressure of 100 mBar and at 1000°C.

4.4 Thermocouple temperature measurement verification

The thermocouples were tested to verify their accuracy as described in subsection 3.3 and the result of the measurement is seen in Table 1. The result indicates that the experienced temperature of the thermocouple is approximately 50 °C lower than the actual temperature of the susceptor. The thermocouples tested with the graphite thread have standard deviations according to Table 1 which are significantly lower than the standard deviations without the graphite thread in Table 2. Standard deviation, σ, is calculated according to Equation 22.

$$\sigma = \sqrt{\frac{\sum_{i=1}^{N}(x_i - \bar{x})^2}{N-1}} \qquad \text{Equation 22}$$

Where $\{x_1, x_2, \ldots, x_N\}$ are the temperatures measure by the thermocouples, $\bar{x}$ the mean temperature and N the number of data points which is equal to the number of thermocouples.

Susceptor T [°C]	TC1 [°C]	TC2 [°C]	TC3 [°C]	TC4 [°C]	TC5 [°C]	Mean T [°C]	Std. Dev. σ [°]
Ref. T [°C]	19.4	19.0	17.6	17.9	17.5	18.28	0.9
600	548	545	549	550	547	547.8	1.9
800	752	748	751	752	750	750.6	1.7
1000	944	939	943	942	942	942	1.9

Table 1 Thermocouple temperature measurement with graphite threads result.

The thermocouples tested *without* the graphite thread shows result in Table 2 Thermocouple temperature measurement with no graphite threads result.

Susceptor T [°C]	TC1 [°C]	TC2 [°C]	TC3 [°C]	TC4 [°C]	TC5 [°C]	Mean T [°C]	Std. Dev. σ [°]
Ref. T [°C]	17.9	17.7	18.1	19.0	17.2	17.98	0.7
450	406	408	409	393	391	401.4	8.7
600	553	557	557	534	542	548.6	10.2
800	755	751	757	732	731	745.2	12.7
1000	950	959	950	922	920	940.2	17.9

Table 2 Thermocouple temperature measurement with no graphite threads result.

4.5 Verification of Computational Fluid Dynamic simulations

The *Computational Fluid Dynamic*, CFD, simulations have been performed at Linköping University with a supercomputer. The simulations show a uniform distribution in consideration with the displayed temperature and velocity distributions in Figure 110 and Figure 111. The simulations predict a laminar flow with a flat profile and not a typical parabolic symmetry. Although it can be seen the velocity of the gas is decreased towards the walls compared with center temperature, a result of Blasius profile in Figure 8 and Equation 7. The simulations were performed with a total flow of ~ 13 SLM in the ammonia run lines and ~ 11 SLM in the precursor run line. The background pressure was set to 50 mBar and a target process temperature of 1100°C.

5 Discussion

5.1 Result of measurements

New limitations on the system have been found throughout the thesis during the measurements. Such limitations as at which specific background pressures and at which various gas flows are possible for the system. This has resulted in qualified data to be used for future use of the MOCVD system. See test schedule in Appendix C.

One of the found limitations on the system is the pump capacity of the vacuum chamber. When measuring at a constant background pressure of 20 mBar, it was found that the exhaust system could not pump enough at flows higher than 25 SLM to keep the constant pressure of 20 mBar. Therefore, a gas flow limitation at 20 mBar was set to 25 SLM. However, this does not raise a concern since the epitaxial growth usually takes place at around 50 mBar which do not have this system limitation.

When trying to inject gas flows higher than 40 SLM into the system, an additional limitation was found. The external gas piping system did not have high enough pressure to succeed a higher flow than 40 SLM which set a limitation of the maximum possible gas flow in the system. This independent of the background pressure. So, if flows higher than 40 SLM is to be used in the system, the pressure in the N_2 piping needs to be increased.

At a background pressure of 700 mBar it was demonstrated that the system could not sustain a stable gas flow for flows lower than 15 SLM which set a limitation of minimum injected gas flow at 700 mBar to 15 SLM. This does not either raise a concern since the system will not be performing growth at this high background pressure.

A temperature below 400°C was not possible to be used because of the pyrometers' limitations to read any value below 400°C. Therefore, a value of 450°C was chosen instead to give a margin of 12.5 % above the lowest detectable temperature which has showed to be successful. The hot-wall MOCVD system has been tested at two different temperatures; the 450°C measurements to mitigate the heating effect on the thermocouples from the heated walls and at 1000°C to simulate a conventional hot-wall MOCVD growth temperature. The most relevant temperature range was to measure the gas behavior inside the growth window which accordingly to REF (Chen, et al., 2013) is between 980°C to 1080°C for GaN-on-SiC since the system will not perform growth outside this temperature range. Limitations on the N type thermocouples set the maximum measure temperature to 1000°C which is inside of the growth window. Together with the CFD simulations performed on the hot-wall MOCVD system it can be demonstrated that a laminar flow within the liner and deposition area is to be expected when performing growth.

In Figure 28 and Figure 30 the temperature is plotted at the different flows over the thermocouples for 1000°C and at 50 respectively 100 mBar background pressure. The trendlines in the figures for the thermocouples indicate a linear behavior up to 25 SLM with a mean gas velocity of 1.21 cm/s. For TC1 and TC5 the trendlines are linear throughout the experiment, but for TC2 and TC4 their x^2 terms start to dominate at the higher flows. This could be indications of their specific heat and how fast they dissipate the heat. Since the gas velocity increases with the increased flow it could be that the gas is not heated fast enough to transport

the heat which would result in colder gas in the center. The specific heat is though increasing with increased temperature for a gas, but as described the gas velocity could be increasing even faster than it can conduct the heat which would result in the obtained diagrams throughout the result section.

In Figure 29 a weak non-linearity can be seen, and the data shows that the gas is equally cooled for every constant increase of the gas flow. TC2 and TC4 have the same trend but with slightly increased amplification with increased flow. The data therefore indicates a higher gas flow is present at TC2 and TC4, but they are decreasing less in a more rapid way and becomes more like TC1 and TC5. If there would have been secondary effects such as warmer gas at lower flows the cooling of the gas would not have been increased with lower flows. Aside from TC3, the temperature profile is planar at lower flows and a parabolic profile that appears. This is in accordance with developing laminar flows. The data for TC3 shows minimal decreasing of delta T for increasing flows which is an interesting behavior. The highest flow in the liner should be located in the center, but this is not what the data shows. Therefore, it can be concluded no cold finger is present in the center since the temperature reduction would have been larger in that case. It is more likely an effect of the temperature heating in the other parts of the liner which then increase in gas velocity and therefore TC5 receives a relative lower velocity.

Comparing this reasoning with the same position at 3A at 450°C and at 2B in Figure 32 and Figure 25 respectively the data indicates the thermocouples are cooled down at higher temperatures. This gives rise to a smaller temperature decrease at higher flows. In Figure 25 it is clearly seen that the temperature of TC2 and TC4 are so cooled down that there is no difference in temperature when increasing the flow from 35 to 40 SLM. This phenomenon is then a possibility of that the gas is more or less warm. In Figure 27, the same appearance of the profile is seen which is most likely attributed to that the gas is to warm and cannot cool enough.

An extra stagnant layer can be seen at TC1 and TC5 in Figure 25 where a lower flow is present. Along the walls the gas is accelerated because of the heated walls, but in the center of the profile it is seen that the gas is not expanding at the same pace since it is cold, and a lower gas velocity is seen. In a perfect world there would not be any quadratic term in the equation, and it would be linear, but since the highly heated gas it will be acting as a result of a non-linear behavior.

The obtained results in the 3D diagrams will give indications whether a laminar flow has been established or not. It will also demonstrate under which conditions this result is valid for.

At alternating pressures, the heat radiation from the walls to the thermocouples will be unchanged but for increasing pressures the thermal conductivity will increase within the gas. This since the density is increasing and there are more molecules in the same volume to transport the heat to the center from the walls in this case. Therefore, a lower temperature measured at the thermocouple will be the result of decreasing the pressure since the heat conduction is affected, but not the heat radiation. The reason why a lower temperature is measured for higher pressures which are demonstrated throughout section 4 is due to the gas velocity has increased to be more dominating over the heat conduction of the gas. With increasing background pressures and high temperatures, the measured temperatures at the thermocouples are decreased compared than for higher pressures, consistent with results at

position 1B, 15 SLM, 1000°C in Figure 80. In section 4.2.2 the phenomenon is unambiguously demonstrated at position 2A at 15 and 35 SLM, 450°C, Figure 83 and Figure 85, and at 1000°C at 15, 25 and 35 SLM in Figure 86, Figure 87 and Figure 88. This reasoning is valid for all the measurements with alternating background pressures. The same phenomenon is also exhibited at higher flows. This is e.g. clearly seen in for position 3A with condition 450°C and 1000°C Figure 70, Figure 71, Figure 72, Figure 73, Figure 74, Figure 75, Figure 33 in section 4.1.5 where a coherent decreased temperature is demonstrated for TC1 to TC5.

A more unstable temperature reading is attributed to conditions with high flows and high background pressures. It appears to be increased fluctuations within the temperature readings with increased gas flow and background pressure. But, at the tests with low pressures, such as conventional growth conditions of 50 mBar up to 40 SLM, the fluctuations are not present even though the gas flow is increased within the system limitations mentioned above.

These fluctuations indicate that a turbulent flow could be developing or presence of buoyancy effect. Since the turbulent flow does not appear immediately after the laminar flow has reached its limitations, this described behavior suggests that the gas flow is moving into the turbulent flow regime which is investigated in e.g. Figure 45 in a condition of 450°C at 700 mBar with flows higher than 25 SLM. It is consistent with the temperature fluctuations on TC2 and TC5. The buoyancy effect is more strongly present at higher temperatures and pressures.

The specific signs of turbulence or buoyancy are then the fluctuations in the temperature measurements when the thermocouple does not reach any stable value and also when the temperature reduction for higher flows becomes non-linear as demonstrated in Figure 28 and Figure 30. These fluctuations are for one specific thermocouple and can be seen when reading the value of the thermocouple. In some of the graphs a certain thermocouple shows higher or lower temperature compared to the others which deviates from their pattern. This by itself is a sign of turbulence behavior. It can also be seen when the thermocouples for e.g. position TC2 and TC4 show higher temperature than their neighboring thermocouples, TC1, TC3 and TC5. That is also an indication on turbulent behavior since it is a sign for higher flows along the walls and the center or intermixing gas velocities.

If a laminar flow is obtained at position 3A there must also be laminar flow at the earlier positions, such as 2A and 1A, if 1A had been in the scope of measurements. The positions measured at were carefully determined in consideration of the gas behavior in the liner and at which positions it is of great importance to know the gas behavior. Position 1B was studied because of its strategic location of the lower half of the liner height. This region is of higher importance due to it being closer to the liner bottom which in its turn is closer to the substrate surface. No measurements were conducted at position 1A due to the risk of a too weak gas flow to detect temperature differences in.

The gas flow needs to be sufficiently high to perturb the gas in the vicinity of the thermocouples. This perturbation will either result in a higher or lower measured temperature at the thermocouple. Since the thermocouples will act as black bodies there will be a radiating heat from the thermocouple to the gas, a heat absorption of the gas to the thermocouple and a heat radiation from the liner walls to the thermocouple. If the measurements had been carried out in absolute vacuum, the radiation effect had not had any impact on the measured temperature.

In Appendix H in Figure 70 Position 3A at 20 mBar background pressure and at a susceptor temperature of 450°C., Figure 71 Position 3A at 50 mBar background pressure and at a susceptor temperature of 450°C. and Figure 72 Position 3A at 700 mBar background pressure and at a susceptor temperature of 450°C. the data indicate a laminar flow up to 20 SLM regardless of background pressure condition, except for 700 mBar where the data indicate a laminar flow at 35 and 40 SLM. Further investigation of the results at the conventional growth condition of 50 mBar strongly indicates a laminar flow profile up to a gas flow of 35 SLM. With a decreasing background pressure to 20 mBar, the data suggests a laminar flow profile up to at least 25 SLM. At 100 mBar the data indicates a laminar flow within the range of 30 SLM.

This data is consistent with the measurements conducted at position 2A in identical conditions in Appendix H in Figure 50 Position 2A at 20 mBar background pressure and at a susceptor temperature of 450°C., Figure 51 Position 2A at 50 mBar background pressure and at a susceptor temperature of 450°C. and Figure 52 Position 2A at 700 mBar background pressure and at a susceptor temperature of 450°C. In position 2A the data indicates a laminar flow at 20 mBar up to 25 SLM which is entirely consistent with position 3A. At 50 mBar, position 2A, the data indicates a slightly lower gas flow of 20 SLM to obtain a laminar gas flow profile. It shall though be noticed that a turbulent flow at position 2A within 20 to 35 SLM cannot be present since the flow is strongly indicated in the data to be laminar up to 35 SLM at position 3A, 50 mBar.

Due the data indicates laminar flow in position 3A it leads to that the limitations of the conditions are consecutive determined for position 1A (theoretical position) and 2A in position 3A.

In Appendix H in Figure 73 Position 3A at 20 mBar background pressure and at a susceptor temperature of 1000°C., Figure 74 Position 3A at 50 mBar background pressure and at a susceptor temperature of 1000°C., and Figure 75 Position 3A at 700 mBar background pressure and at a susceptor temperature of 1000°C. the data indicates a laminar flow up to 25 SLM regardless of background pressure, except for 700 mBar indicating turbulent flow already at 15 SLM. At 20 and 200 mBar the laminar flow limit is, according to the data, estimated to be even higher and reaching a value of 35 SLM.

In Appendix H in Figure 53 Position 2A at 20 mBar background pressure and at a susceptor temperature of 1000°C., Figure 54 Position 2A at 50 mBar background pressure and at a susceptor temperature of 1000°C. and Figure 55 Position 2A at 700 mBar background pressure and at a susceptor temperature of 1000°C. the laminar flow limit is indicated to be at least 25 SLM regardless of background pressure and at 100 mBar at 30 SLM. This data in consideration with the data of position 3A under same conditions gives strong indications of laminar flow.

The thermocouples have been tested to ensure the accuracy of the recorded value which was described in section 4.4. The result of the temperature verification indicates that a minimal misalignment of the thermocouples, although to measure at the same position, could result in more than 20°C spread in the same measurement. The standard deviation for the thermocouples which were not forced together by the graphite thread at test condition 1000°C was more than nine times the standard deviation for the same experiment condition, compared to measurements with the graphite thread. Since the measurement was conducted

in the interface of the liner and susceptor, the gas should according to the simulations be well mixed and its fully developed profile should be present.

A case which also is suggested to be the reality is described as following. The depression at TC3 is deeper at 1000°C compared to 450°C under the same conditions in (varied flow) position 3A. With the temperature being increased from 450°C to 1000°C, the volume of the gas under constant pressure and gas flow is more than two times larger according to Equation 3. The gas viscosity is also increasing with increased temperature according to Equation 1. The two equations together result in that the viscosity of the gas increases and the gas density decreases. This leading to that a higher velocity of the gas is possible and this could be the case for the gas along the walls, ceiling and bottom of the liner. Therefore, it could be that the gas is colder in the center. This together with that heat transfer in the gas is conducted by convection is a result of a slower convection course because of lower density and higher gas velocity, hence a colder finger will be the result of a qualitative laminar flow. In Figure 34, Figure 35, Figure 36 and Figure 37 it can be seen that the temperature is measured to be constant up to 100 to 200 mBar depending on heating temperature and flow. This shows that for the Re number the background pressure does not affect the measured temperature since the gas velocity will account for this and even out Reynold's number. This shows that it is possible that the specific heat is increasing, and the gas is fully heated leaving no cold finger. Therefore, the measured temperature is not dependent of the background pressure since the process is in a good equilibrium and managing to heat the entire gas. With higher pressures the density will increase and the heat convection as well resulting in this constant trendline.

The Reynold's number in Equation 1 and the characteristic linear dimension in Equation 2 gives a hint on the gas behavior since up to a limit of 2300 it is suggested that a laminar flow is indicated and at > 2300 a turbulent flow is indicated to be developed. Reynold's number is calculated for a rectangular geometry (0.3 x 0.023 m), the kinematic viscosity for N_2 at 651°C is $108.03*10^{-6}$ m^2/s (Engineering ToolBox, 2018), cross-sectional area 0.0069 m^2, gas velocity of N_2 at 651°C is 4.84 m/s according to Equation 25 and the circumference as 0.646 m in Equation 23.

$$Re = \frac{uL}{\nu} = \frac{ud_h}{\nu} = \frac{u}{\nu}\frac{4A}{O} = \frac{3.84*4*0.0069}{108.03*10^{-6}(0.3*2+0.023*2)} \approx 2412.19 > 2300 \qquad \text{Equation 23}$$

From the result of 2412.19 > 2300 it indicates a transit to turbulent flow, but from Figure 74 in Appendix H the result of the data indicates a laminar flow. An important note to make is that the velocity is the driving parameter for this Reynold's value and the kinematic viscosity which is strongly driven by the temperature. A decreased temperature would increase Reynold's number flow since it would give a lower viscosity, but the gas velocity would decrease which as well is the driving parameter for the Reynold's number since a decrease in the temperature would give a larger change of Re than for the viscosity. So, too minimize the Reynold's number, the temperature should be decreased to obtain a laminar flow according to Reynold's number. Therefore, the experiments at high temperatures will reach a turbulent flow more rapidly than at the flows with lower temperatures. Although it is seen for the experiments at 1000°C that they can obtain laminar flow at higher flow rates and background pressures.

Calculating the Reynold's number for the same position 3A at 700 mBar, 1000°C and gas flow of 15 SLM, in Appendix H Figure 75, results in a much lower Reynold's number. The kinematic viscosity for N_2 at 667.8°C is $111.5*10^{-6}$ m^2/s (Engineering ToolBox, 2018) and the gas velocity is calculated to 0.573 m/s. See Equation 24.

$$Re = \frac{u}{\nu}\frac{4A}{O} = \frac{0.573*4*0.0069}{111.5*10^{-6}(0.3*2+0.023*2)} \approx 219.56 \ll 2300 \qquad \text{Equation 24}$$

The Reynold's number is much lower than the limit for laminar flow which should be a good and strong indication on laminar flow. Although it indicates laminar flow, it can be seen in the same figure, Appendix H in Figure 75, that according to the relative temperatures there are indications on a turbulent behavior of the gas at this elevated background pressure. Since the gas velocity is calculated to be much lower at this high background pressure it results in a low Reynold's number. When the viscosity increases, that will say that the temperature is increased, and the pressure is increased it results in decreasing the velocity. The decreased velocity with the increased viscosity is the resulting in a lower Reynold's number. It also shows that it is possible to obtain a very low Reynold's number at high pressures even though the flow is turbulent.

The two equations, Equation 23 and Equation 24, then both indicates that a laminar or turbulent flow can be obtained even though Reynold's number is above 2300 and below 2300. This means that Reynold's number is not limiting the transition from laminar to turbulent behavior, which means there must be something more that is a source of this transition. Important to notice is that the Reynold's number is also strongly dependent on the geometry which means that a small Reynold's number on a rough surface would still result in vortexes and therefore a turbulent flow would arise.

In the second case when the Reynold's number is very small even though the flow is clearly turbulent, it is due to the high pressure which will produce a low Reynold's number since the gas velocity is clearly decreased.

Another possible reason could have been physical perturbations on the top, bottom or wall surfaces in terms of gaps between the graphite pieces or uneven surfaces. This is though not the case since these surfaces are extremely smooth. It shall be noticed that the indications of turbulent behavior are not concluded to be simply turbulent behavior, but it could also be sign of buoyancy effect resulting in perturbed temperature readings and unstable flows. The buoyancy effect would result in heat waves perturbing the gas flow in such way it could create local heating of the gas which would be the result of a complex pattern.

In summary, the low Reynold's number of 219.56 is indicated to be a result of a high background pressure resulting in decreased gas velocity.

5.2 Stabilization time

Different stabilization times for the measurements with the thermocouples have been ranging from five to ten mins which could have an effect in the tolerance of the recorded process value. At some values the thermocouples experienced temperature fluctuations which did not stabilize over time. At those values, a mean value was calculated when the fluctuations were as mitigated as possible. This value could then be a few degrees offset which could be enough to conclude the incorrect flow type. This has though only been a problem in the extreme cases of background pressures at 700 mBar and high flows which is not of highest importance for the thesis purpose.

5.3 Thermocouples

At initial state different measurement techniques were investigated. These were using an IR camera with an optical fiber to extract the data about the temperature distribution inside the liner. This would have been the fastest method to use since this would have projected a visualization of the temperature distribution on the liner as a result of the colder gas injected. This could have been a good method, but since the cable to IR camera which were investigated could not be installed in such way that a vacuum could be obtained in the reactor. This method was excluded. This was not the only reason, but this fiber equipment could not be located, and it would have resulted in a regular IR camera without the fiber. That would not have been an optimal solution to the problem.

Instead of using thermocouples, the experiment could have been designed without these measurements and tuning the growth with performing test-growths on substrates. By analyzing the growth profile of the epitaxial layer, suggestions to adjustments could have been extracted from the data. This would though not have been feasible at this point of time because of the reactor needs to be tuned with additional measurements to even use the precursors as process gas and not only N_2. The advantages would have been a fast result and easily foreseeable data since just by using OM or the naked eye, the growth profile could have been seen. With additional characterization methods such as XRD, the composition profile of the epiwafer could have been extracted from the data and visualized. The susceptor could also have been inspected to see how the deposition profile looks like since the entire susceptor bottom and wafer is deposited in a growth run.

Using a pitot tube to measure the gas velocity was also a possible measurement technique in the discussion phase. Then the gas velocity would have been extracted immediately and a gas flow velocity profile could have been created instead of using relative temperature measurement such as thermocouples. The problem once again came down to the pitot tube since this tube was too thick to fit in the already manufactured vacuum flange lock where the thermocouples were inserted into the reactor. A thinner tube was not found after a qualitative study and the idea was excluded.

The thermocouple measurement technique was then deeper examined. It was found that the thermocouples were cost-effective and easily read since the accompanied software gave a good overview of the data during the measurements and it was easy to extract the data into Excel after conducted measurements. They were suitable for the vacuum flange and could be used (the N type) at desired temperatures of maximum 1000 °C. If the thermocouples would have been placed in another type of arrangement that ensures they are not misaligned. Since this type of measurements have not been carried out before in this scale, this thesis is the first

published paper on this subject. Among the references found, this type of temperature measurement with thermocouples are of course well-known. But, by conducting this experiment with five thermocouples creating a temperature distribution map it is one of its kind.

Using solely five thermocouples has indicated the limit of collecting enough data in some cases when the data have been difficult to interpret. Increasing the number of thermocouples used in the measurements would lead to less blank spaces in between the five data points recorded in this thesis. Even though the five thermocouples have shown to be enough in the conclusions it would have improved the certainty and accuracy of the result even more.

Using thermocouples as measurement method has been shown to be a qualitative approach on this problem. It demonstrates good accuracy and the result shows statistical behavior in the variating flows, heating temperatures and background pressures. By later presenting the data in 3D flow charts let the data be more easily interpreted and understood. It has also shown to be the only method where a solution regarding the graphite's need for vacuum at high temperatures was found.

Studies regarding measuring the temperature distribution in a MOCVD has in REF (Tsai, et al., 2014) been performed with thermocouples. The measurements have then been compared to CFD simulations which are in accordance in the paper. The thermocouple consisting of two thermoelements is a well-known method for industrial thermal measurements and distribution maps.

5.4 Comparison with CFD simulations

What can be seen throughout the data is a depression for TC3 at position 2B, 2C and 3A at varied background pressures, see figures in section 4.2.3, 4.2.4 and 4.2.5. It can also be seen in the data for section 4.1.3, 4.1.4 and 4.1.5 at position 2B, 2C and 3A. This is in accordance with the CFD simulations which simulate a planar profile at process gases. Since this depression is present in most of the measurements at different conditions, the data suggests that a cold finger is present in the gas flow profile which indicates a laminar flow.

The velocity profile in Appendix H in Figure 111 shows that the gas composition should experience a velocity of about 4 to 5 m/s in the downstream liner in the vicinity of the susceptor. According to the calculations made in Equation 21 at the same background pressure of 50 mBar, gas flow of 25 SLM, setpoint temperature of 1000°C and the measured temperature at position TC3, 3A in Appendix H in Figure 74 and Figure 107 at 651°C. This resulted in a roughly estimated velocity seen in Equation 25.

$$w_2 = (A_1 w_1)(\rho_1/\rho_2)(1/A_2) = 0.00042 * \left(20 * \frac{651+273}{20+273}\right) * \left(\frac{1}{0.0069}\right) \approx 4.84 \frac{m}{s} \quad \text{Equation 25}$$

This calculated value is based on that the N_2 is injected at initial pressure of 1 Bar and initial temperature of 20 °C. Compared to the CFD simulations which are based on a gas flow around 24 SLM and at a gas composition containing the process gas mixture. The calculated gas velocity in Equation 25 is not a function of the position which will also result in a rough estimation. The calculated velocity is though calculated to be in the expected interval of 4 to 5 m/s which is a good indication of similarity between the experiment and the simulations. A lower pressure in the liner would result in even higher gas velocity or at decreased temperature. What can be seen is that the calculated velocity from the measurement result is close to the simulated velocity. The gas is in fact simulated with a higher temperature at the same position which also would contribute to a lower velocity. The summary is that the simulated and the measured velocity is similar.

In Equation 23 and Equation 24 the Reynold's number is calculated to 2412.19 respectively 219.56 for N_2 which together with the Blasius profile in the latter case indicates two laminar flows in the series of experiments. The Reynold's number calculated for the case of Equation 23 which contains almost the same gas flow (25 SLM) as the CFD simulations (24 SLM), but now with hydrogen instead. The kinematic viscosity for H_2 at 651 °C and 50 mBar is given by table values from (Engineering ToolBox, 2018) in Equation 26 and the Reynold's number is calculated in Equation 27.

$$\frac{1}{\nu} = \frac{\rho}{\mu} \Leftrightarrow \nu = \frac{\mu}{\rho} = \frac{19*10^{-6}}{0.0263*5*10^{-2}} = 0.01445\,\frac{m^2}{s} \qquad \text{Equation 26}$$

$$Re = \frac{u}{\nu}\frac{4A}{O} = \frac{4.84*4*0.0069}{0.01445*(0.3*2+0.023*2)} \approx 14.3 \qquad \text{Equation 27}$$

Since the viscosity is increased for the hydrogen with a factor of hundred it results in a much lower Reynold's number. This indicates that a higher composition of the H_2 in the gas mixture would result in a lower Reynold's number indicating laminar flow. In summary, a lower Reynold's number would be calculated if the similar gas mixture was used in the experimental measurements as already used in the CFD simulations.

The reason why a turbulent behavior of the gas is experienced could also be as a result from the CFD simulations where the design of the injector is changed throughout the simulations since a turbulent behavior is seen when the gap between the wedge (triangular shaped piece in each injector outlet) and the injector outlet walls where each tapered wedge are placed. It was seen in the simulations that a narrower gap would result in higher output pressure of the gas and higher velocity which would result in turbulence and creating a vortex outside of the injector perturbing the gas flow profile. When this gap was increased it could be seen that the vortexes were not present anymore which resulted in a laminar flow all the way. If this is the reason which needs further investigation, it is a possibility that the gap might be to narrow and the gap between the tapered wedge and the wall need adjustments. If a high Reynold's number would be present already at the injector outlet it would result in a turbulent flow all along the liner and susceptor.

6 Conclusions

The conclusions will put answers to the initial questions in section 1.3 Problem formulation which reflect the purpose of the thesis.

- To what degree can a laminar gas flow profile be obtained in the hot-wall MOCVD system?

Conclusively, strong indications regarding the laminar gas flow profile is supported and extracted from the data within the thermocouple measurements.

At 1000 °C a laminar flow is strongly indicated to be obtained at position 3A, closest to the growth area, within the range of 25 SLM regardless of background pressure, except for 700 mBar indicating turbulent flow for 15 SLM and up if not would be a result of the buoyancy effect which would need further examination. At 20 and 200 mBar the laminar flow limit is, according to data, estimated to be even higher and reaching a value of 35 SLM.

At 450 °C the data indicate a laminar flow up to 20 SLM at position 3A regardless of background pressure condition, except for 700 mBar where the data indicate a laminar flow at 35 and 40 SLM. 50 mBar strongly indicates a laminar flow profile up to a gas flow of 35 SLM. With a decreasing background pressure to 20 mBar, the data suggests a laminar flow profile up to at least 25 SLM. At 100 mBar the data indicates a laminar flow within the range of 30 SLM.

- To what degree is the gas flow profile in accordance with the computational fluid dynamics simulations?

The increased Reynold's number in the experimental measurements compared to the CFD simulations is indicated to be a result of that only N_2 is used which is not the case in an actual growth run, increased gas velocity in the center which is a result of increased temperature along the liner resulting in lower gas density.

The measured velocity according to the calculations made are in the expected gas velocity interval according to the CFD which indicates that the measured result is what to expect.

Further investigations also need to be performed for the injector outlet if the gap between the tapered wedge and the wedge wall needs to be thicker to rule out that the Reynold's number is increased in the experiment compared to the CFD simulations.

- What system limitations have been discovered and concluded?

New limitations on the system have been found throughout the thesis during the measurements. Such limitations as at which specific background pressures and at which various gas flows are possible for the system. This has resulted in qualified data for future use of the MOCVD system.

One of the found limitations on the system is the pump capacity of the vacuum chamber. At a constant background pressure of 20 mBar, it was found that the exhaust system could not pump enough at flows higher than 25 SLM to keep the constant pressure of 20 mBar. The maximum gas flow limitation at 20 mBar was concluded to 25 SLM.

When trying to inject gas flows higher than 40 SLM into the system, an additional limitation was found. The external gas piping system did not have high enough pressure to succeed a higher flow than 40 SLM which set a limitation of the maximum possible gas flow in the system. This independent of the background pressure.

At a background pressure of 700 mBar it was demonstrated that the system could not sustain a stable gas flow for flows lower than 15 SLM which set a limitation of minimum injected gas flow at 700 mBar to 15 SLM.

A temperature below 400°C was not possible to be used because of the pyrometers' limitations to read any value below 400°C.

- To what degree can the laminar velocity profile be controlled i.e. can a concave velocity profile be obtained?

A laminar velocity profile is clearly obtained which looks exactly as what was expected from the pre-studies and the measurements of the newly built hot-wall MOCVD reactor system. A concave velocity profile with a parabolic symmetry was obtained under certain conditions and it was also shown that with adjusted flows in the injector, a fully concave profile can be performed. Concluded was also that the measurements should have been performed with no external heating of the liner and susceptor from the beginning to eliminate the effect of secondary effects or heating perturbations such as buoyancy effect and such.

It is also concluded that a cold finger is not present even though some data indicates a depression for TC3 in the 3D graphs, but it is more likely attributed to that the gas is heated up, so it is not cooling of the thermocouples even though the flow is increased which instead would have created a cold finger.

A buoyancy effect is also thought to be present at high temperatures and higher pressures which would result in fluctuations of the temperature measurements. The fluctuations were at the initial investigation attributed to turbulence but has more or less been concluded to be a result of the buoyancy effect.

7 Future work

Next step from this thesis would be to inject the precursors and the process gases to be used in the growth and do a test growth. The growth profile on the wafer would reveal if a laminar flow is obtained or not and act as an additional motivator of the data result. This profile could be analyzed with optical microscopy which is a non-destructive characterization method of an epiwafer to extract information about the surface morphology.

The grown epiwafer could then be investigated by suitable characterization methods such as *X-ray Diffraction* among others to extract the composition and quality. Another method to extract the composition of the surface layers is *Time-of-Flight Secondary Ion Mass Spectrometry.*

As already described in the discussion regarding the number of thermocouples used in the measurements. A suggestion was to use more thermocouples and find a more effective and accurate way of fixing the thermocouples during the measurements so the possibility of misalignment with the thermocouples is eliminated. This is something that is suggested to be investigated before proceeding to the growth process optimization in a new hot-wall MOCVD system. Repeating the measurements with no heating at room temperature would also be of great interest since this would result in an elimination of radiative heat, change of gas viscosity and the gas density which resulted in cold fingers. The measurements should start at room temperature and then slowly increasing the temperature to see the changes in the profile. If a laminar would be obtained with no heating, it should not change when heating to process temperature. This at a constant gas flow and background pressure. This could have resulted in easier interpretations of the data which would have given a more certain answer to the problem formulation.

An analyzation and optimization of the gas composition will also be of interest to extract information about the intermixing of the organometals and the hydride gases. This could be conducted by a series of experiment with mass spectrometry by inserting the probe into the gas flow in different locations to analyze the uniformity of the composition.

A suggested method to be used instead of thermocouples in the thesis was to use thermal imaging which would measure the temperature profile at the bottom of the liner to see how the gas cools the walls. In this way to extract the gas flow profile and directly see if a laminar flow is obtained or not. This would result in indirect measurements since the gas temperature is not measured, but the liner bottom temperature is the measured.

This infrared camera could have been a more convenient measurement method since it easier could have displayed the profile at all positions inside the liner and not only in the pre-drilled holes of the liner. The problem to be solved before using an IR camera with a fiber extension would have been to maneuver the fiber camera in a non-visual system. Since the graphite cannot be heated to too high temperatures in Oxygen rich environments because of oxidation of the carbon in the graphite, it would need to be a closed system to mitigated Oxygen impurities.

8 References

© 1996-2018 HORIBA, L. A. r. r., 2018. *What is a Mass Flow Controller?.* [Online] Available at: http://www.horiba.com/what-is-a-mass-flow-controller/ [Accessed 03 10 2018].

Amano, H., Sawaki, N., Akasaki, I. & Toyoda, Y., 1986. Metalorganic vapor phase epitaxial growth. *Applied Physics Letter,* 48(353).

Chen, D. J.-T., 2015. *MOCVD growth of GaN-based high electron mobility transistor structures.* Dissertation No. 1662 ed. Linköping: Linköping Studies in Science and Technology.

Chen, J.-T., Forsberg, U. & Janzén, E., 2013. Impact of residual carbon on two-dimensional electron gas properties in AlxGa1-xN/GaN heterostructure. *Applied Physics Letter,* 102(193506).

Csanyi, E., 2017. *Electrical engineering Portal - Resistive heating explained in details.* [Online] Available at: https://electrical-engineering-portal.com/resistive-heating-explained-in-details [Accessed 22 01 2019].

Engineering ToolBox, 2018. *Nitrogen - Dynamic and Kinematic Viscosity..* [Online] Available at: https://www.engineeringtoolbox.com/nitrogen-N2-dynamic-kinematic-viscosity-temperature-pressure-d_2067.html [Accessed 24 01 2019].

Grand View Research, Inc, 2017. *Gallium Nitride (GaN) Semiconductor Devices Market Analysis By Product (GaN Radio Frequency Devices, Opto-semiconductors, Power Semiconductors), By Wafer Size, By Application, By Region, And Segment Forecasts, 2018 - 2025.* [Online] Available at: https://www.grandviewresearch.com/industry-analysis/gan-gallium-nitride-semiconductor-devices-market [Accessed 03 01 2019].

Hitchman, A. C. J. a. M. L., 2009. Overview of Chemical Vapour Deposition. In: w. Royal Society of Chemistry, ed. *Chemical Vapour Deposition: Precursors, Processes and Applications.* Liverpool, Glasgow: Royal Society of Chemistry, pp. 1-36.

INOR Process AB, 2014. *Temperaturskolan.* [Online] Available at: https://www.krohne-inor.se/temperaturskolan/teori-termoelement/#1530615840995-621280b2-6403 [Accessed 03 01 2019].

J. M. Redwing, M. A. T. J. S. F. S. E. M. A. R. S. N. a. W. C. M., 1996. Two-dimensional electron gas properties of AlGaN/GaN heterostructures grown on 6H– SiC and sapphire substrates. *Applied Physics Letter,* 69(963).

Kordina, O., 1994. *Growth and Characterization of Silicon Carbide Power Device Material.* Dissertations No. 352 ed. Linköping: Linköping Studies in Science and Technology.

Lee, G., 2016. *EDN Network, Thermocouples: Basic principles and design essentials.* [Online] Available at: https://www.edn.com/design/test-and-measurement/4442672/Thermocouples--Basic-principles-and-design-essentials
[Accessed 14 09 2018].

M. Asif Khan, J. N. K. J. M. V. H. N. P. a. J. C., 1992. Observation of a two-dimensional electron gas in low pressure metalorganic chemical vapor deposited GaN-AlxGa1−xN heterojunctions. *Applied Physics Letter,* 60(3027).

Nationalencyklopedin, 2018. *Pitotrör.* [Online] Available at: https://www.ne.se/uppslagsverk/encyklopedi/lång/pitotrör
[Accessed 18 10 2018].

Nordtec Instrument AB, 2018. *Anslutningsslang.* [Online] Available at: https://www.nordtec.se/tillbehor/anslutningsslang-0
[Accessed 18 10 2018].

Nordtec Instrument AB, 2018. *Pitotrör.* [Online] Available at: https://www.nordtec.se/givare/pitotror-4
[Accessed 18 10 2018].

R. Nave, Georgia State University, 2016. *HyperPhysics: Kinetic Temperature.* [Online] Available at: http://hyperphysics.phy-astr.gsu.edu/hbase/Kinetic/kintem.html
[Accessed 20 09 2018].

Scervini, D. M., 2009. *Thermoelectric materials for thermocouples at University of Cambridge MSM.* [Online] Available at: https://www.msm.cam.ac.uk/utc/thermocouple/pages/ThermocouplesOperatingPrinciples.html
[Accessed 13 09 2018].

Storck, K. et al., 2016. *Formelsamling i termo- och fluiddynamik.* LiTH-IKP-S-508 ed. Linköping: Institutionen för ekonomisk och industriell utveckling på Tekniska högskolan vid Linköpings universitet.

SweGaN™, 2018. *SweGaN - Aspiring for perfection.* [Online] Available at: https://swegan.se/
[Accessed 20 09 2018].

Tsai, M.-L., Fang, C.-C. & Lee, L.-Y., 2014. Numerical simulation of the temperature distribution in a planetary MOCVD reactor. *Chemical Engineering and Processing: Process Intensification,* Volume 81, pp. 48-58.

U.S. Secretary of Commerce on behalf of the United States of America, 1995/2018. *NIST ITS-90 Thermocouple Database.* [Online] Available at: https://srdata.nist.gov/its90/main/
[Accessed 13 09 2018].

Vincent Summers, Sciencing, 2018. *How to Calculate Velocity From Temperature.* [Online] Available at: https://sciencing.com/calculate-velocity-temperature-6234001.html [Accessed 20 09 2018].

World Semiconductor Trade Statistics, 2018. *WSTS Semiconductor Market Forecast Spring 2018.* [Online] Available at: https://www.wsts.org/esraCMS/extension/media/f/WST/3540/WSTS_nr-2018_05.pdf [Accessed 3 01 2019].

9 Appendices

9.1 Appendix A

Appendix A contains information regarding the MFC of brand Horiba and model number with specification SEC-N124 MGMR-07 N2 10SLM 4CR. See attached pdf-file *HORIBASTEC MFC SEC-N124MGM N100 series*.

9.2 Appendix B

Appendix B contains information regarding the differential pressure gauge of brand VELOCICALC® Plus model 8360. See attached pdf-file *Velocicalc 8360*.

9.3 Appendix C

Appendix C contains the test schedule with the five thermoelements of type N. See attached pdf-file *Test schedule v4.*

9.4 Appendix D

Appendix D contains data sheet regarding the thermoelements of type N. See attached pdf-file *Katalogblad_Toleranser_termoelement_SV.pdf*.

9.5 Appendix E

Appendix E contains data sheet regarding the thermoelements of type N. See attached pdf-file *Katalogblad_Temperaturtabeller_termoelement_SV.pdf*.

9.6 Appendix F

Appendix F contains the raw data of the temperature measurements. See attached pdf-file *Graphs changed pressure and flow v6.pdf*.

9.7 Appendix G

Appendix G contains tables of the thesis.

Total flow [SLM]	**RL1 [SLM]**	**RL2 [SLM]**
5	2.73	2.27
10	5.45	4.55

15	8.18	6.82
20	10.90	9.10
25	13.64	11.36
30	16.36	13.64
35	19.10	15.90
40	21.82	18.18
45	24.55	20.45
50	27.73	22.27

Table 3 Total flow rate over run line 1 and run line 2.

9.8 Appendix H

Appendix H contains graphs from the thesis.

9.8.1 Temperature over flows at fixed pressures

9.8.1.1 Position 1B

At 450 °C, in Figure 44 the temperature profile is planar with a slightly elevated bulge between TC2 up to TC5 which is more elevated for higher flows. This is seen for the background pressures 20, 50, 100 and 200 mBar with flows ranging from 0 to 25 SLM at 20 mBar and flows ranging from 5 to 40 SLM at the other pressures. The result is presented at 20 mBar and the laminar flow limitation at 700 mBar. The results show strong indications of laminar flow in the vicinity of the injector. In Figure 45 at 700 mBar, flows higher than 25 SLM show indication of a turbulent flow a rapidly temperature increase of TC5 from 20 SLM to 25 SLM, but with no temperature increase at TC1.

At 1000 °C, in Figure 46 the temperature profile is planar with a slightly elevated bulge between TC2 up to TC5 which is more elevated at higher flows. There is also a depression between TC1 and TC2 at 5 to around 15 SLM. This profile is seen for the background pressures 20, 50, 100 and 200 mBar with flows ranging from 0 to 25 SLM at 20 mBar and flows ranging from 5 to 40 SLM at the other pressures. The result is presented at 20 and 50 mBar and the laminar flow limitation at 700 mBar. The results show indications on laminar flow in the vicinity of the injector at 20, 50, 100 and 200 mBar. There is no clear limit where the flow transits from laminar to turbulent flow and no strong indications of either laminar or turbulent flow. In

Figure 47 it is seen that at 50 mBar at 10 SLM, TC4 increases in temperature compared to TC5 indicating a turbulent flow is developing. This occurs for TC2 and TC1 with an equal scenario at 20 SLM. In Figure 48 it is seen that a turbulent flow is indicated for higher flows and equal to 30 SLM.

In Figure 49 trendline of ΔT is shown, where ΔT is the temperature difference between the maximum and minimum of the measured temperature at 15, 20 and 25 SLM. This indicates that the temperature difference between the maximum and minimum is almost constant throughout the measurements independent of the background pressure. A planar trend line indicates a more stable flow and can be an indicator that a laminar flow is present.

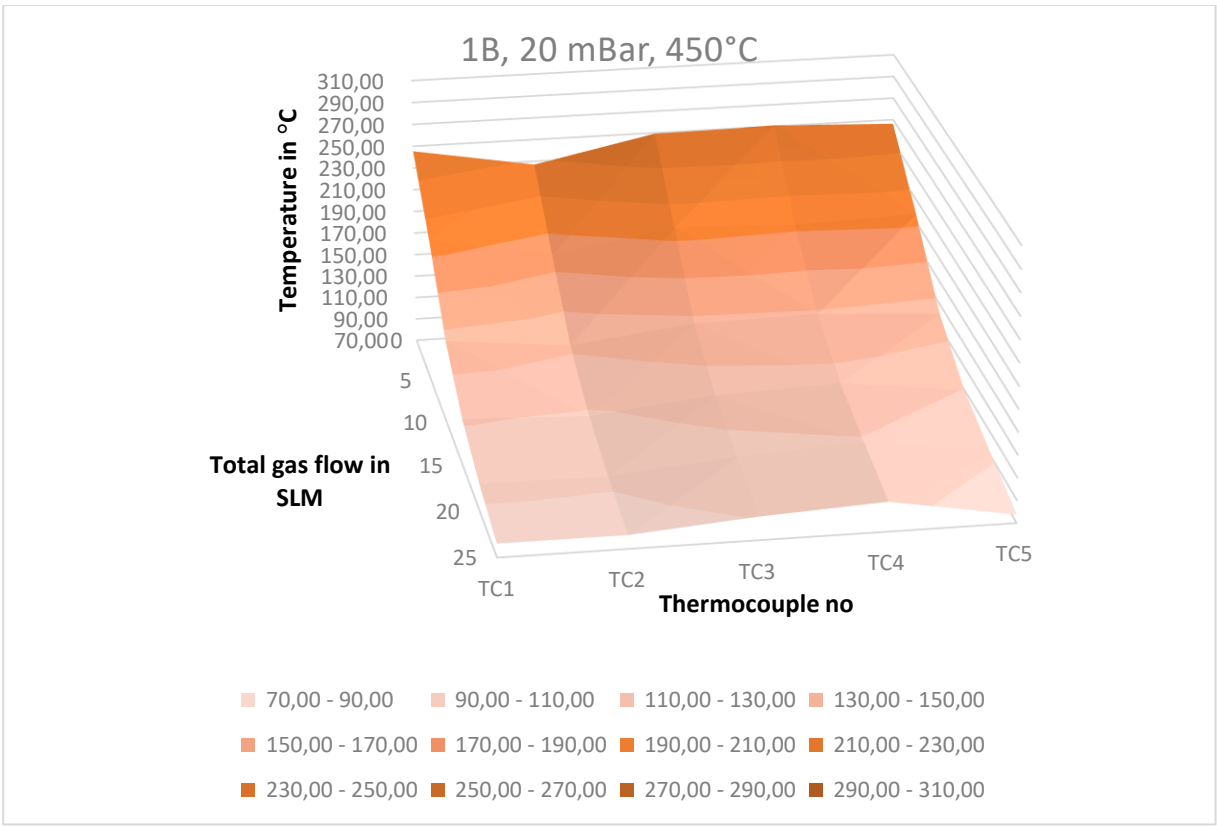

Figure 44 Position 1B at 20 mBar background pressure and at a susceptor temperature of 450°C.

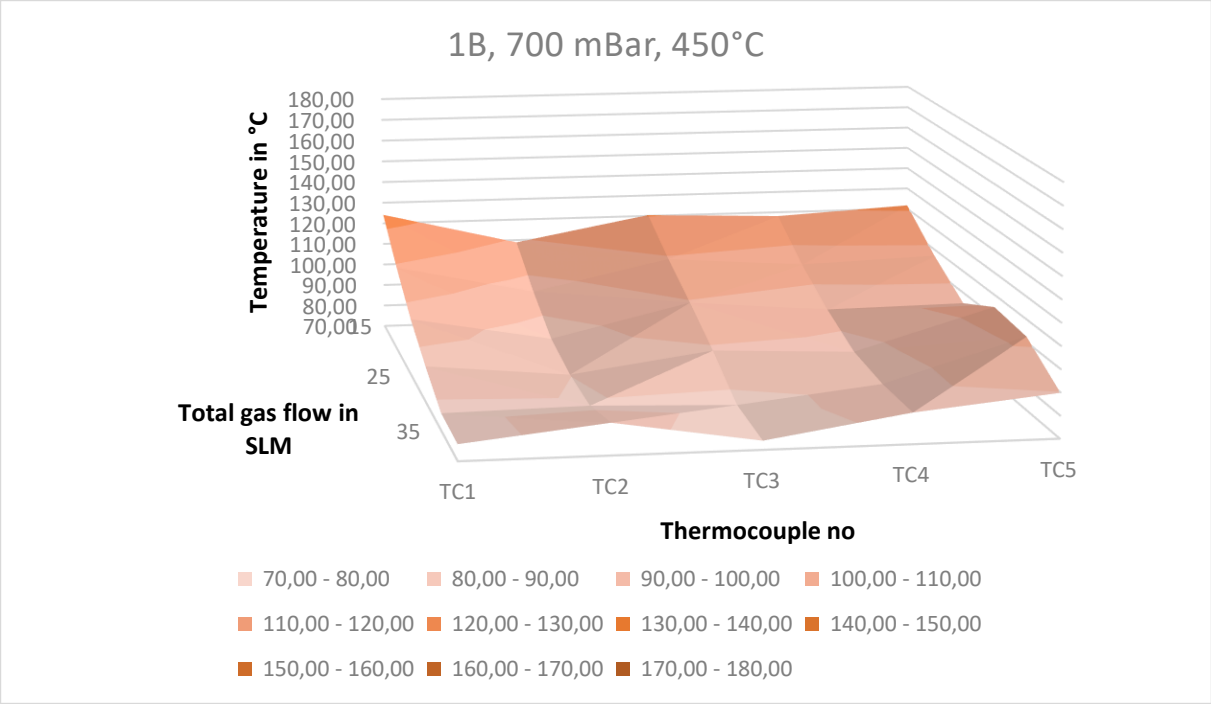

Figure 45 Position 1B at 700 mBar background pressure and at a susceptor temperature of 450°C.

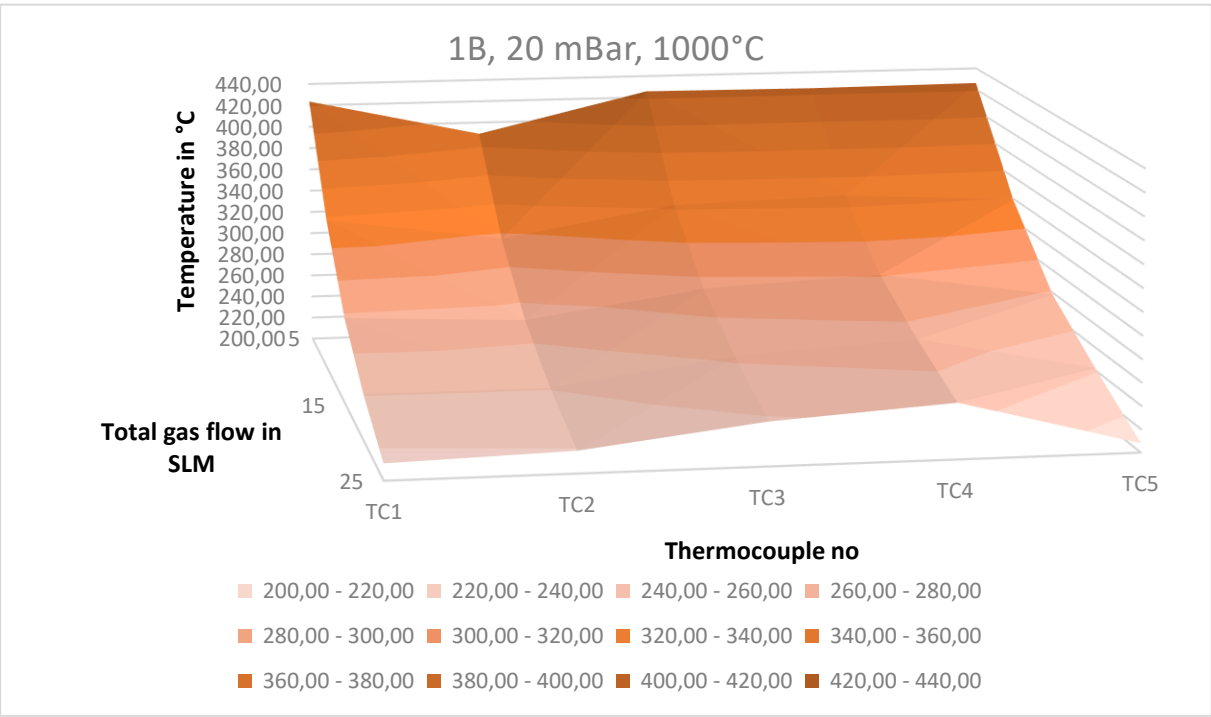

Figure 46 Position 1B at 20 mBar background pressure and at a susceptor temperature of 1000°C.

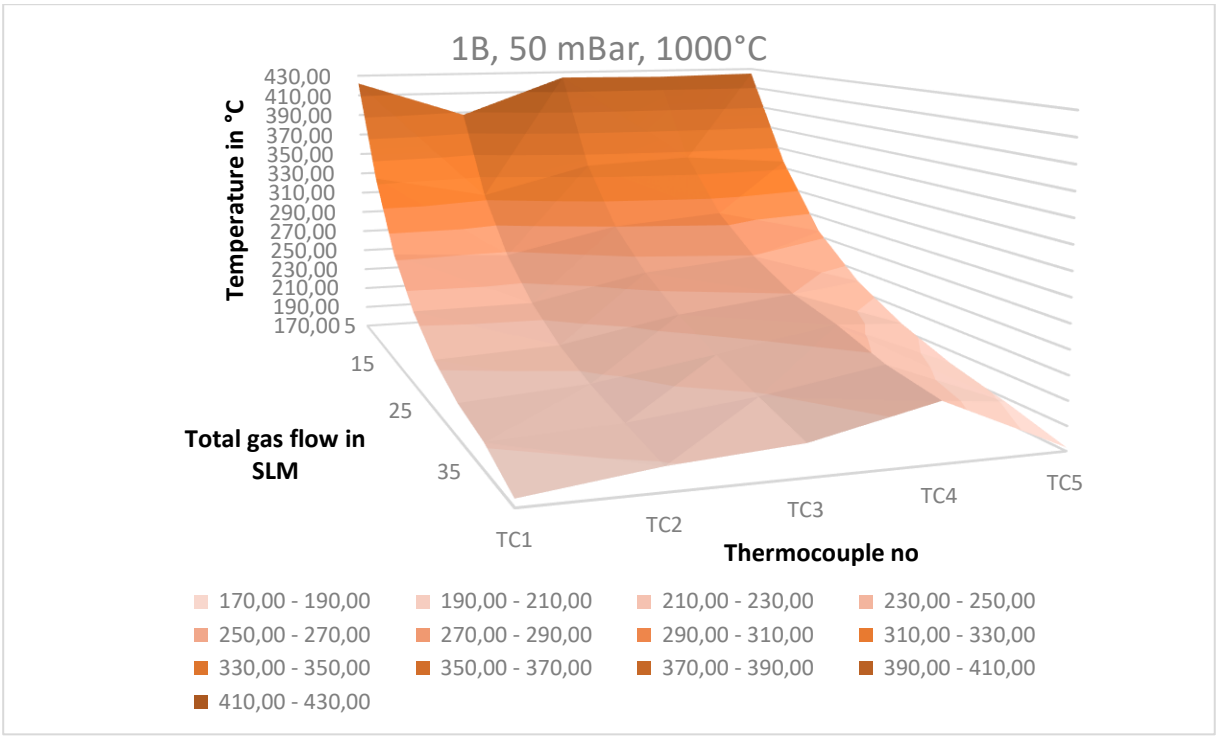

Figure 47 Position 1B at 50 mBar background pressure and at a susceptor temperature of 1000°C.

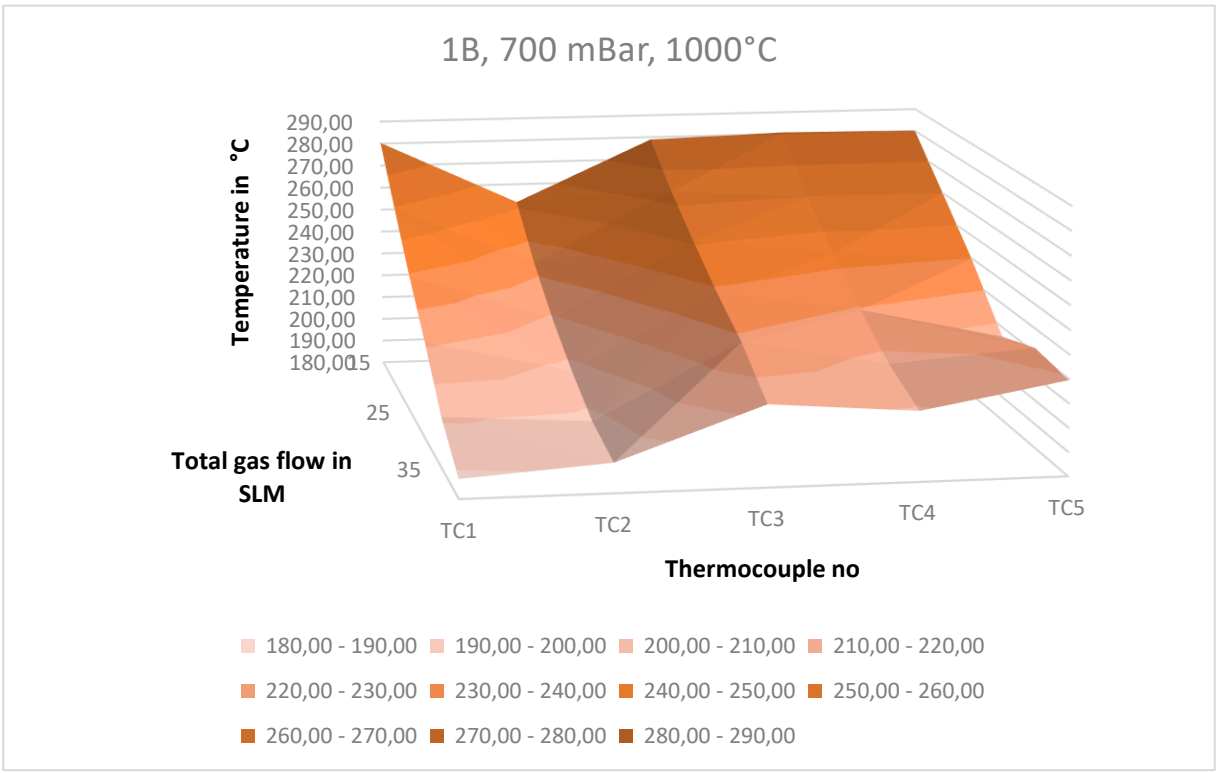

Figure 48 Position 1B at 700 mBar background pressure and at a susceptor temperature of 1000°C.

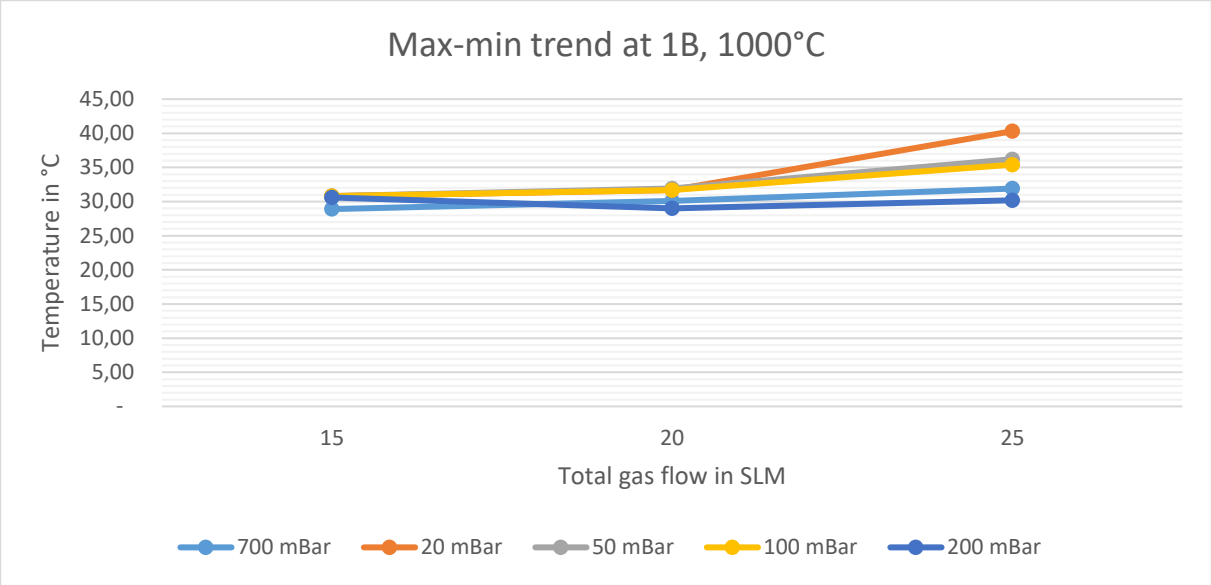

Figure 49 Max-min trendline at position 1B at susceptor temperature of 1000°C at total gas flows 15, 20 and 25 SLM.

9.8.1.2 Position 2A

At 450 °C, in Figure 50 the temperature profile is planar with a slightly elevated bulge at TC3 which is more elevated at higher flows. This profile is seen for background pressure 20 mBar with flows ranging from 0 to 25 SLM. At 50, 100 and 200 mBar it is seen with flows ranging from 5 to 40 SLM and the profile is like Figure 51 at 50 mBar. The profile is showing increased temperatures at TC2 and TC4 for flows above 20 SLM. The result is presented at 20 and 50 mBar and the laminar flow limitation at 700 mBar. The results show indications on laminar flow at 20, 50, 100 and 200 mBar. At 20 mBar up to 25 SLM, at 50 mBar up to 20 SLM, at 100 mBar up to 15 SLM and at 200 mBar up to 10 SLM. There is no clear limit where the flow transits from laminar to turbulent flow and no strong indications of turbulent flow for 200 mBar. In Figure 52 it is seen that a turbulent flow is indicated for higher flows and equal to 30 SLM.

At 1000 °C, in Figure 53 the temperature profile is planar with a slightly elevated bulge at TC3 and TC2 which is more elevated at higher flows. This profile is seen for background pressure 20 mBar with flows ranging from 0 to 25 SLM. At 50, 100 and 200 mBar it is seen with flows ranging from 5 to 40 SLM and the profile is like Figure 54 at 50 mBar. The profile in Figure 54 is showing increased temperatures at TC2 and TC4. The result is presented at 20 and 50 mBar and the laminar flow limitation at 700 mBar. The results show indications on laminar flow at 20, 50, 100 and 200 mBar. At 20 mBar up to 25 SLM, at 50 mBar up to 25 SLM with a parabolic profile and between 30 to 40 SLM a profile with its maximum at TC2, at 100 mBar up to 30 SLM and at 200 mBar up to 25 SLM. In Figure 55 it is seen that a turbulent flow is indicated for higher flows and equal to 15 SLM.

In Figure 56 a trendline of ΔT is shown, where ΔT is the temperature difference between the maximum and minimum of the measured temperature at 15, 20 and 25 SLM. The result indicates that the temperature difference between the maximum and minimum is almost constant throughout the measurements independent of the background pressure. A planar trend line indicates a more stable flow and can be an indicator that a laminar flow is present.

For flows higher than 100 mBar it is indicated that a turbulent flow is developed at an earlier stage compared to the others.

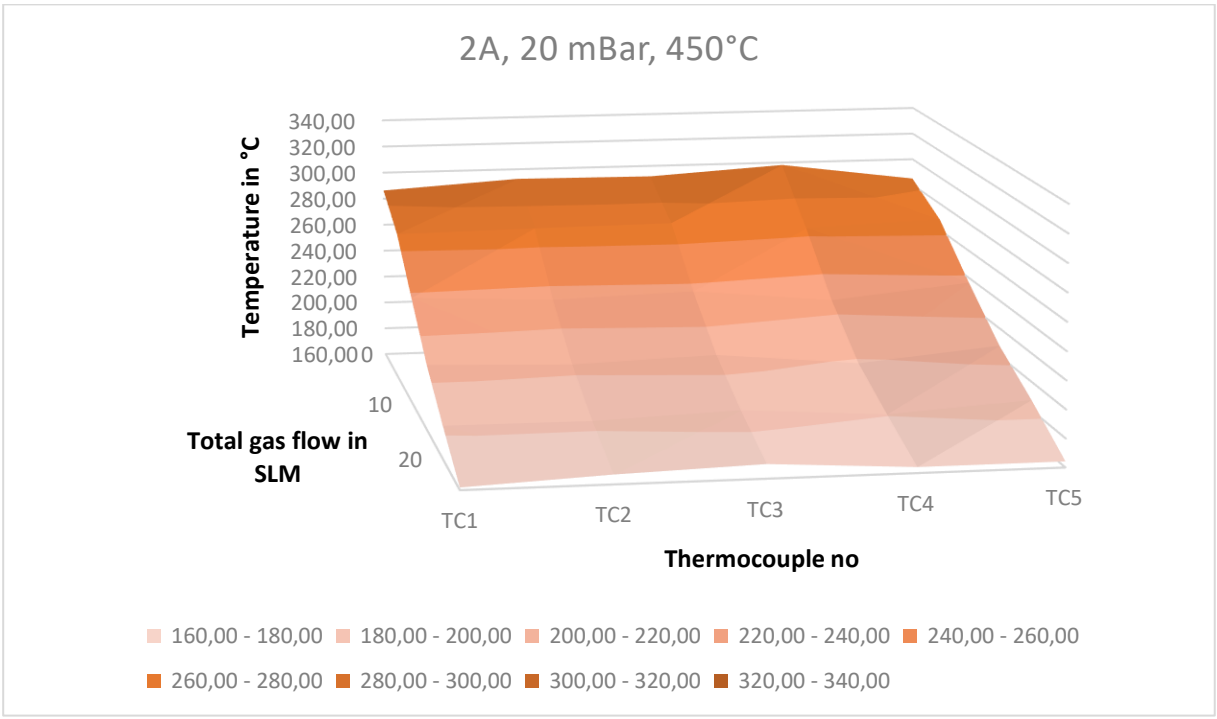

Figure 50 Position 2A at 20 mBar background pressure and at a susceptor temperature of 450°C.

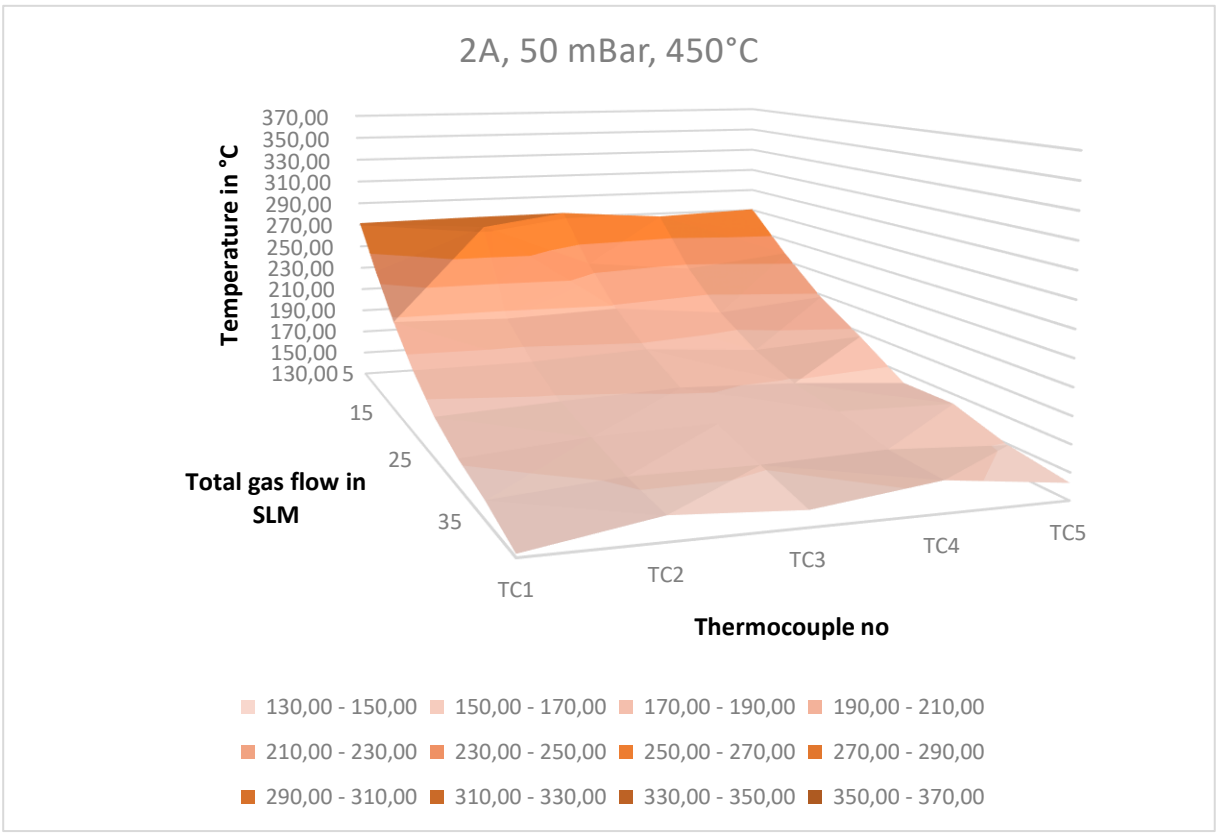

Figure 51 Position 2A at 50 mBar background pressure and at a susceptor temperature of 450°C.

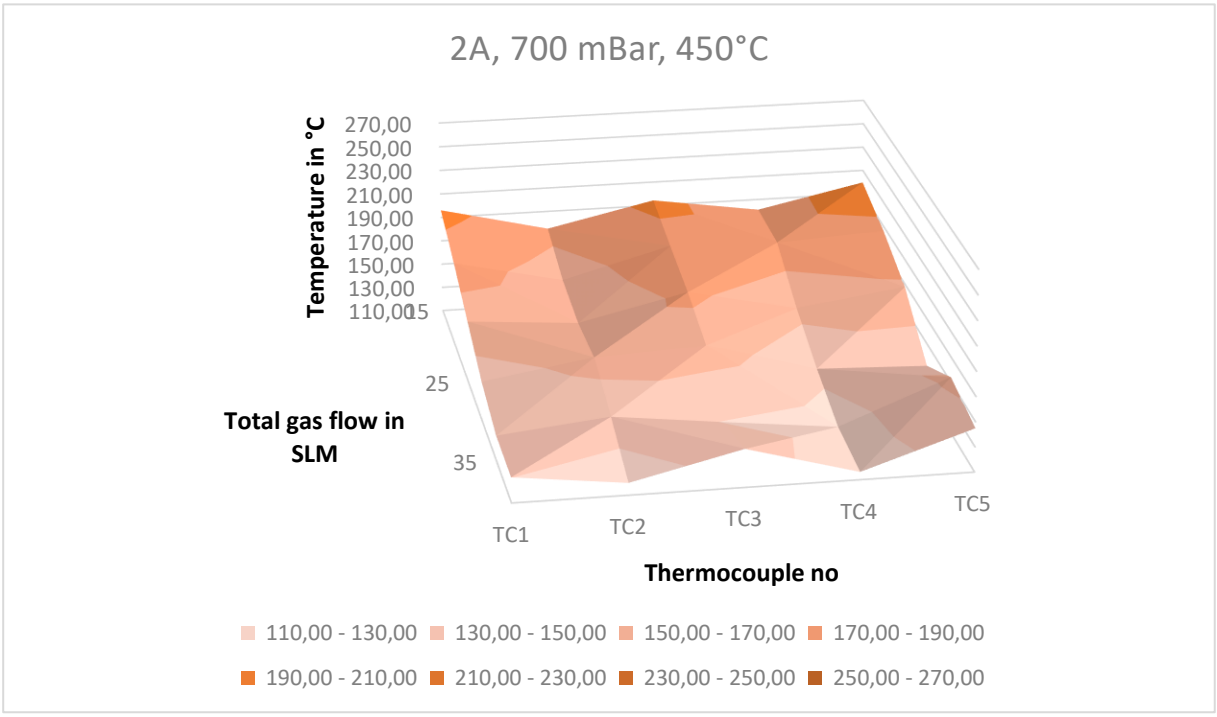

Figure 52 Position 2A at 700 mBar background pressure and at a susceptor temperature of 450°C.

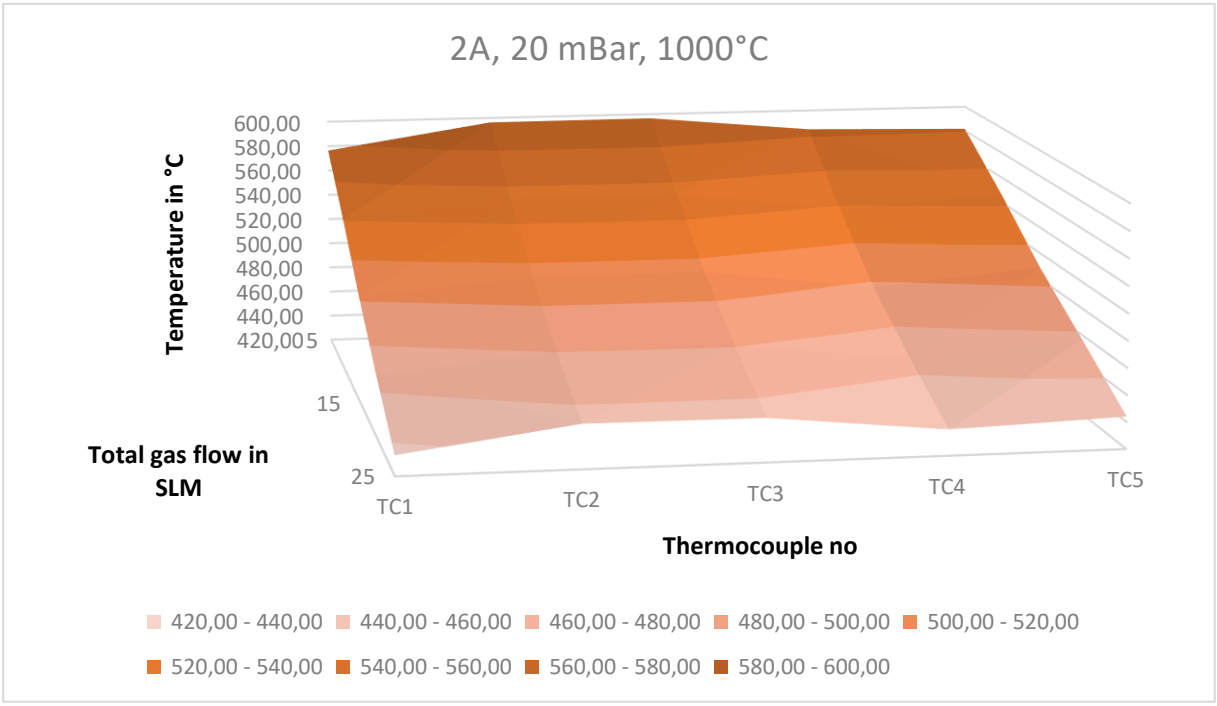

Figure 53 Position 2A at 20 mBar background pressure and at a susceptor temperature of 1000°C.

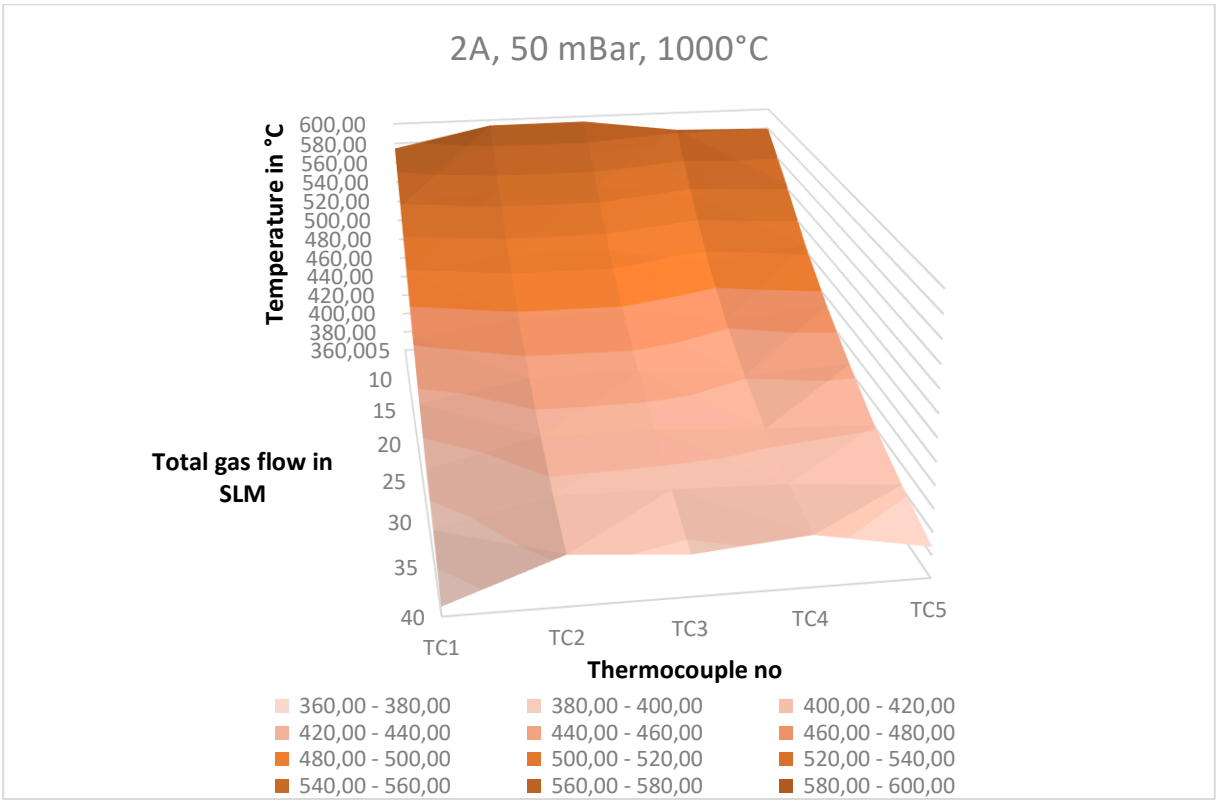

Figure 54 Position 2A at 50 mBar background pressure and at a susceptor temperature of 1000°C.

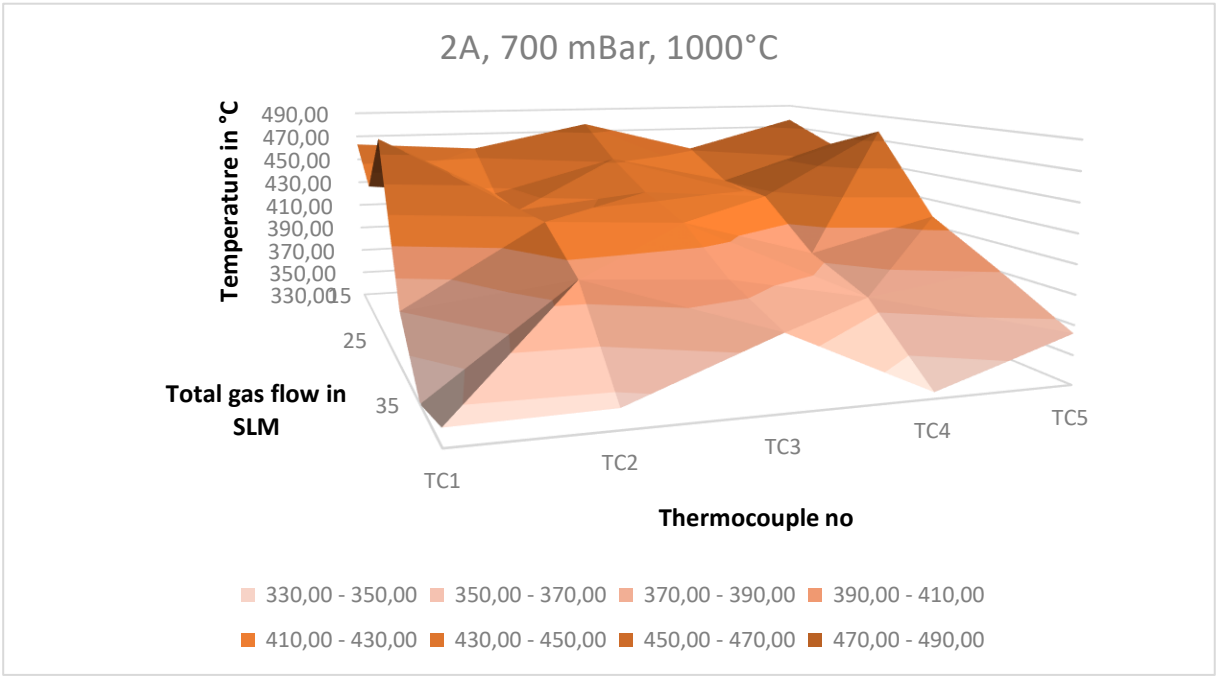

Figure 55 Position 2A at 700 mBar background pressure and at a susceptor temperature of 1000°C.

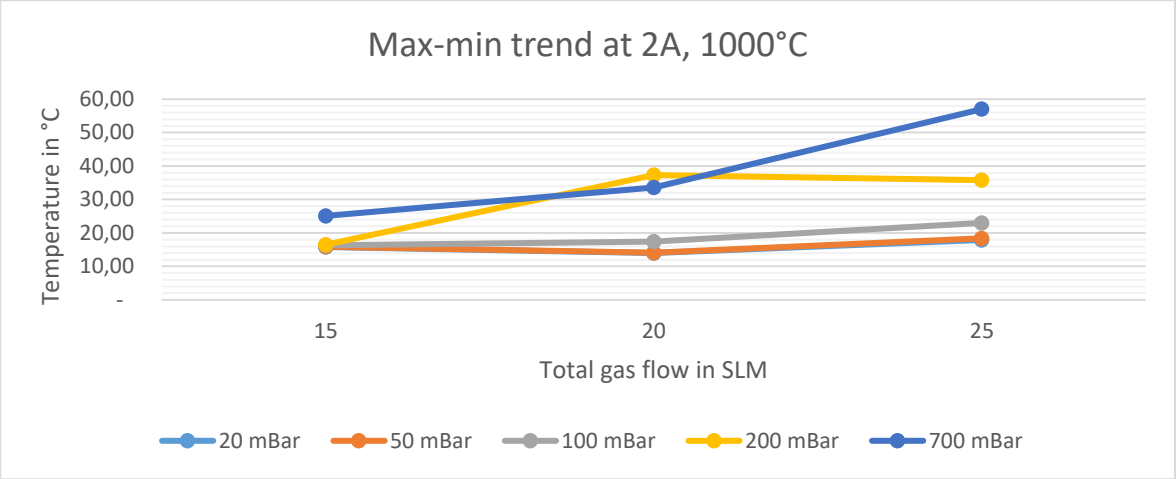

Figure 56 Max-min trendline at position 2A at susceptor temperature of 1000°C at total gas flows 15, 20 and 25 SLM.

9.8.1.3 Position 2B

At 450 °C, in Figure 57 the temperature profile is planar with a concave bulge at TC3. This profile is seen for background pressure 20 mBar with flows ranging from 0 to 25 SLM. At 50, 100 and 200 mBar it is seen with flows ranging from 5 to 40 SLM and the profile is like Figure 58 at 50 mBar. The result is presented at 20 and 50 mBar and the laminar flow limitation at 700 mBar. The results show indications on laminar flow at 20, 50, 100 and 200 mBar. At 20 mBar up to 20 SLM, at 50, 100 and 200 mBar up to 25 SLM. In Figure 59 at 700 mBar it is seen that a turbulent flow is indicated for higher flows and equal to 25 SLM.

At 1000 °C, in Figure 60 the temperature profile is planar with a concave bulge at TC3. This profile is seen for background pressure 20 mBar with flows ranging from 0 to 25 SLM. At 50, 100 and 200 mBar it is seen with flows ranging from 5 to 40 SLM and the profile is like Figure 61 at 50 mBar. The result is presented at 20 and 50 mBar and the laminar flow limitation at 700 mBar. The results show indications on laminar flow at 20, 50, 100 and 200 mBar. At 20 and 50 mBar up to 20 SLM, 100 mBar up to 15 SLM and 200 mBar at 15 SLM and only equal to it. In Figure 62 at 700 mBar it is seen that a turbulent flow is indicated for higher flows and equal to 30 SLM.

In Figure 63 a trendline of ΔT is shown, where ΔT is the temperature difference between the maximum and minimum of the measured temperature at 15, 20 and 25 SLM. The result indicates that the temperature difference between the maximum and minimum is almost constant throughout the measurements independent of the background pressure, except for 50 mBar. A planar trend line indicates a more stable flow and can be an indicator that a laminar flow is present between 15 to 25 SLM.

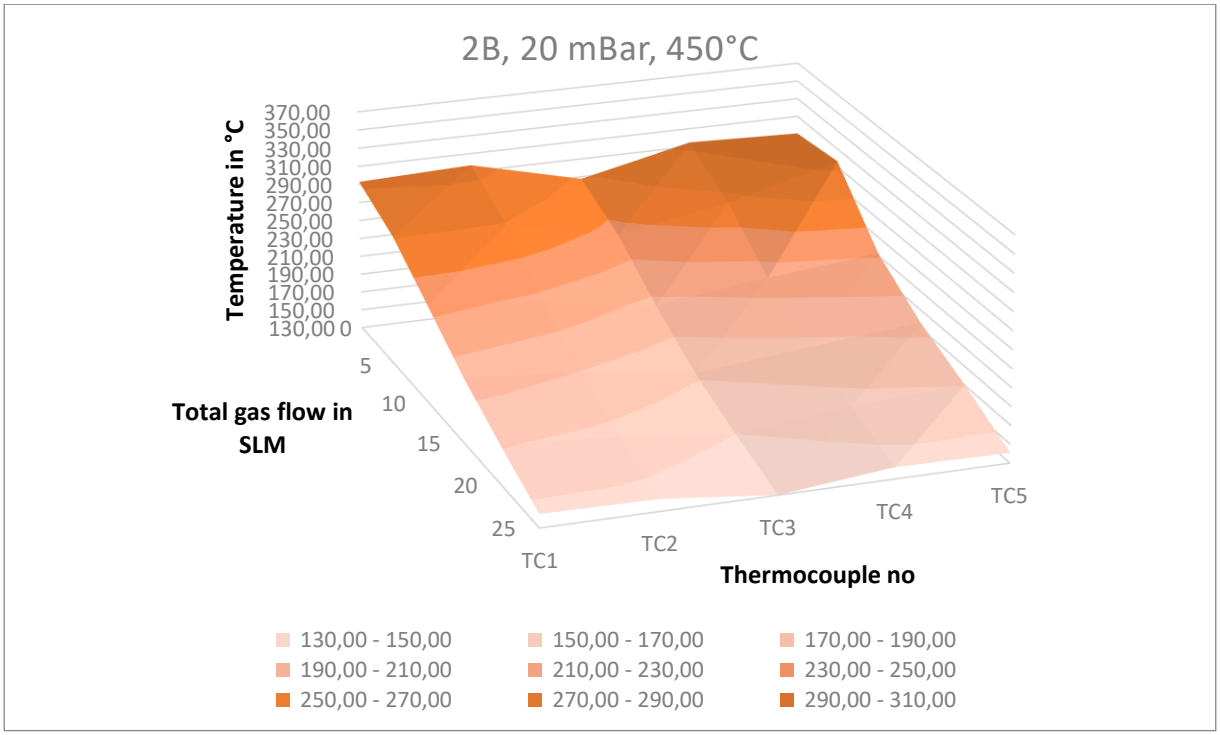

Figure 57 Position 2B at 20 mBar background pressure and at a susceptor temperature of 450°C.

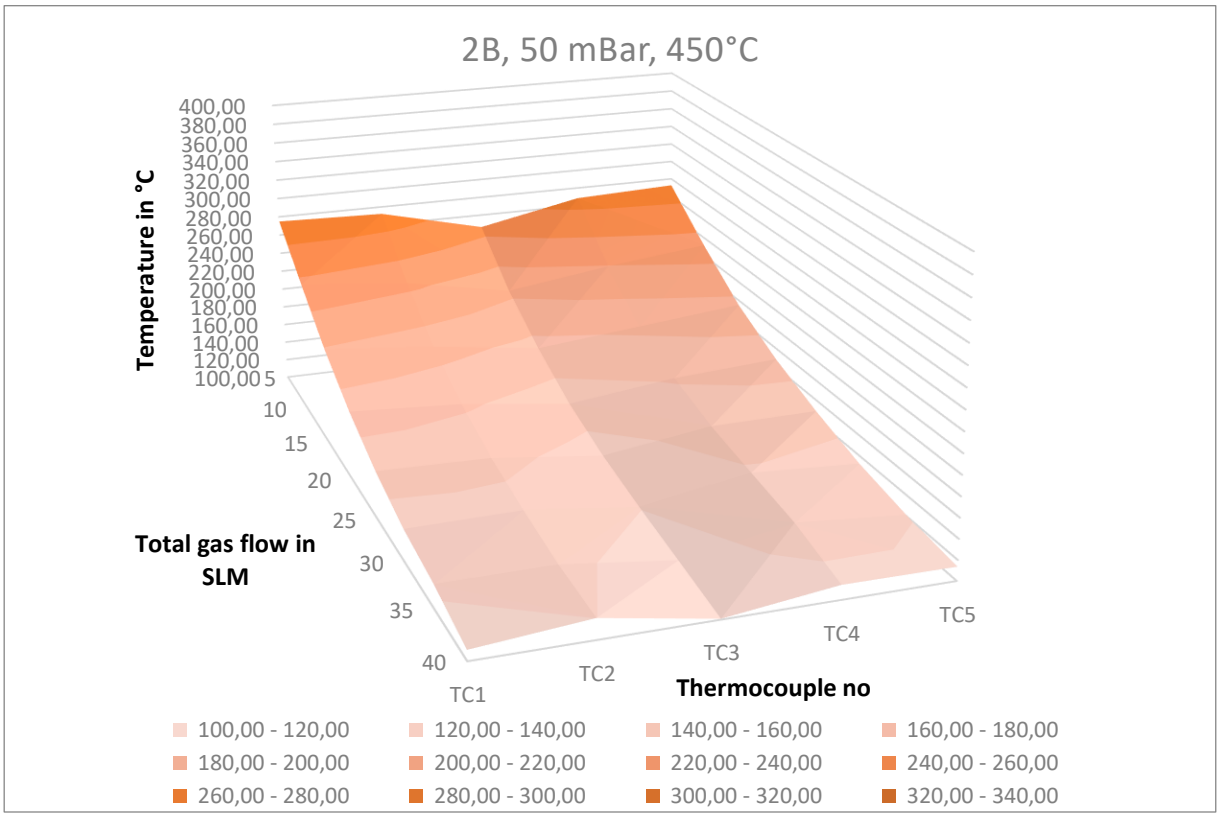

Figure 58 Position 2B at 50 mBar background pressure and at a susceptor temperature of 450°C.

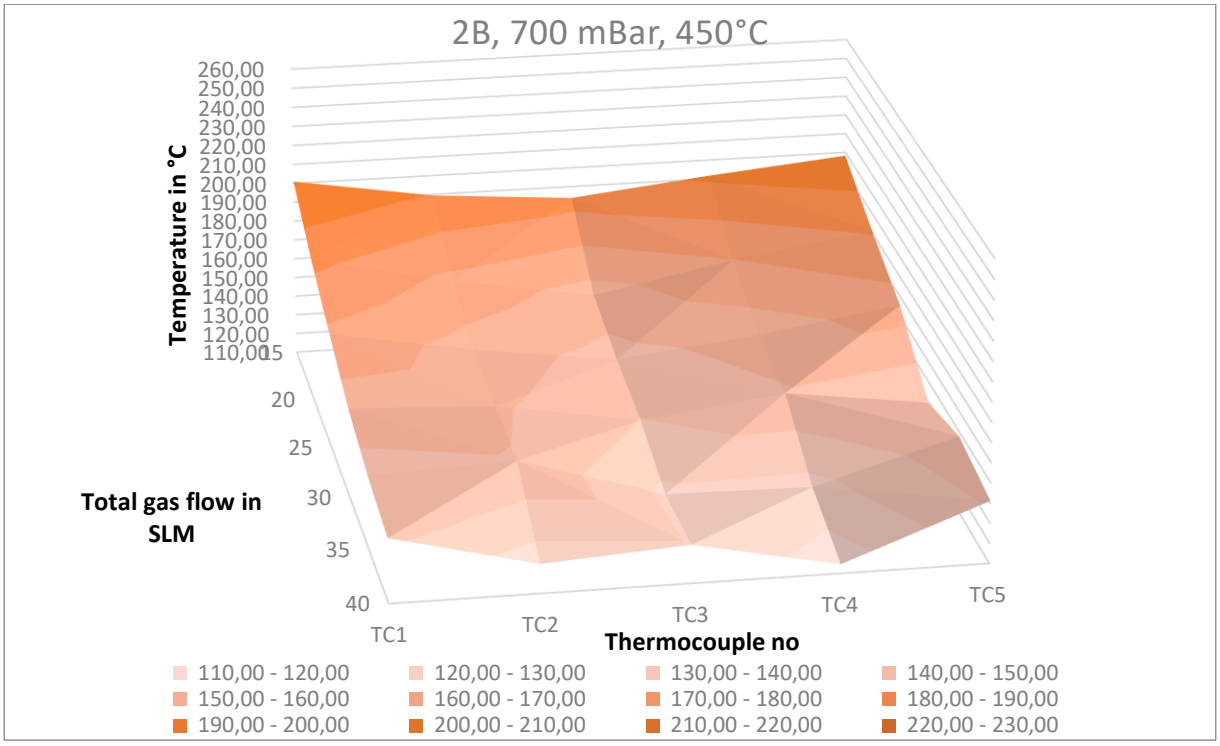

Figure 59 Position 2B at 700 mBar background pressure and at a susceptor temperature of 450°C.

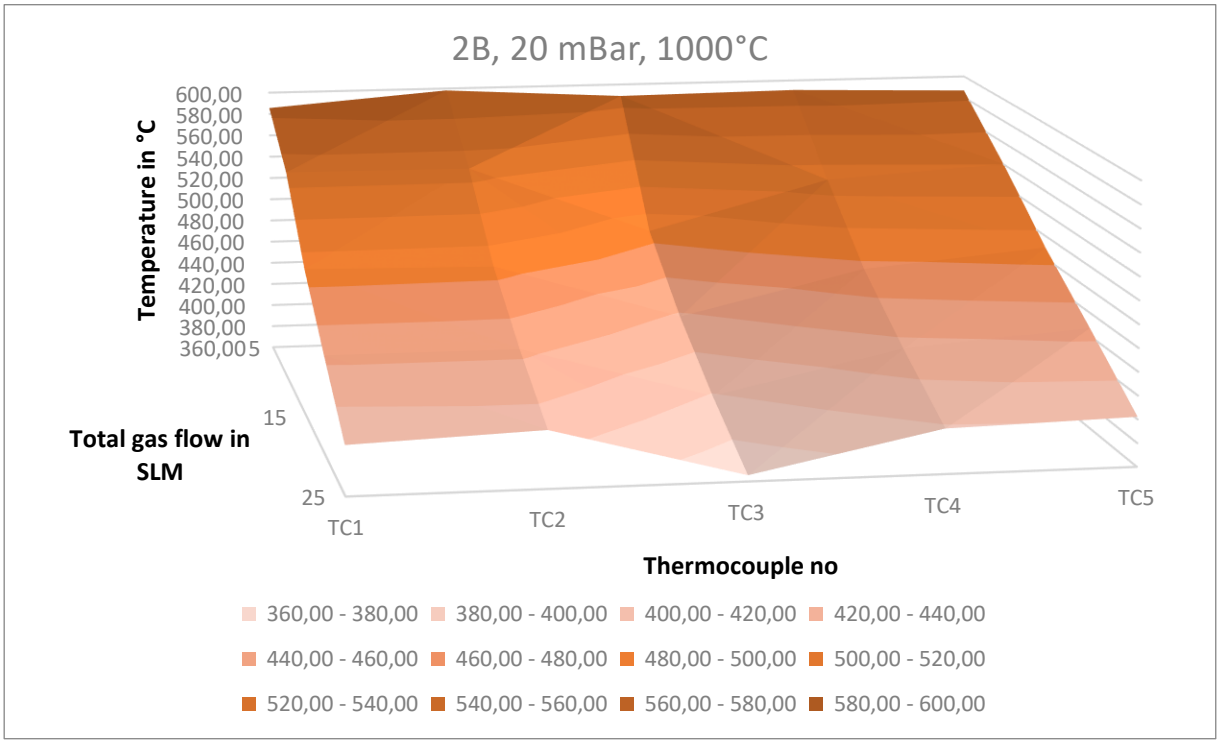

Figure 60 Position 2B at 20 mBar background pressure and at a susceptor temperature of 1000°C.

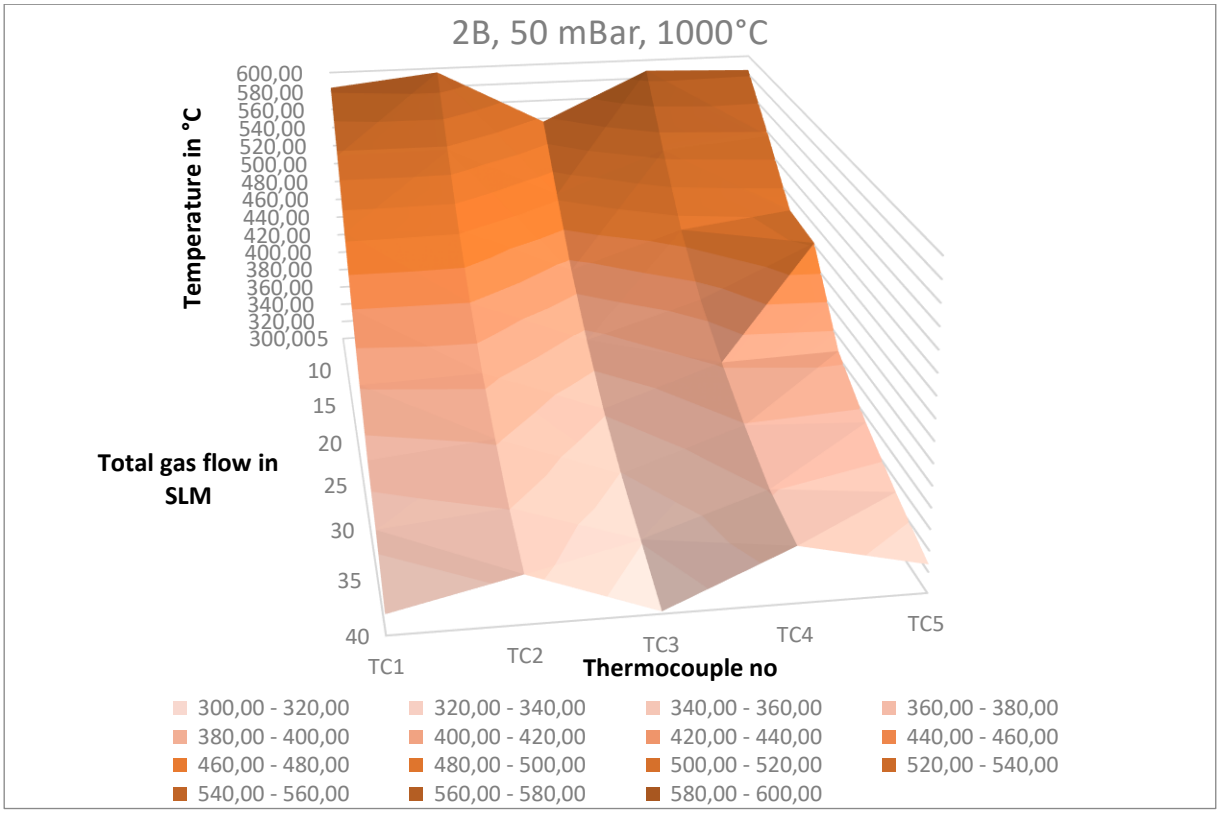

Figure 61 Position 2B at 50 mBar background pressure and at a susceptor temperature of 1000°C.

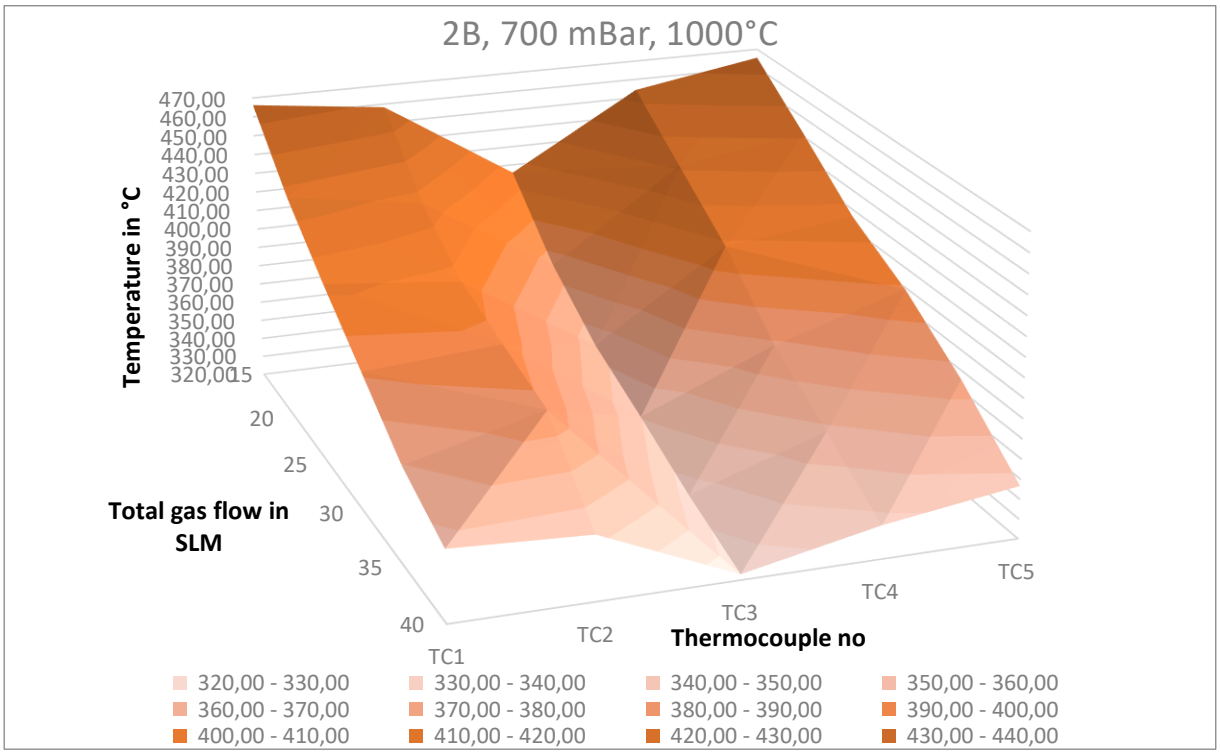

Figure 62 Position 2B at 700 mBar background pressure and at a susceptor temperature of 1000°C.

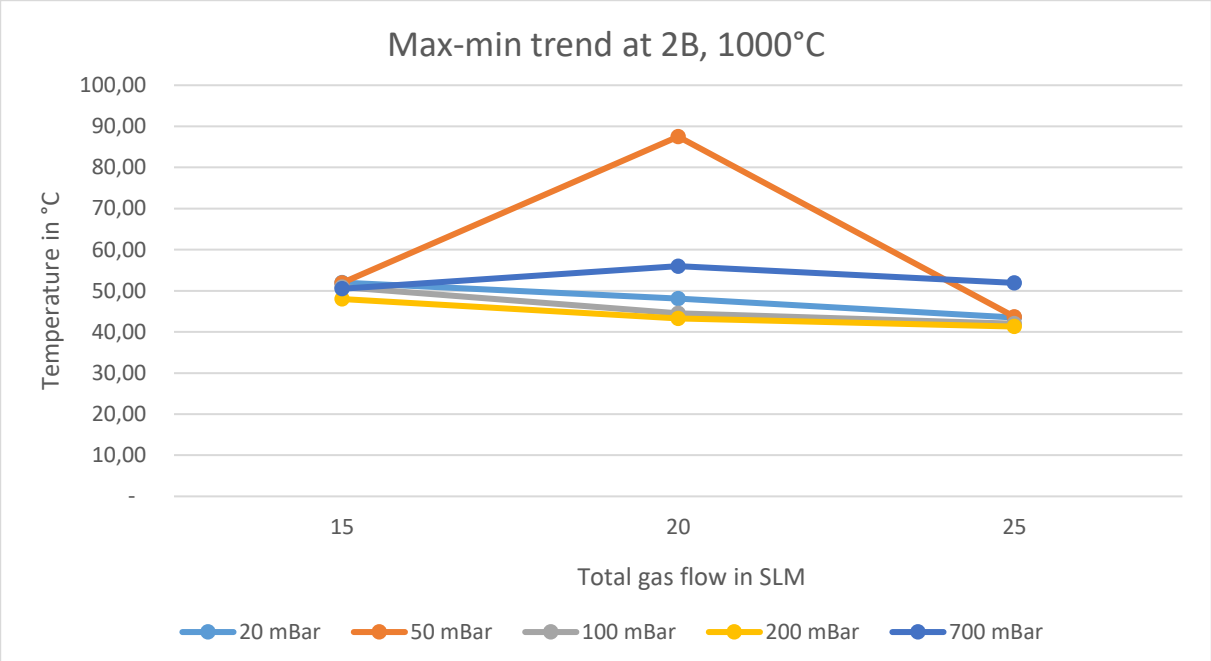

Figure 63 Max-min trendline at position 2B at susceptor temperature of 1000°C at total gas flows 15, 20 and 25 SLM.

9.8.1.4 Position 2C

At 450 °C, in Figure 64 the temperature profile is planar with a concave bulge at TC3. This profile is seen for background pressure 20 mBar with flows ranging from 0 to 25 SLM. At 50, 100 and 200 mBar it is seen with flows ranging from 5 to 40 SLM and the profile is like Figure 64. The result is presented at 20 mBar and the laminar flow limitation at 700 mBar. The results show indications on laminar flow at 20, 50, 100 and 200 mBar. At 20 mBar up to 20 SLM, 50 mBar up to 25 SLM, 100 mBar up to 25 SLM and 200 mBar up to 35 SLM. In Figure 65 at 700 mBar it is seen that a laminar flow is indicated up to maximum tested flow of 40 SLM.

At 1000 °C, in Figure 66 the temperature profile is planar with a concave bulge at TC3. This profile is seen for background pressure 20 mBar with flows ranging from 0 to 25 SLM. At 50, 100 and 200 mBar it is seen with flows ranging from 5 to 40 SLM and the profile is like Figure 67 at 50 mBar. The result is presented at 20 and 50 mBar and the laminar flow limitation at 700 mBar. The results show indications on laminar flow at 20, 50, 100 and 200 mBar. At 20 mBar up to 20 SLM, 50 mBar up to 25 SLM, 100 mBar up to 30 SLM and 200 mBar up to 40 SLM. In Figure 68 at 700 mBar it is seen that a laminar flow is indicated up to maximum tested flow of 30 SLM.

In Figure 69 a trendline of ΔT is shown, where ΔT is the temperature difference between the maximum and minimum of the measured temperature at 15, 20 and 25 SLM. The result indicates that the temperature difference between the maximum and minimum is almost constant throughout the measurements independent of the background pressure, except for 200 and 700 mBar which shows a larger spread at 25 SLM. A planar trend line indicates a more stable flow and can be an indicator that a laminar flow is present between 15 to 25 SLM for 20, 50 and 100 mBar.

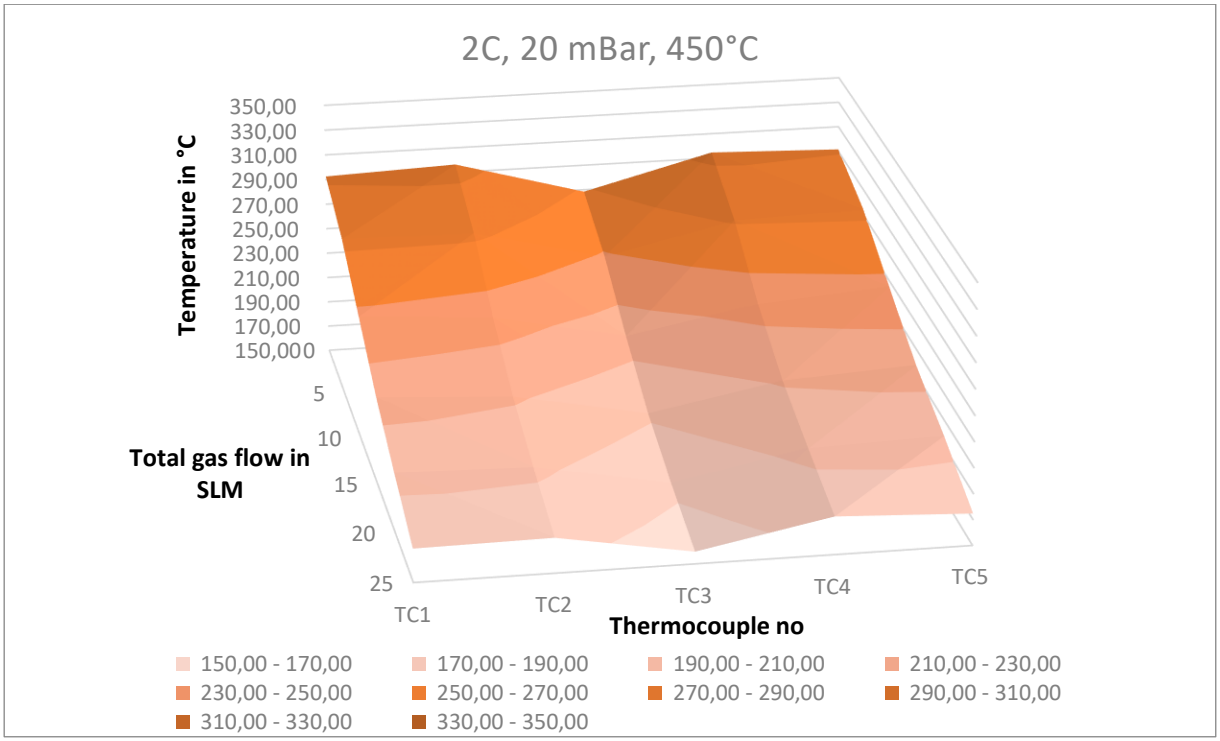

Figure 64 Position 2C at 20 mBar background pressure and at a susceptor temperature of 450°C.

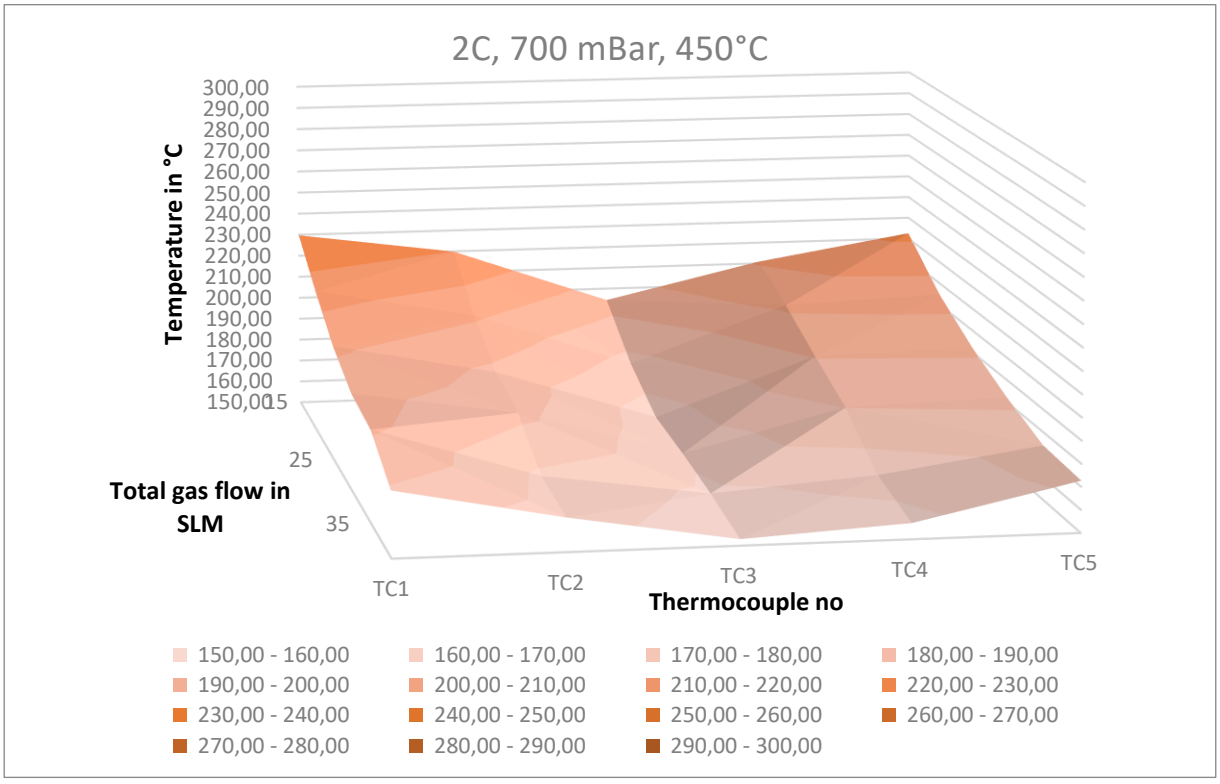

Figure 65 Position 2C at 700 mBar background pressure and at a susceptor temperature of 450°C.

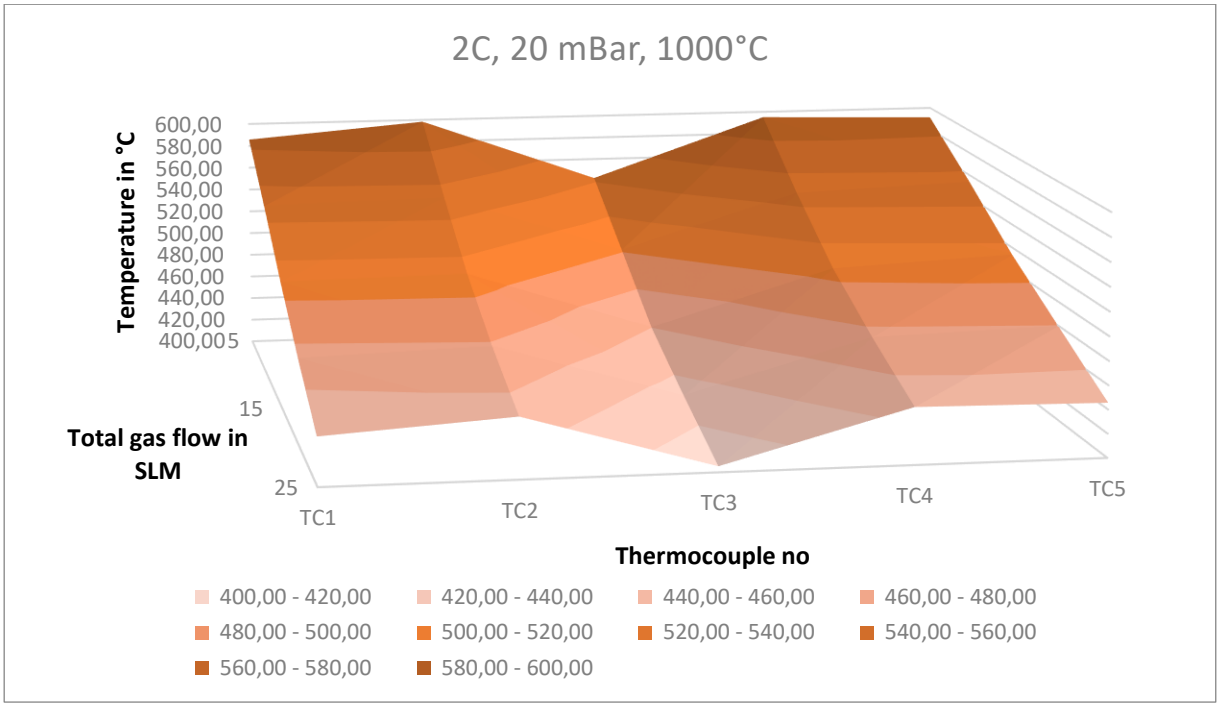

Figure 66 Position 2C at 20 mBar background pressure and at a susceptor temperature of 1000°C.

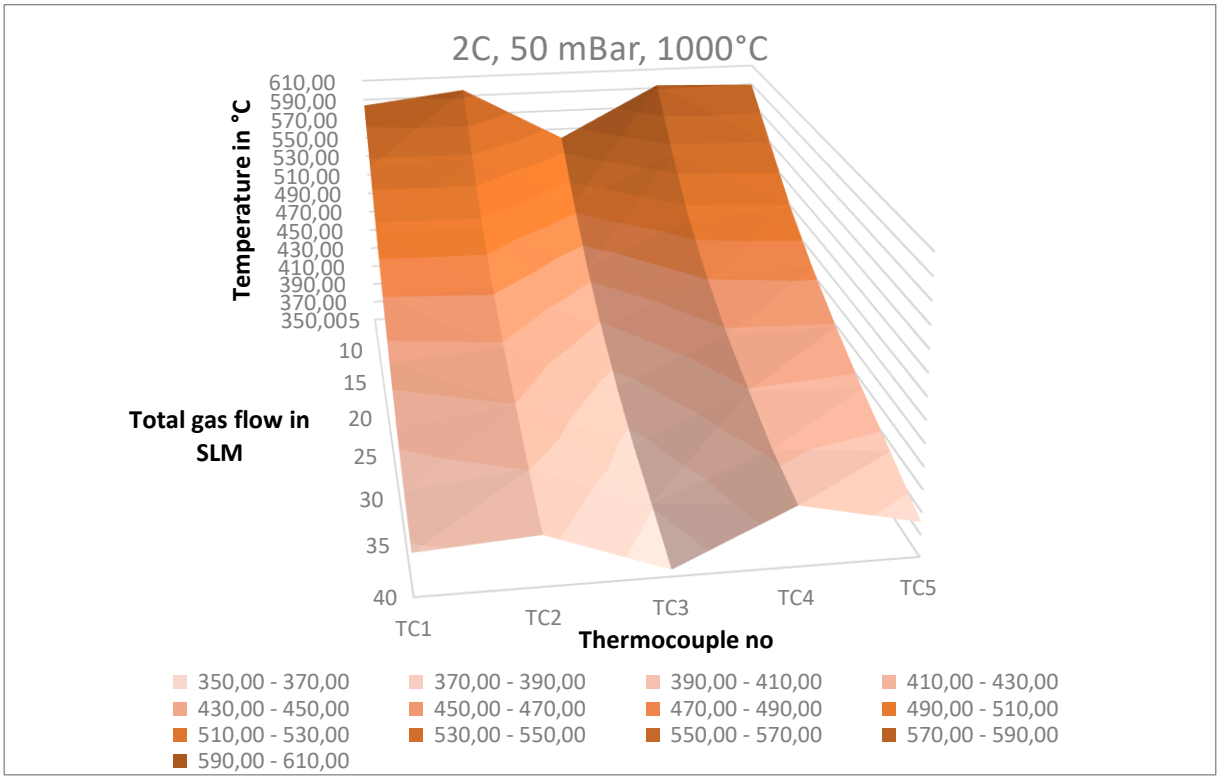

Figure 67 Position 2C at 50 mBar background pressure and at a susceptor temperature of 1000°C.

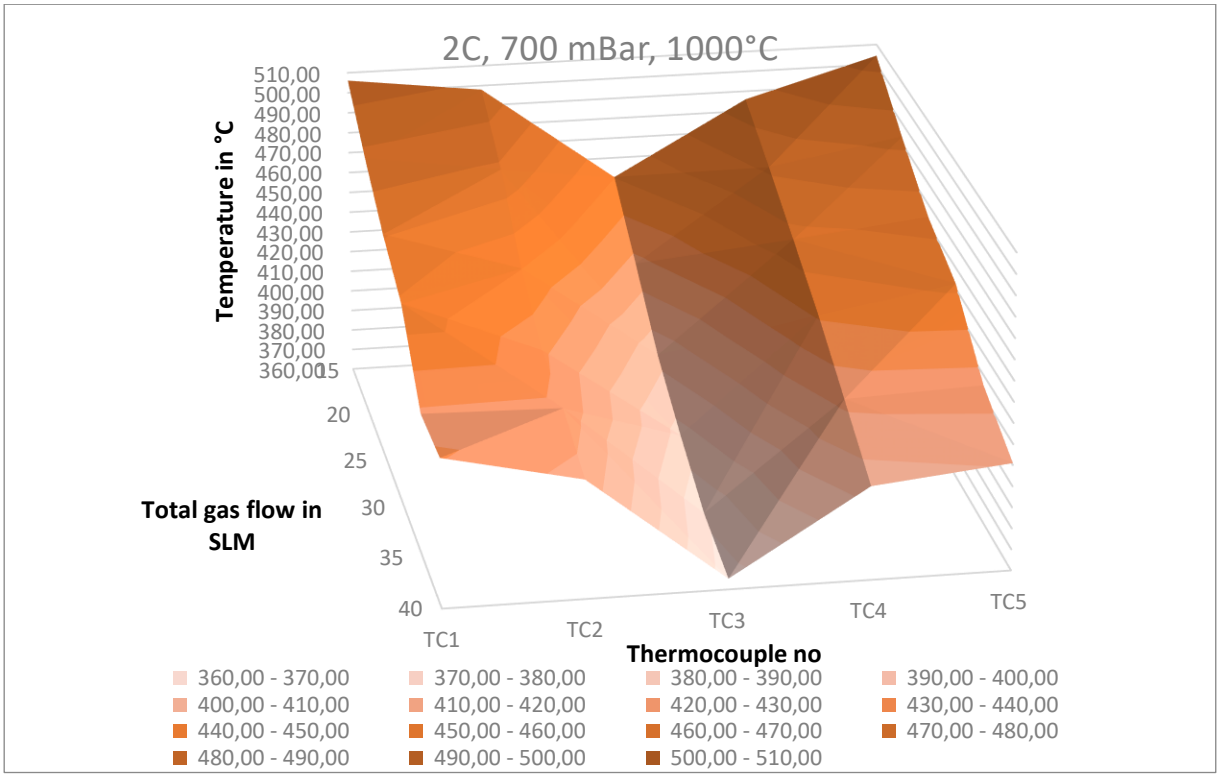

Figure 68 Position 2C at 700 mBar background pressure and at a susceptor temperature of 1000°C.

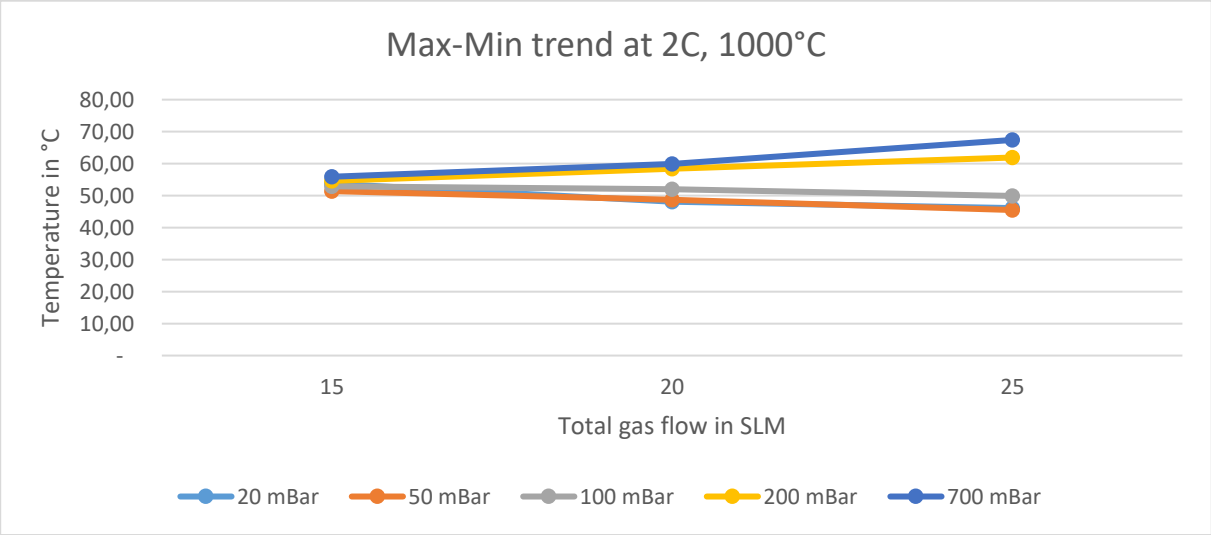

Figure 69 Max-min trendline at position 2C at susceptor temperature of 1000°C at total gas flows 15, 20 and 25 SLM.

9.8.1.5 Position 3A

At 450 °C, in Figure 70 the temperature profile is planar with a concave bulge at TC3. This profile is seen for background pressure 20 mBar with flows ranging from 0 to 25 SLM. At 50, 100 and 200 mBar it is seen with flows ranging from 5 to 40 SLM and the profile is like Figure 71 at 50 mBar. The result is presented at 20 and 50 mBar and the laminar flow limitation at 700 mBar. The results show indications on laminar flow at 20, 50, 100 and 200 mBar. At 20 mBar up to 25 SLM, 50 mBar up to 35 SLM, 100 mBar up to 30 SLM and 200 mBar up to 20 SLM. In Figure 72 the temperature profile is asymmetric and shows no pattern at 700 mBar with flows ranging from 15 to 30 SLM in the vicinity of the susceptor. Flows ranging from 35 to 40 SLM show indications of laminar flow with a depressing profile towards TC3.

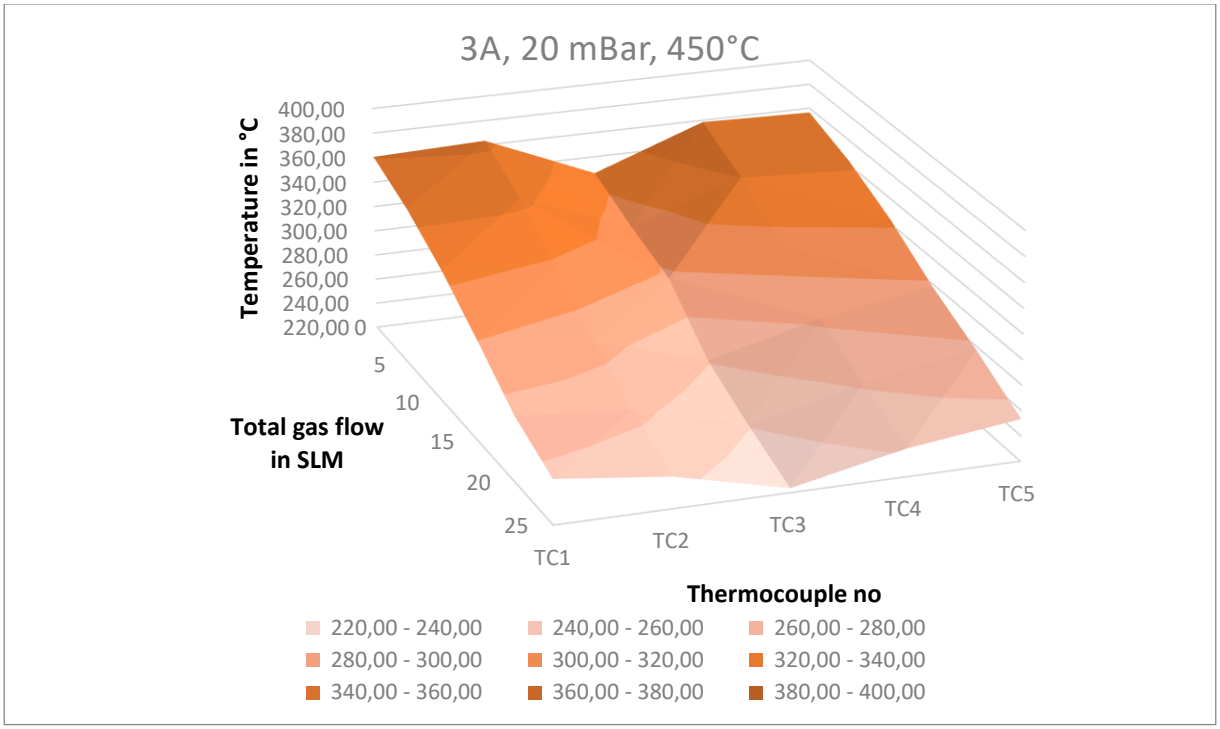

Figure 70 Position 3A at 20 mBar background pressure and at a susceptor temperature of 450°C.

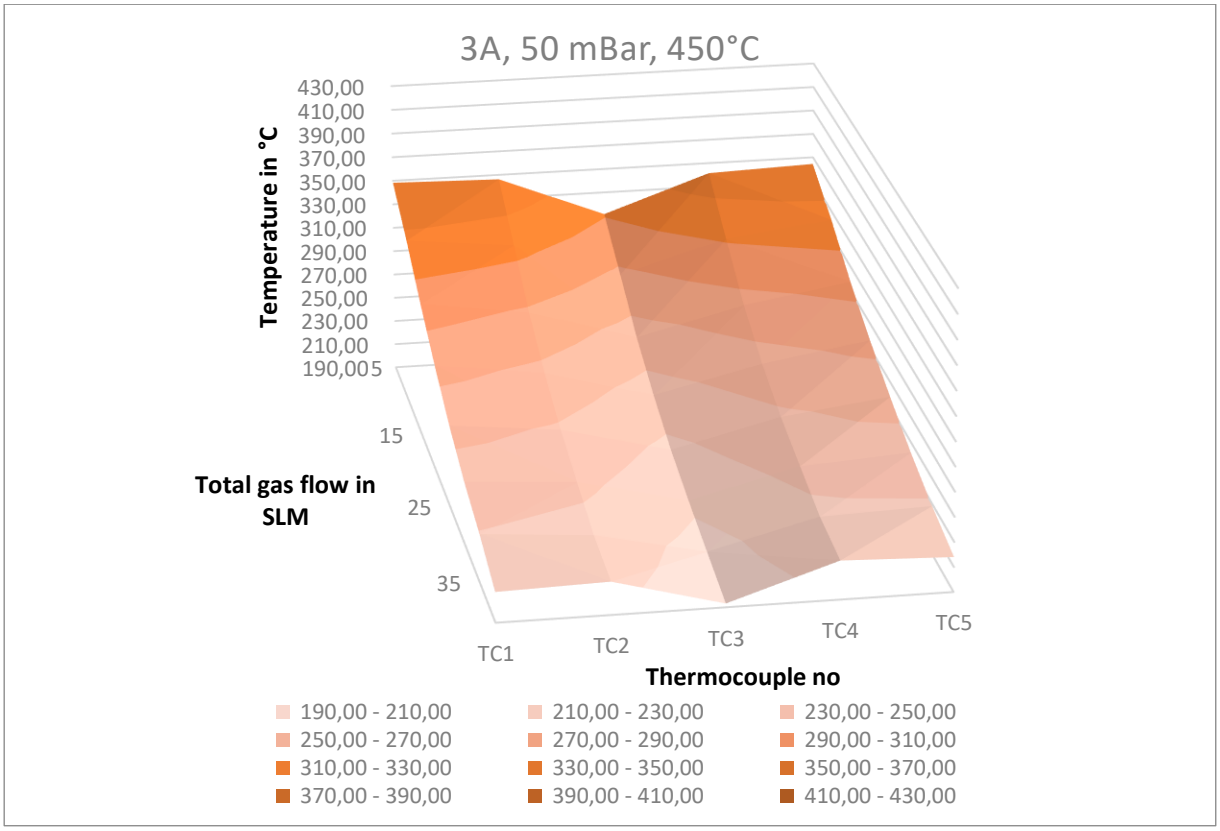

Figure 71 Position 3A at 50 mBar background pressure and at a susceptor temperature of 450°C.

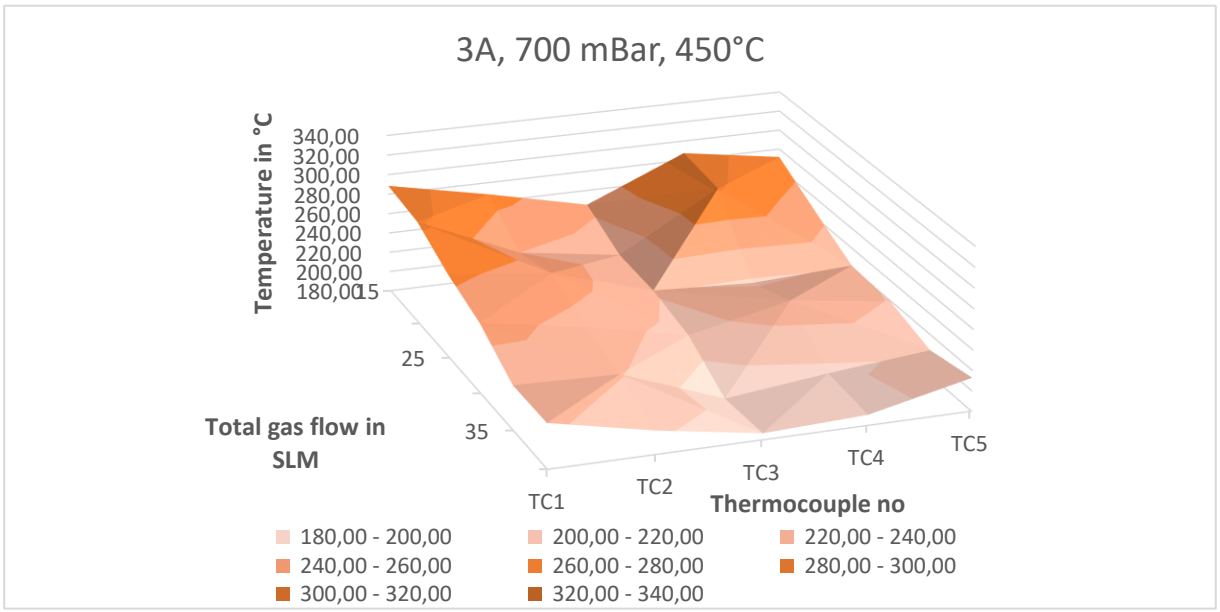

Figure 72 Position 3A at 700 mBar background pressure and at a susceptor temperature of 450°C.

At 1000 °C at 50, 100 and 200 mBar temperature depression creating a concave profile is seen at TC3 with flows ranging from 5 to 40 SLM and the profile is like Figure 74 at 50 mBar. The result is presented at 20 and 50 mBar and the laminar flow limitation at 700 mBar. The results show indications of laminar flow at 20, 50, 100 and 200 mBar. At 20 mBar up to 25 SLM, 50 mBar up to 35 SLM, 100 mBar up to 35 SLM and 200 mBar up to 25 SLM. In Figure 75 at 700 mBar the temperature profile is asymmetric and shows a flow profile depressing towards TC3 which is indicated to be turbulent from 15 SLM and up. This profile is also seen for background pressure 20 mBar in Appendix H in section 9.8.1.5 with flows ranging from 5 to 25 SLM.

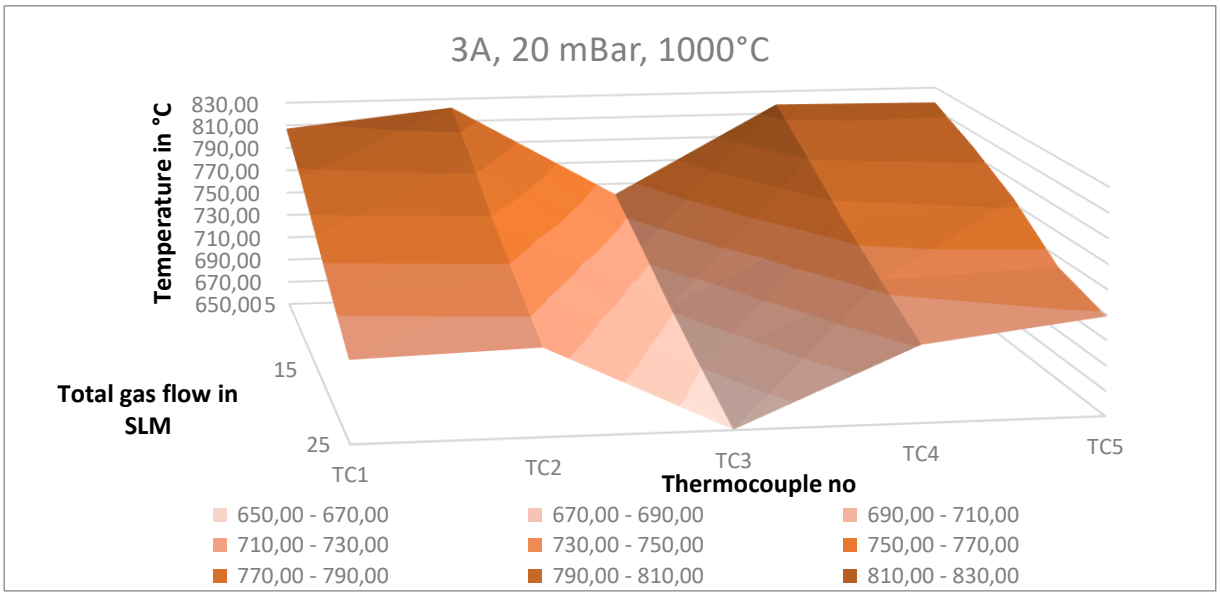

Figure 73 Position 3A at 20 mBar background pressure and at a susceptor temperature of 1000°C.

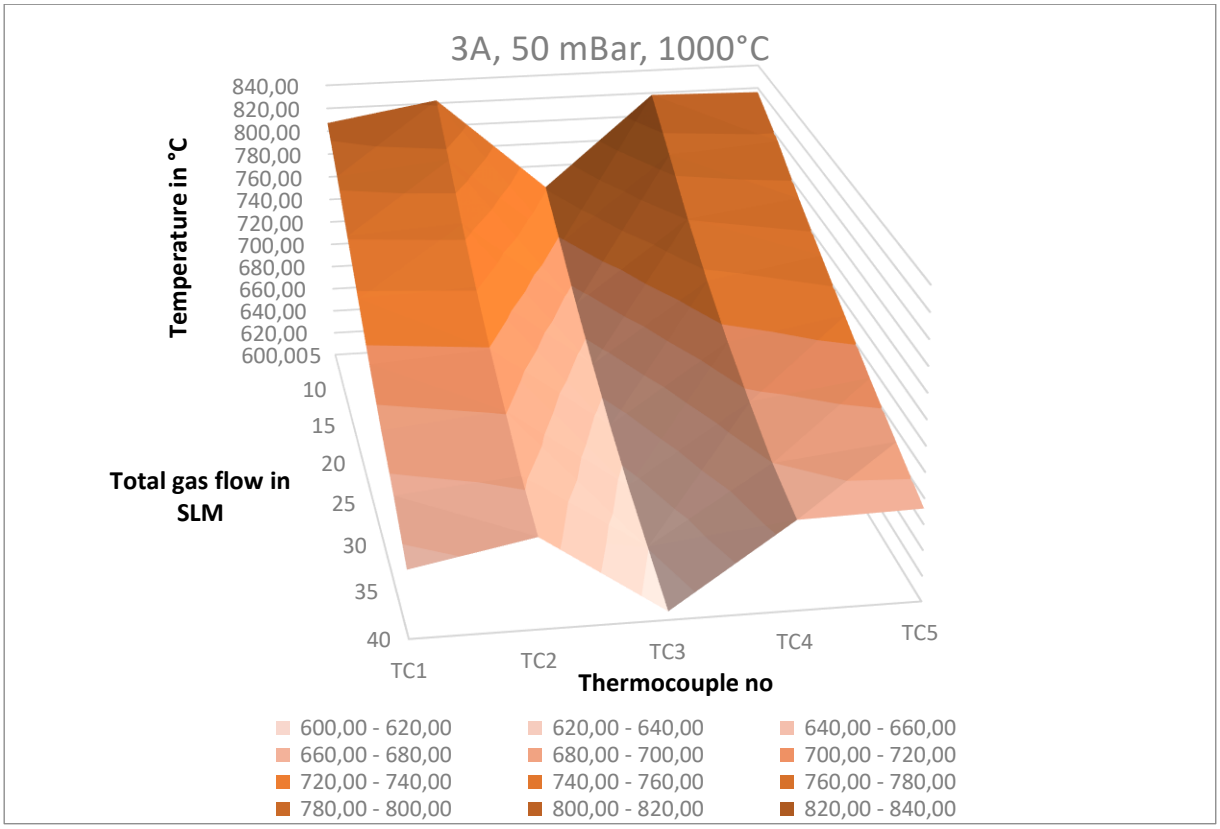

Figure 74 Position 3A at 50 mBar background pressure and at a susceptor temperature of 1000°C.

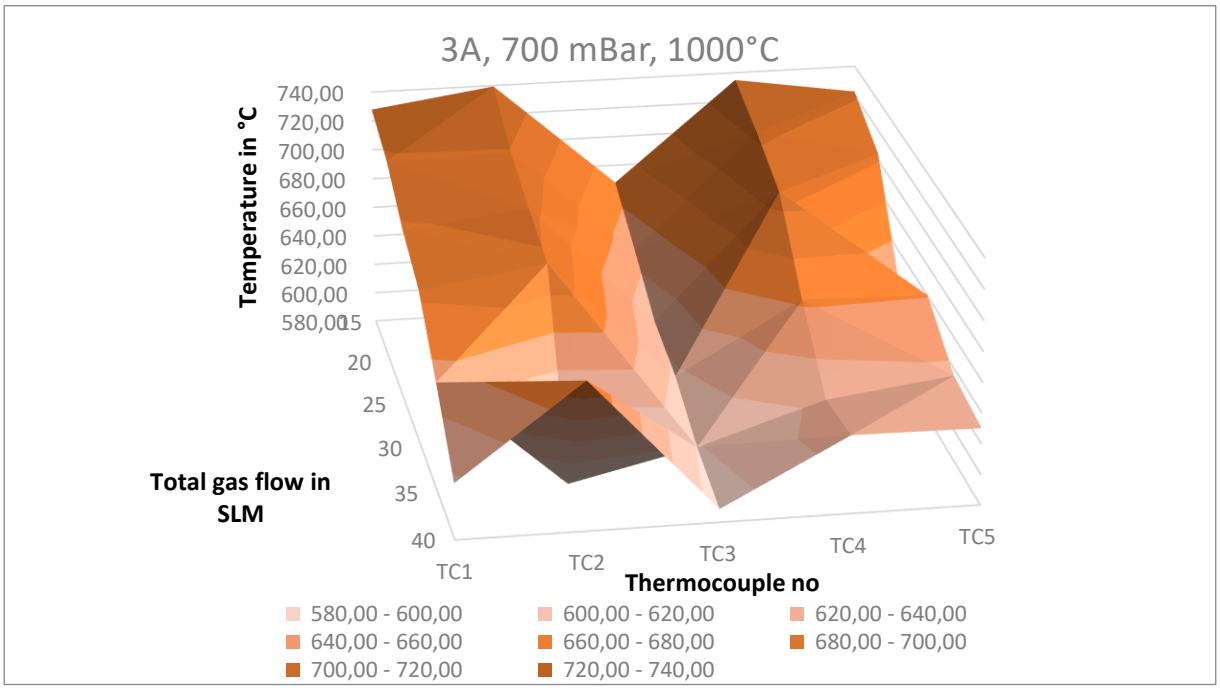

Figure 75 Position 3A at 700 mBar background pressure and at a susceptor temperature of 1000°C.

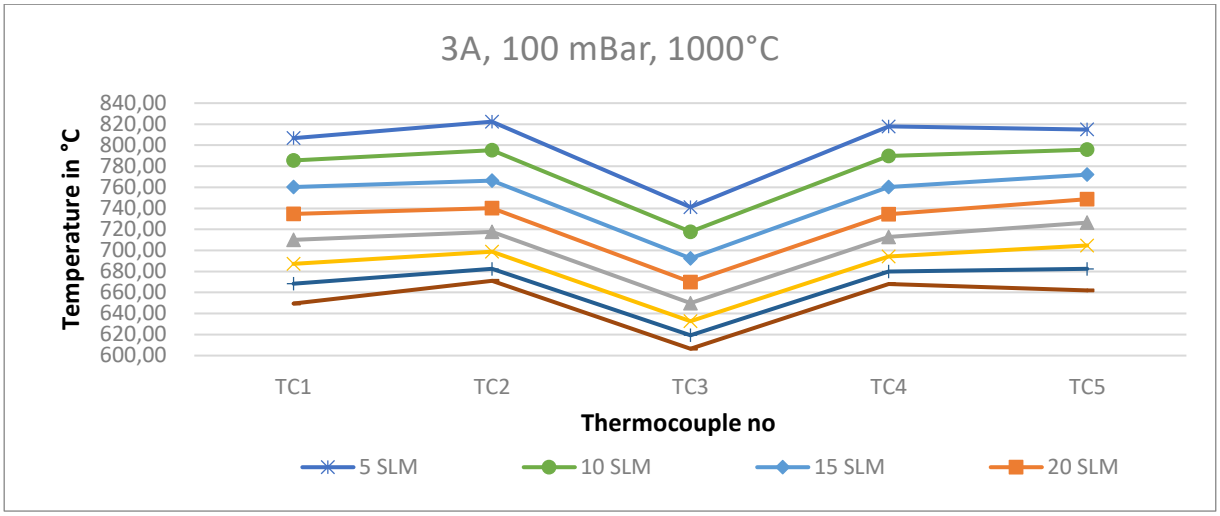

Figure 76 Position 3A with T over TC at 100 mBar background pressure and at a susceptor temperature of 1000°C.

9.8.2 Temperature over pressures at fixed flows

9.8.2.1 Position 1B

At 450 °C, in Figure 77 the temperature profile is planar with a convex bulge between TC3 and TC4. This profile is seen for gas flows at 15, 20, 25, 30 and 35 SLM with background pressures at 20, 50, 100, 200 and 700 mBar and the profile look like Figure 78. The result is presented at 15, 25 and 35 SLM. The results show a depression at TC2 and elevated temperature at TC4 with flows up to 35 SLM. In Figure 79 the temperature profile is planar at 35 SLM up to 200 mBar in background pressure and it also shows elevated temperature at TC4 and a spike at 700 mBar, TC5.

At 1000 °C, in Figure 80 the temperature profile is planar with a convex bulge at TC4. This profile is seen for gas flows at 15, 20, 25, 30 and 35 SLM with background pressures at 20, 50, 100, 200 and 700 mBar and the profile look like Figure 81. The result is presented at 15, 25 and 35 SLM. The results show a depression at TC2 and elevated temperature at TC4 with flows up to 35 SLM. In Figure 82, along with Figure 80 and Figure 81, turbulent flow is indicated.

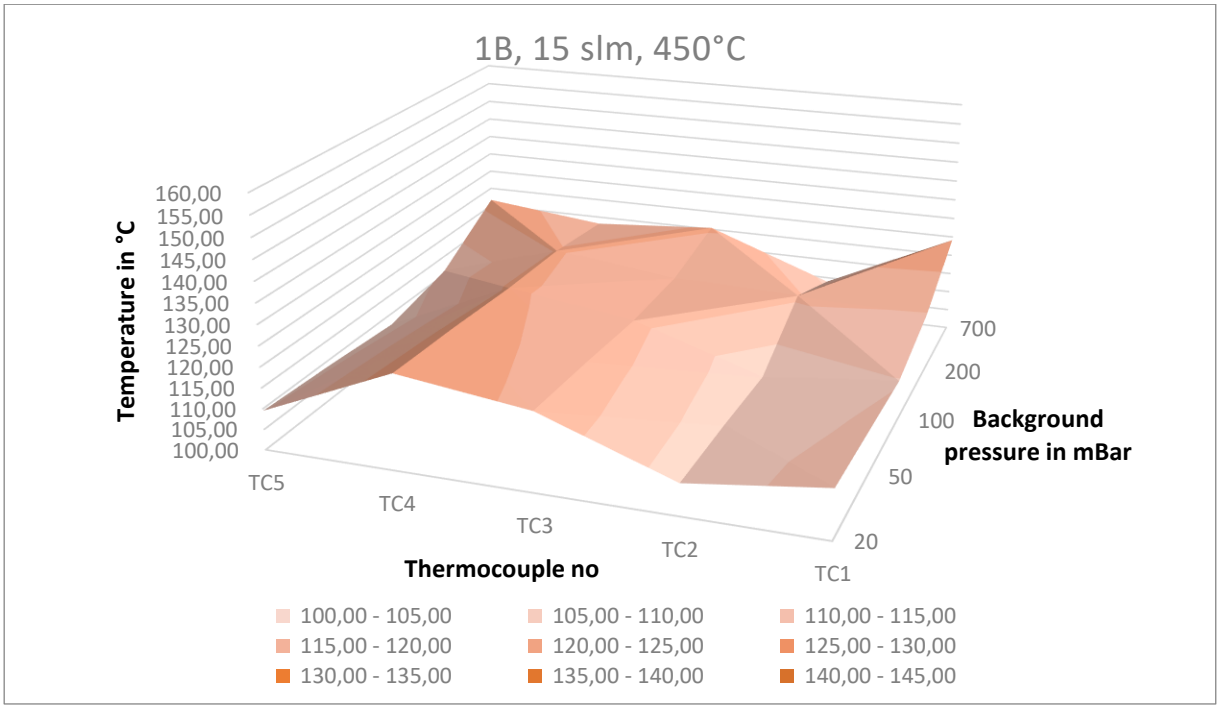

Figure 77 Position 1B at 15 SLM gas flow and at a susceptor temperature of 450°C.

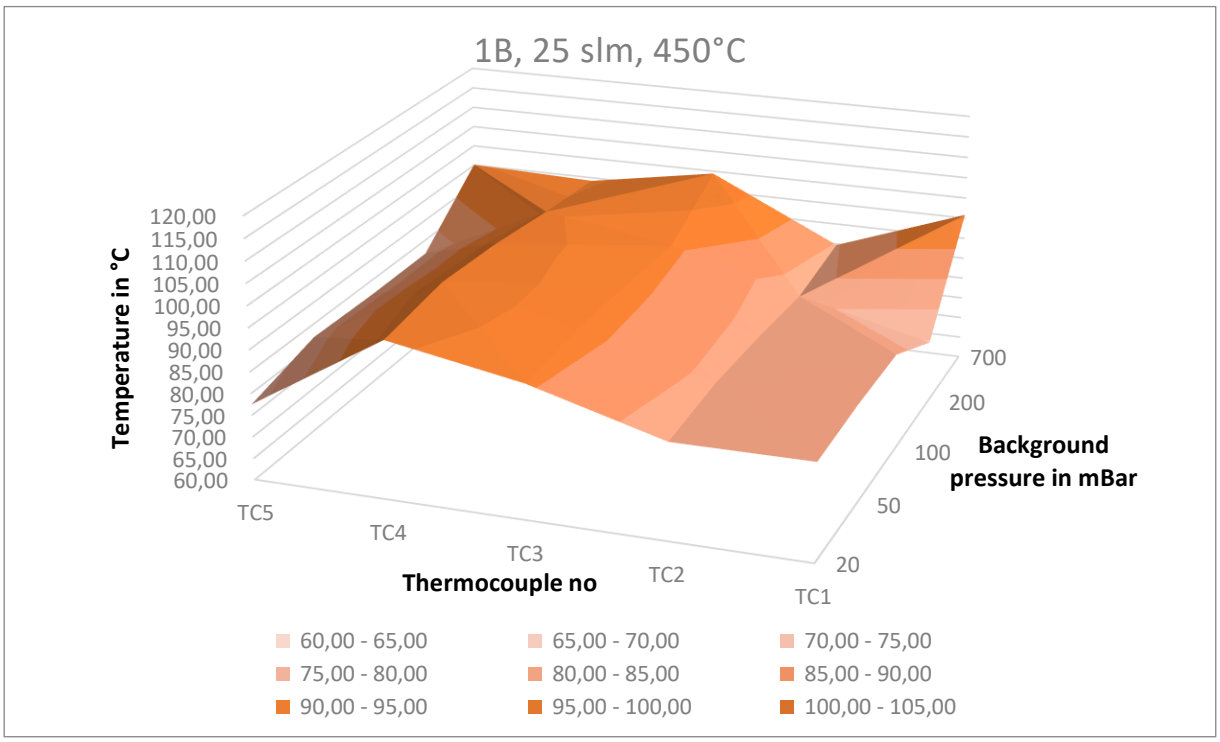

Figure 78 Position 1B at 25 SLM gas flow and at a susceptor temperature of 450°C.

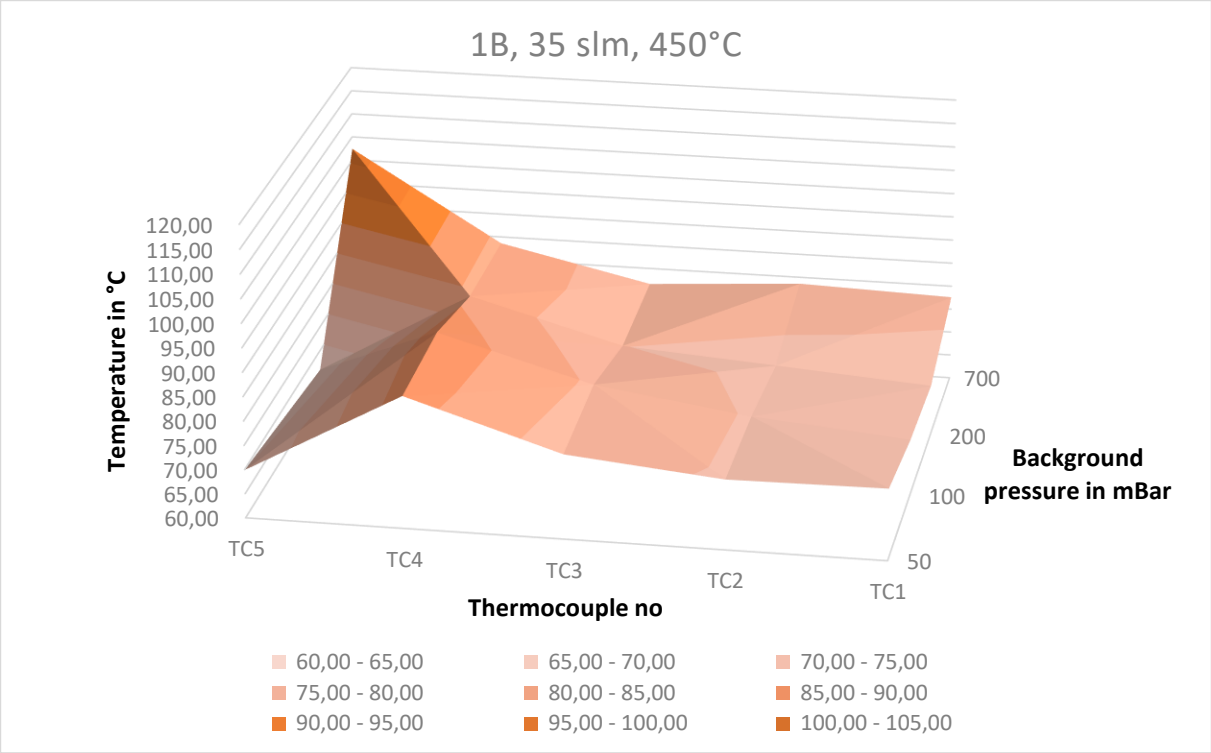

Figure 79 Position 1B at 35 SLM gas flow and at a susceptor temperature of 450°C.

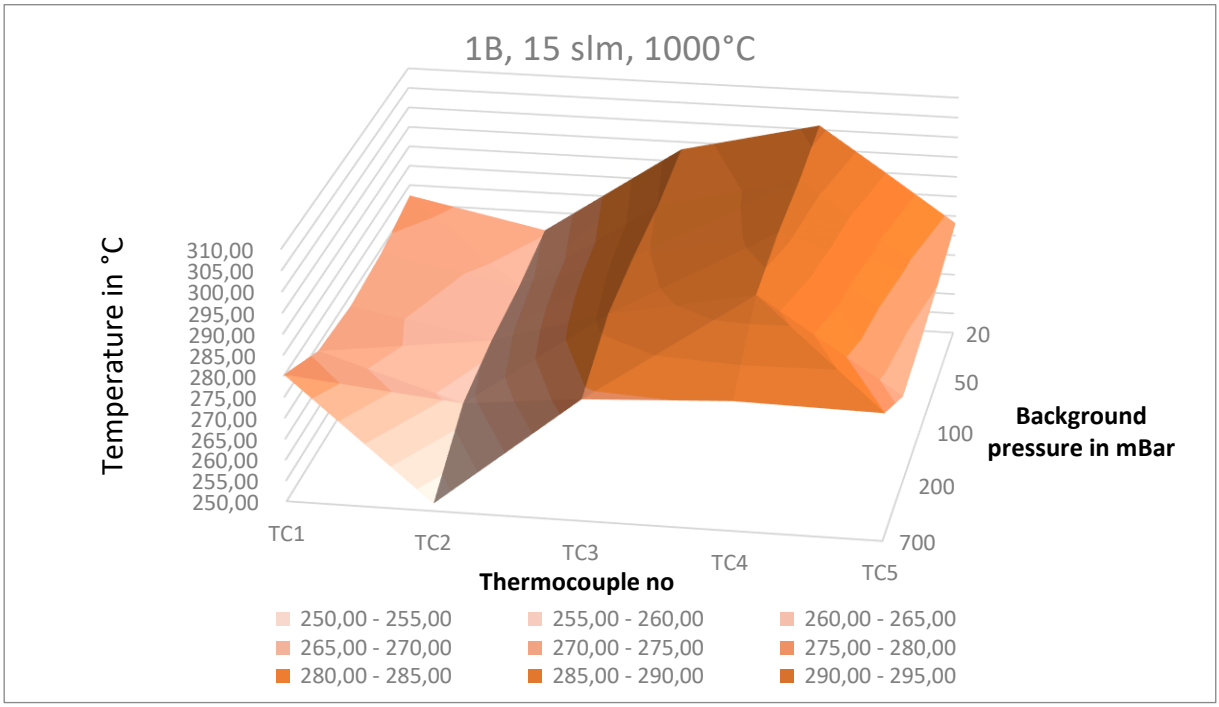

Figure 80 Position 1B at 15 SLM gas flow and at a susceptor temperature of 1000°C.

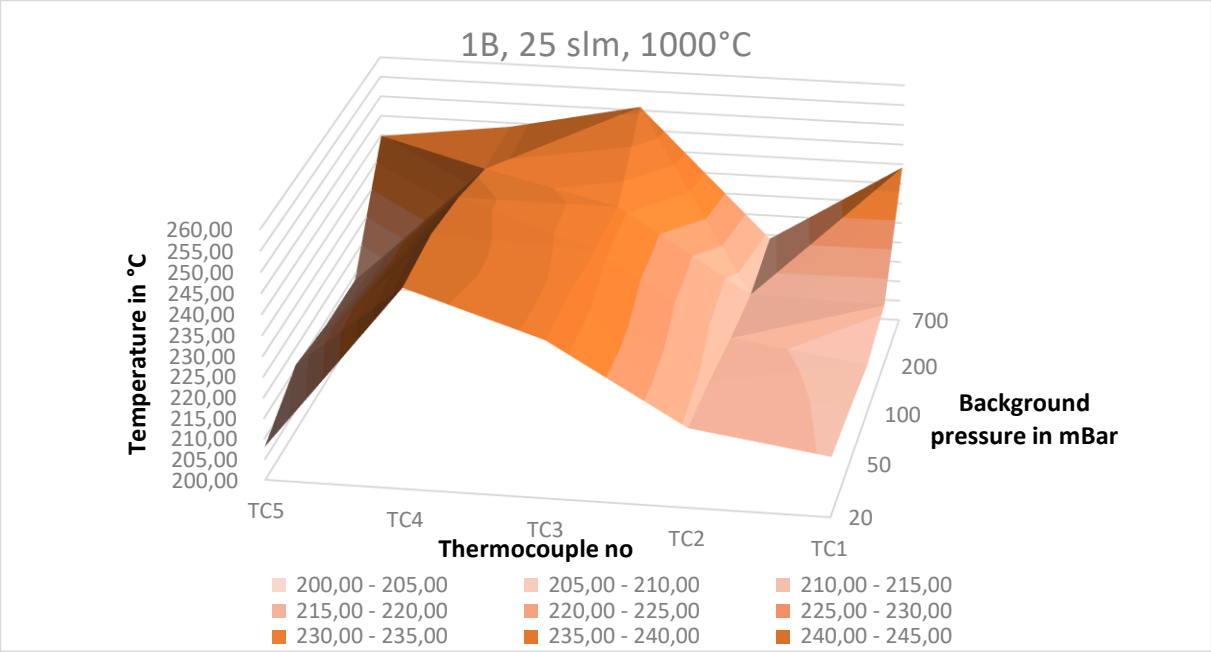

Figure 81 Position 1B at 25 SLM gas flow and at a susceptor temperature of 1000°C.

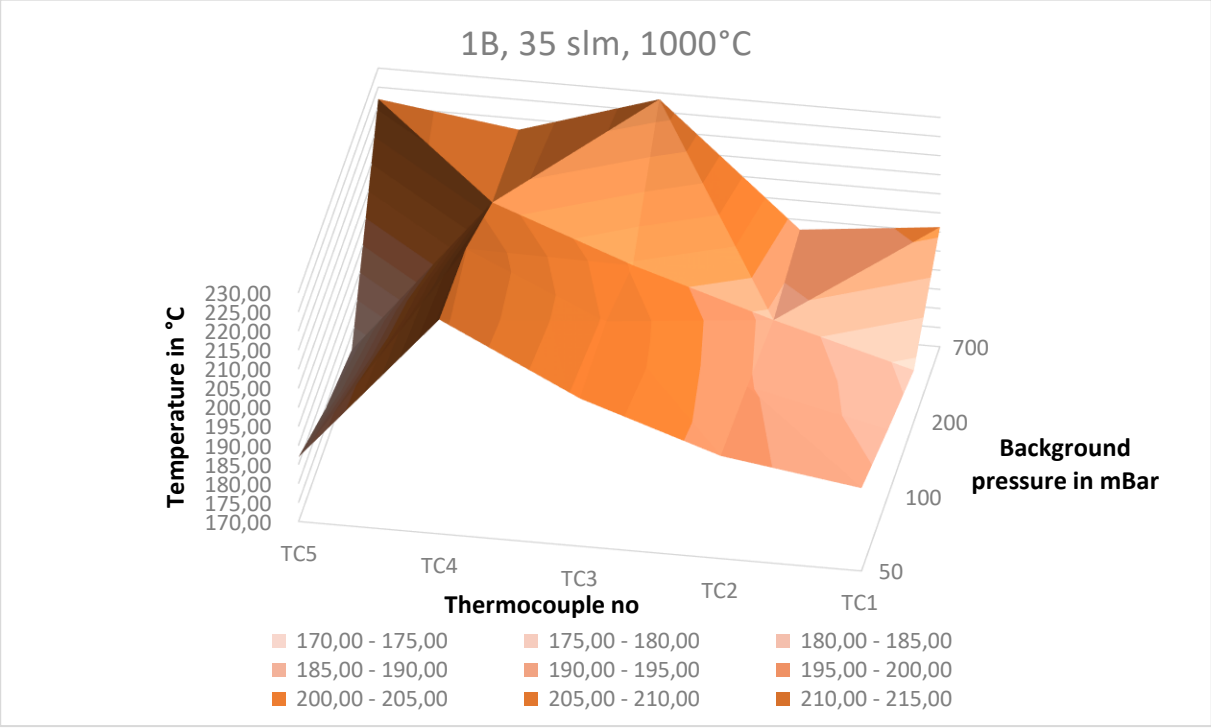

Figure 82 Position 1B at 35 SLM gas flow and at a susceptor temperature of 1000°C.

9.8.2.2 Position 2A

At 450 °C, in Figure 83 the temperature profile is planar with a small convex bulge TC3. This profile is seen for gas flows at 15, 20, 25, 30 and 35 SLM with background pressures at 20, 50, 100, 200 and 700 mBar and the profile look like Figure 84. The result is presented at 15, 25 and

35 SLM. The results show a small depression at TC2 at 15 SLM but is even out with higher flows of 20 SLM and up. The result shows strong indications of laminar flow up to 200 mBar at flows up to 30 SLM and up to 100 mBar at 35 SLM in Figure 85.

At 1000 °C, in Figure 86 the temperature profile is planar with a small convex bulge between TC2 and TC3. This profile is seen for gas flows at 15, 20, 25 and 30 SLM with background pressures at 20, 50, 100, 200 and 700 mBar and the profile look like Figure 87. At 35 SLM the profile is planar between TC2 and TC4 with decreased temperatures at TC1 and TC5. The result is presented at 15, 25, 35 and 40 SLM. The results show a small depression at TC4 at 15 SLM but is even out with higher flows of 30 SLM and up. The result show strong indications of laminar flow up to 200 mBar at flows up to 30 SLM and up to 100 mBar at 35 and 40 SLM in Figure 88 and Figure 89.

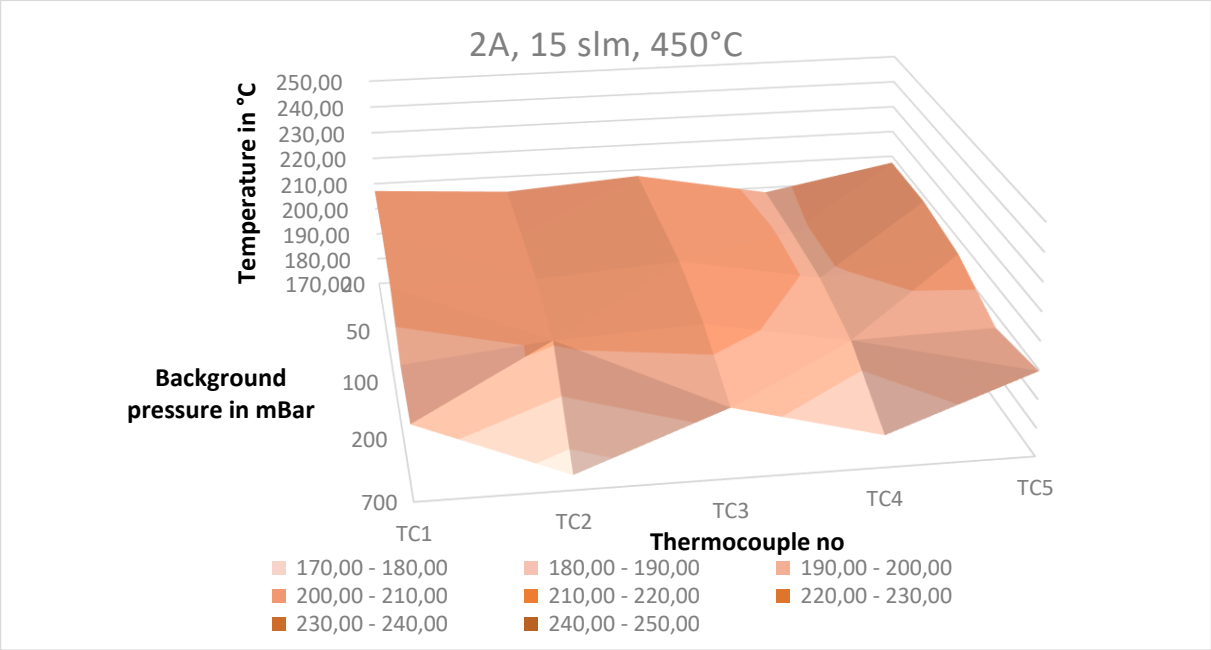

Figure 83 Position 2A at 15 SLM gas flow and at a susceptor temperature of 450°C.

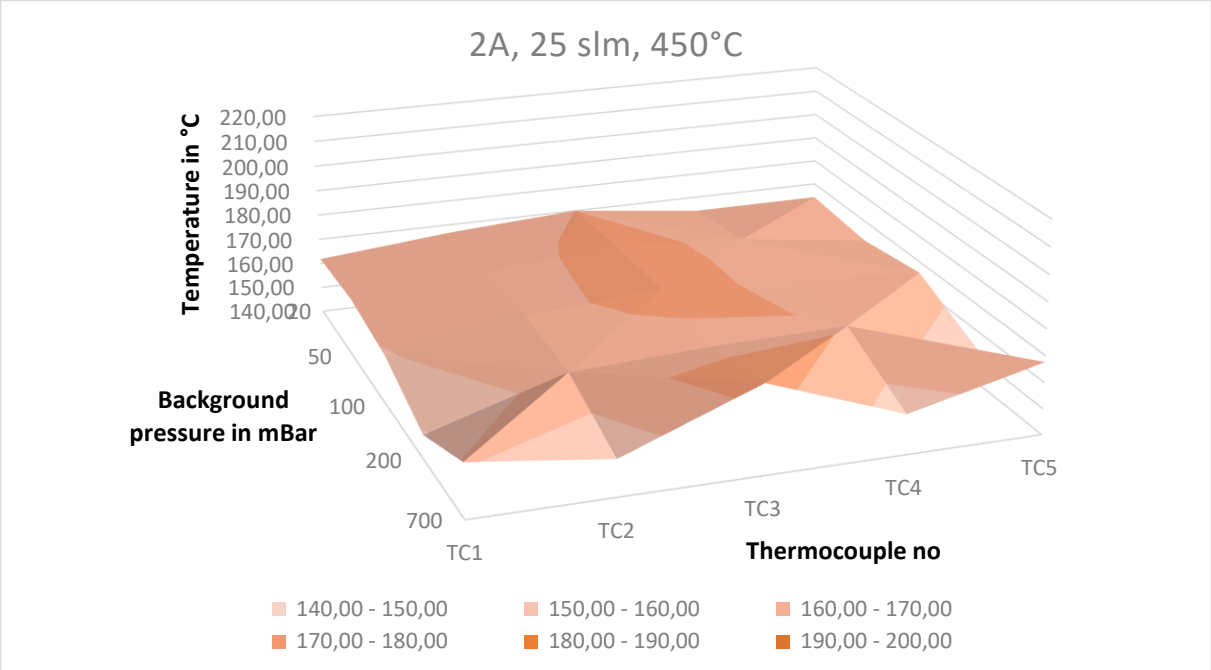

Figure 84 Position 2A at 25 SLM gas flow and at a susceptor temperature of 450°C.

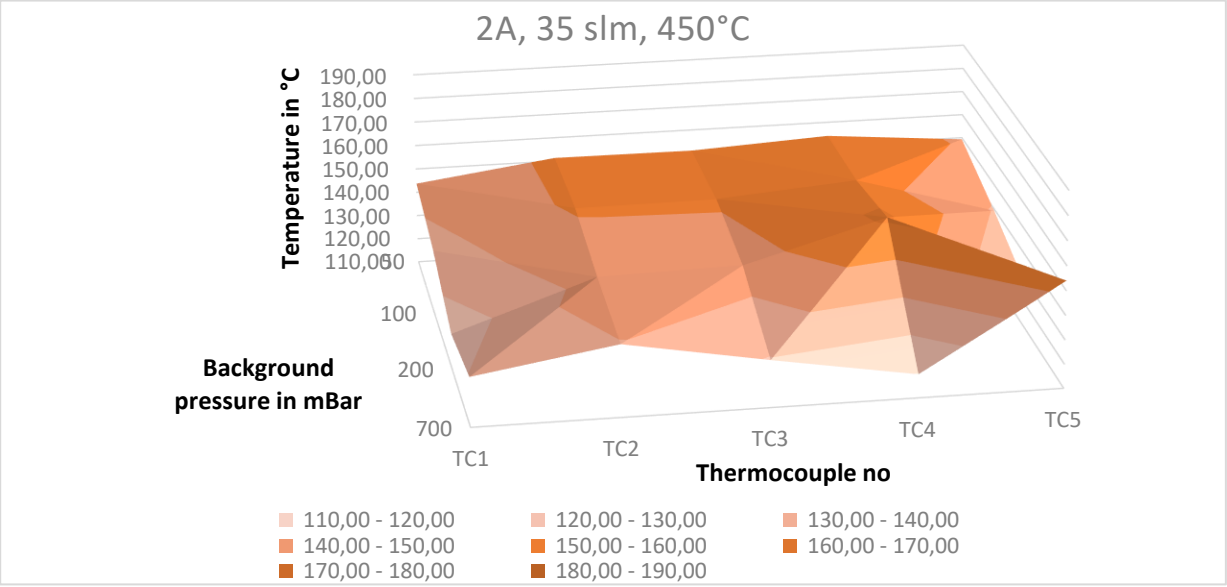

Figure 85 Position 2A at 35 SLM gas flow and at a susceptor temperature of 450°C.

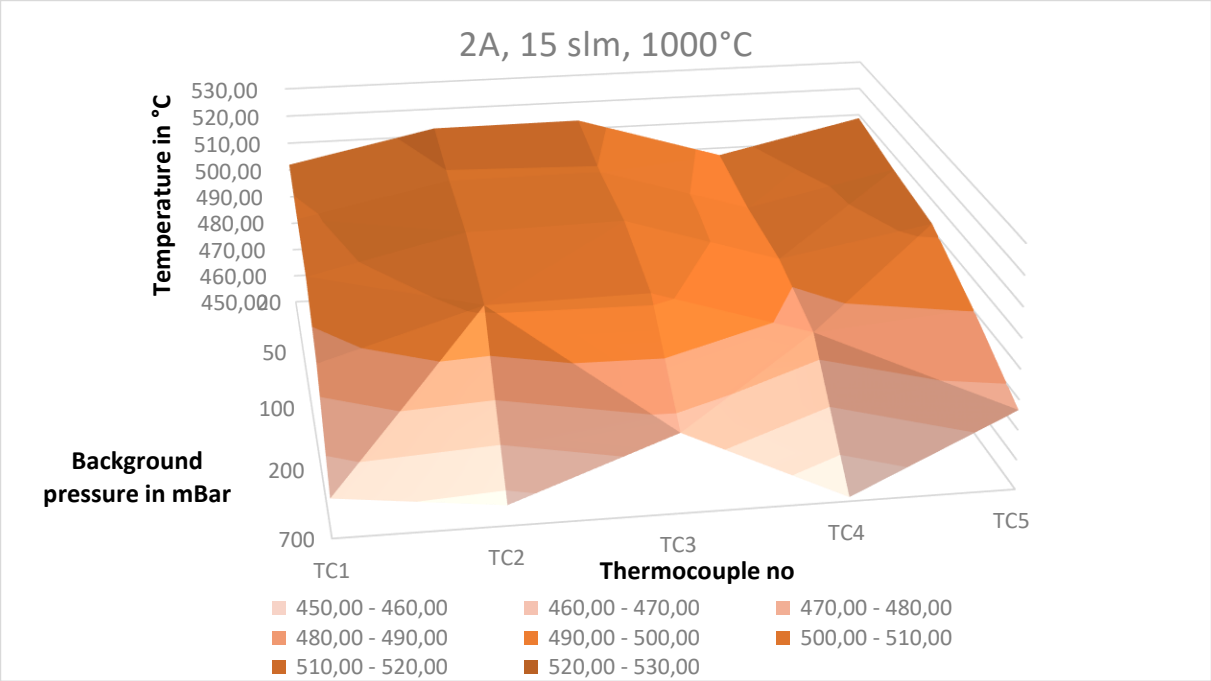

Figure 86 Position 2A at 15 SLM gas flow and at a susceptor temperature of 1000°C.

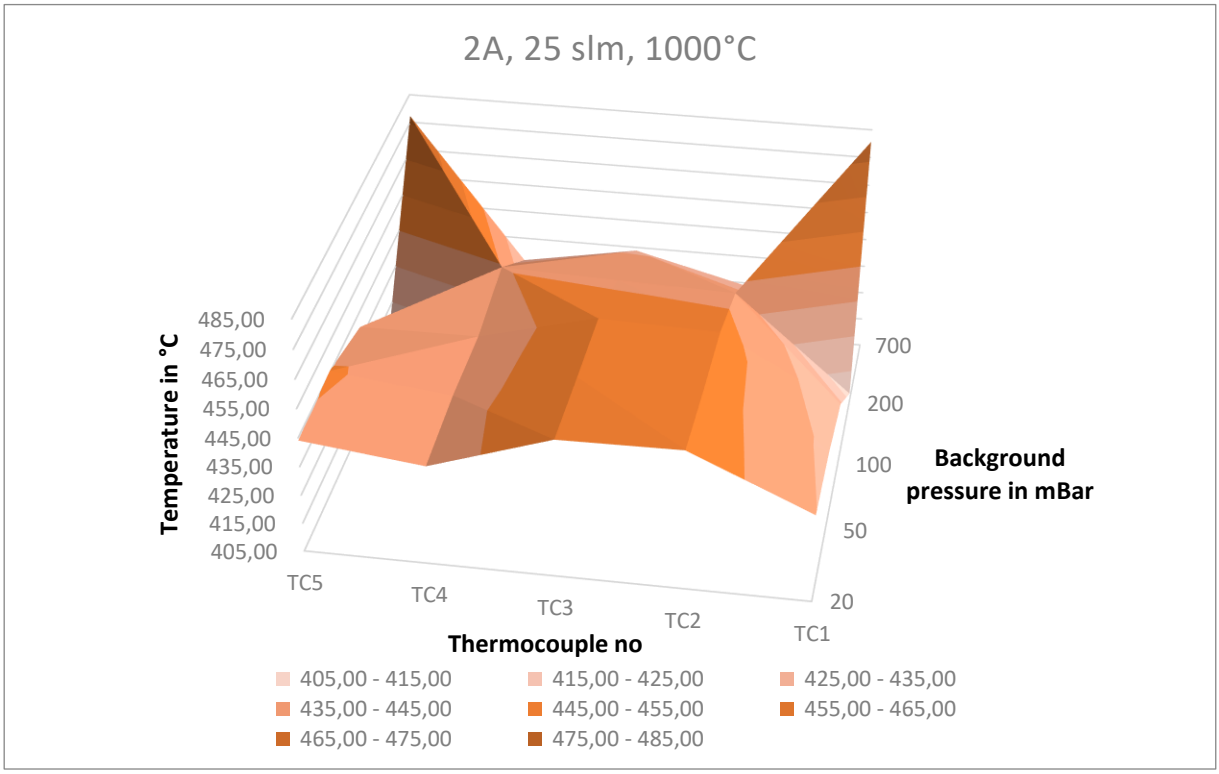

Figure 87 Position 2A at 25 SLM gas flow and at a susceptor temperature of 1000°C.

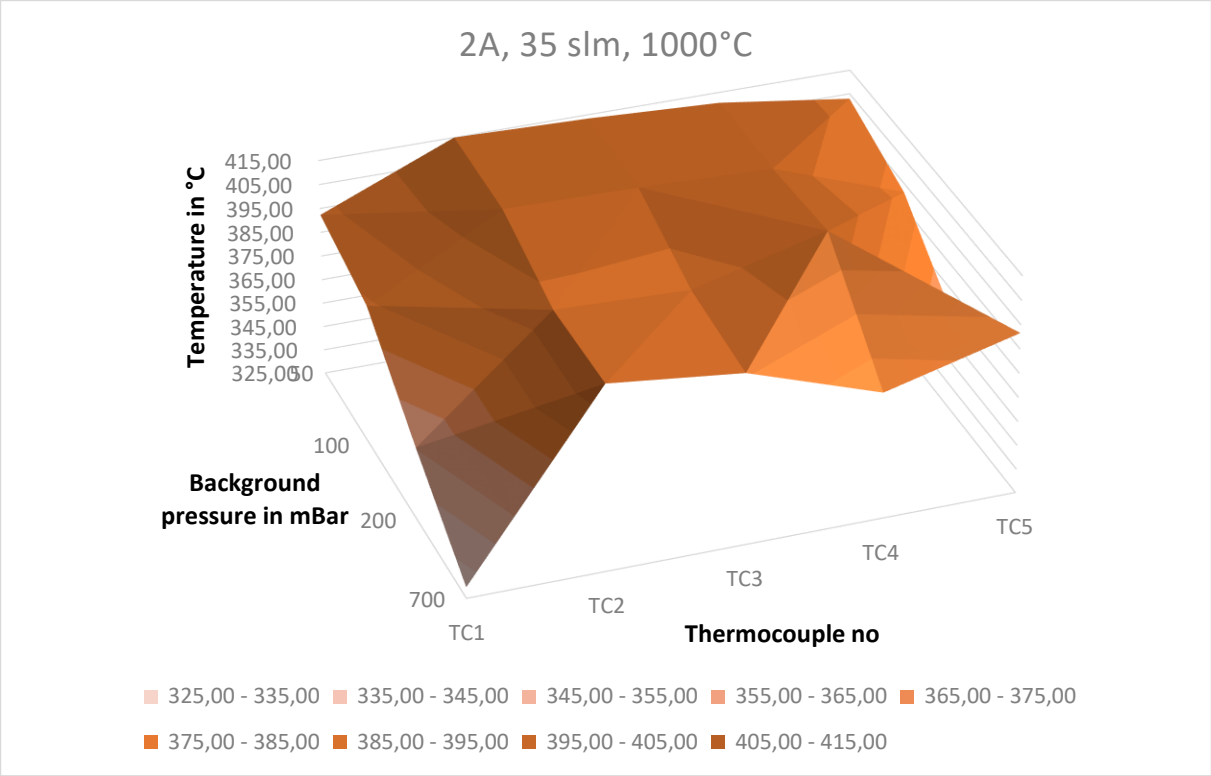

Figure 88 Position 2A at 35 SLM gas flow and at a susceptor temperature of 1000°C.

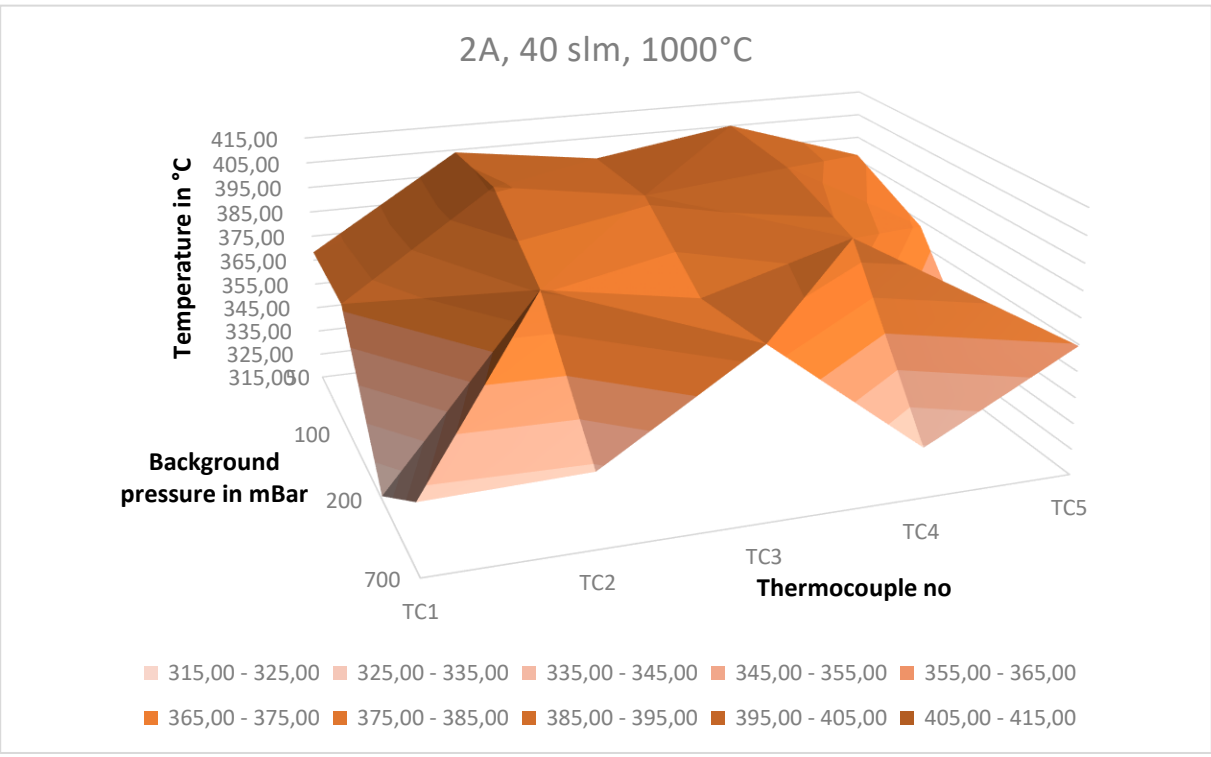

Figure 89 Position 2A at 40 SLM gas flow and at a susceptor temperature of 1000°C.

9.8.2.3 Position 2B

At 450 °C, in Figure 90 the temperature profile is a V-shaped plane with descending temperature towards the center, TC3. This profile is seen for gas flows at 15, 20, 25 and 30 SLM with background pressures at 20, 50, 100, 200 and 700 mBar and the profile look like Figure 91. At 35 SLM the profile shows no indication on laminar flow. The result is presented at 15, 25 and 35 SLM. The result show strong indications of laminar flow up to 700 mBar at flows up to 25 SLM and turbulent flow at all background pressures at 35 SLM in Figure 92.

At 1000 °C, in Figure 93 the temperature profile is a V-shaped plane with descending temperature towards the center, TC3. This profile is seen for gas flows at 15, 20, 25 and 30 SLM with background pressures at 20, 50, 100, 200 and 700 mBar and the profile look like Figure 94. At 35 SLM the profile shows no indication on laminar flow. The result is presented at 15, 25 and 35 SLM. The result show strong indications of laminar flow up to 700 mBar at flows up to 25 SLM and turbulent flow at all background pressures at 35 SLM in Figure 95.

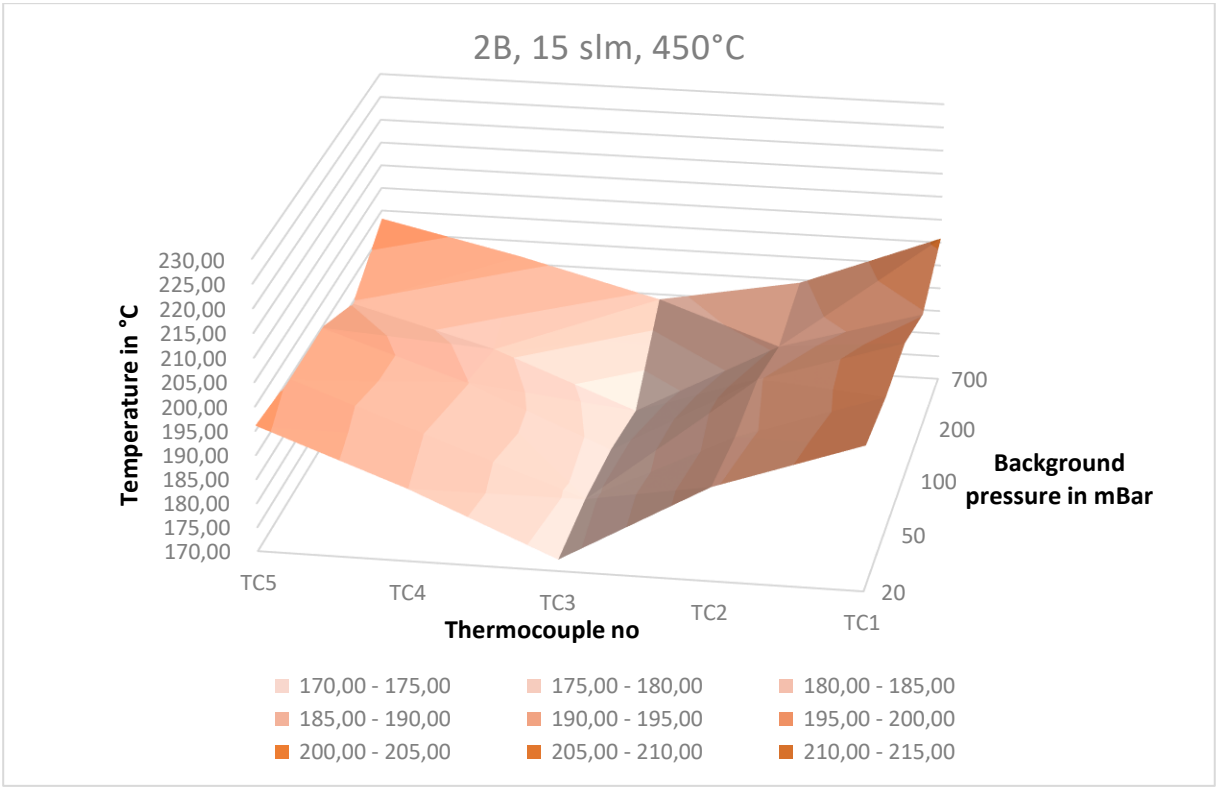

Figure 90 Position 2B at 15 SLM gas flow and at a susceptor temperature of 450°C.

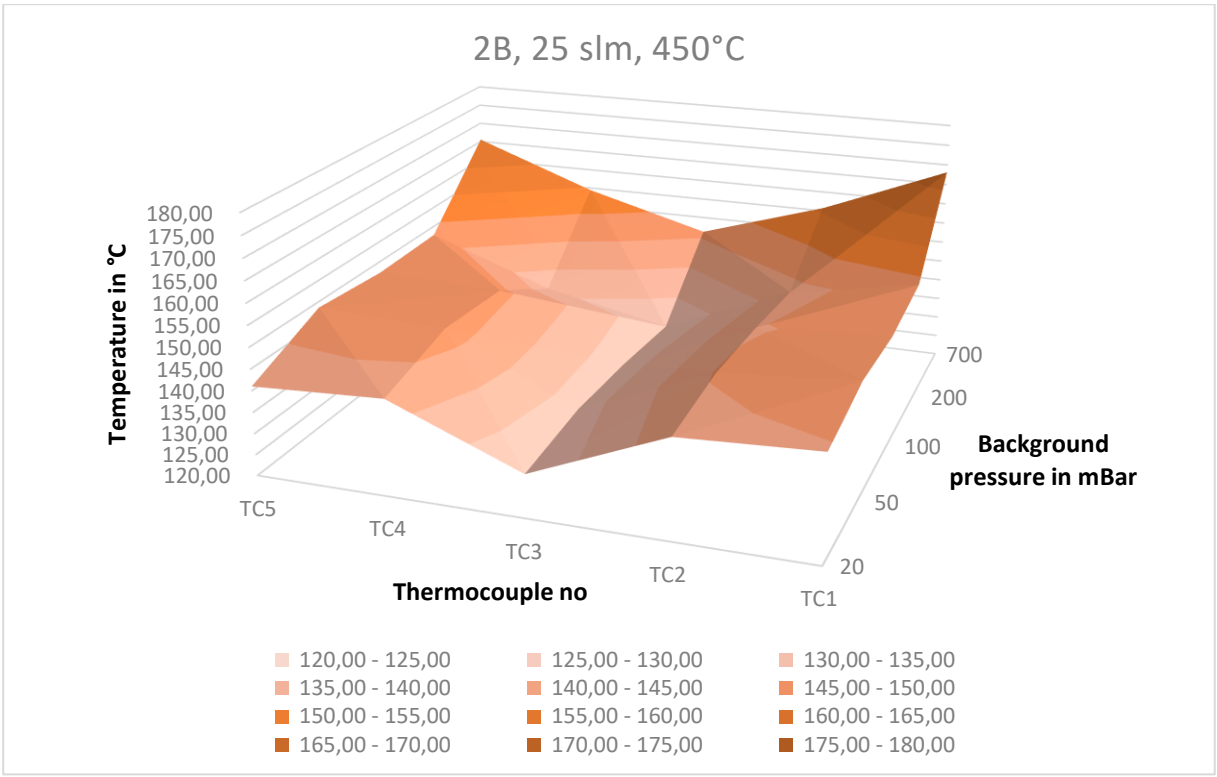

Figure 91 Position 2B at 25 SLM gas flow and at a susceptor temperature of 450°C.

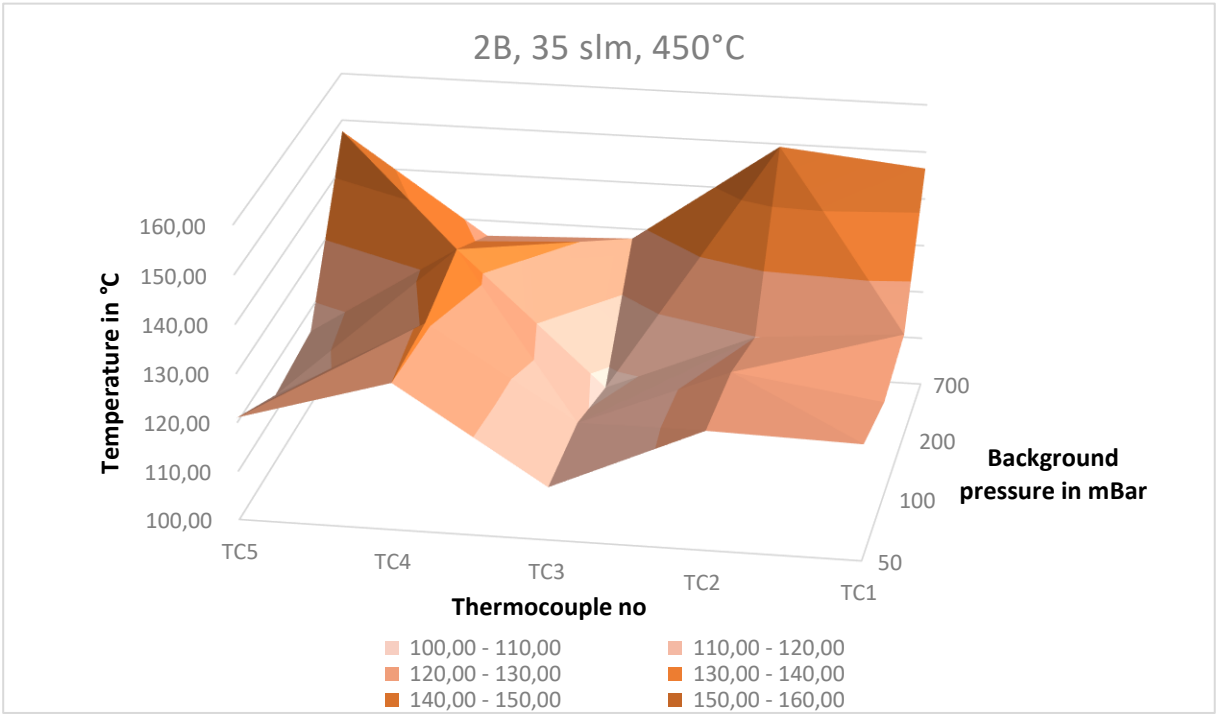

Figure 92 Position 2B at 35 SLM gas flow and at a susceptor temperature of 450°C.

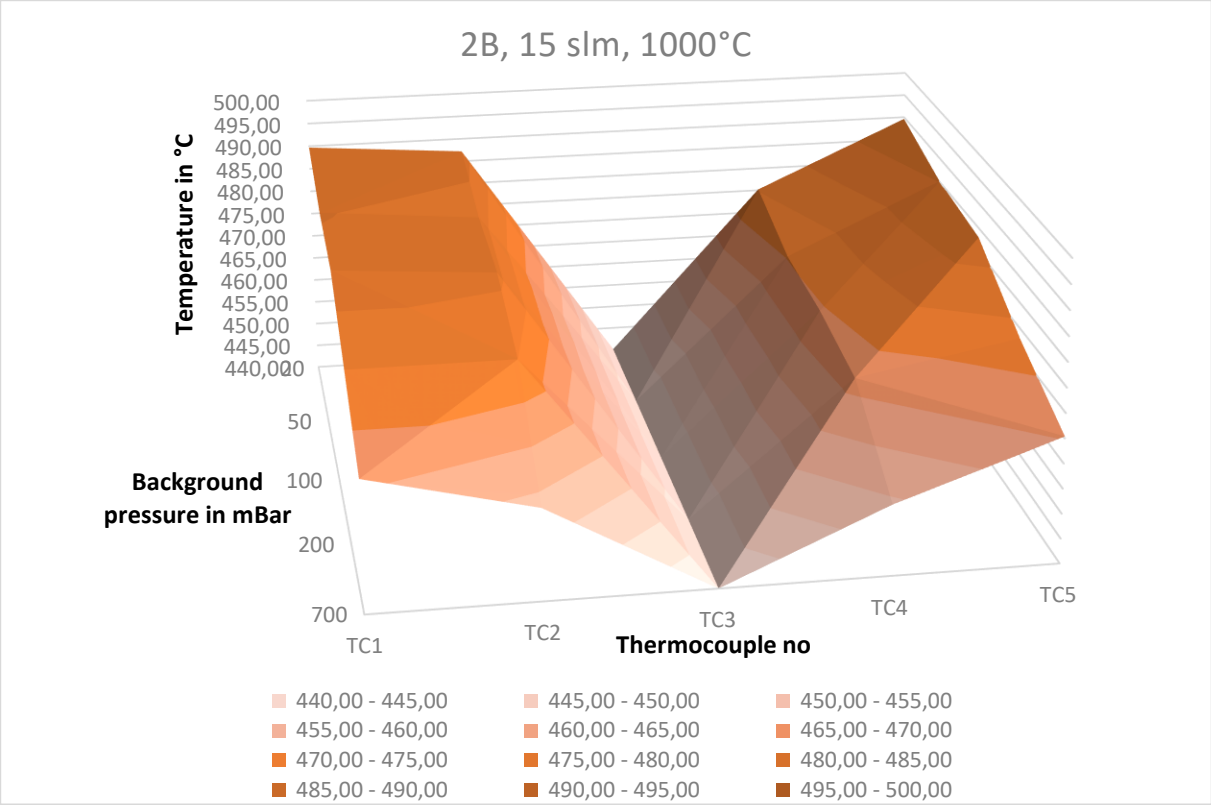

Figure 93 Position 2B at 15 SLM gas flow and at a susceptor temperature of 1000°C.

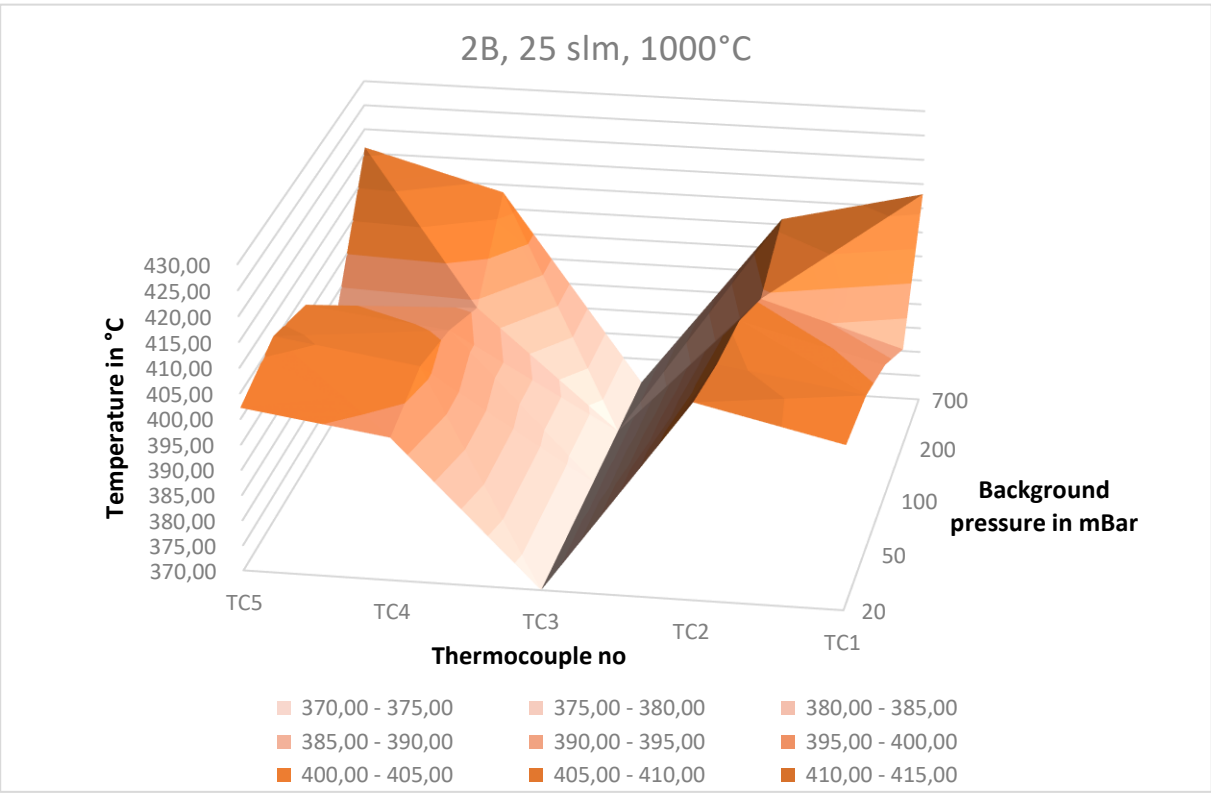

Figure 94 Position 2B at 25 SLM gas flow and at a susceptor temperature of 1000°C.

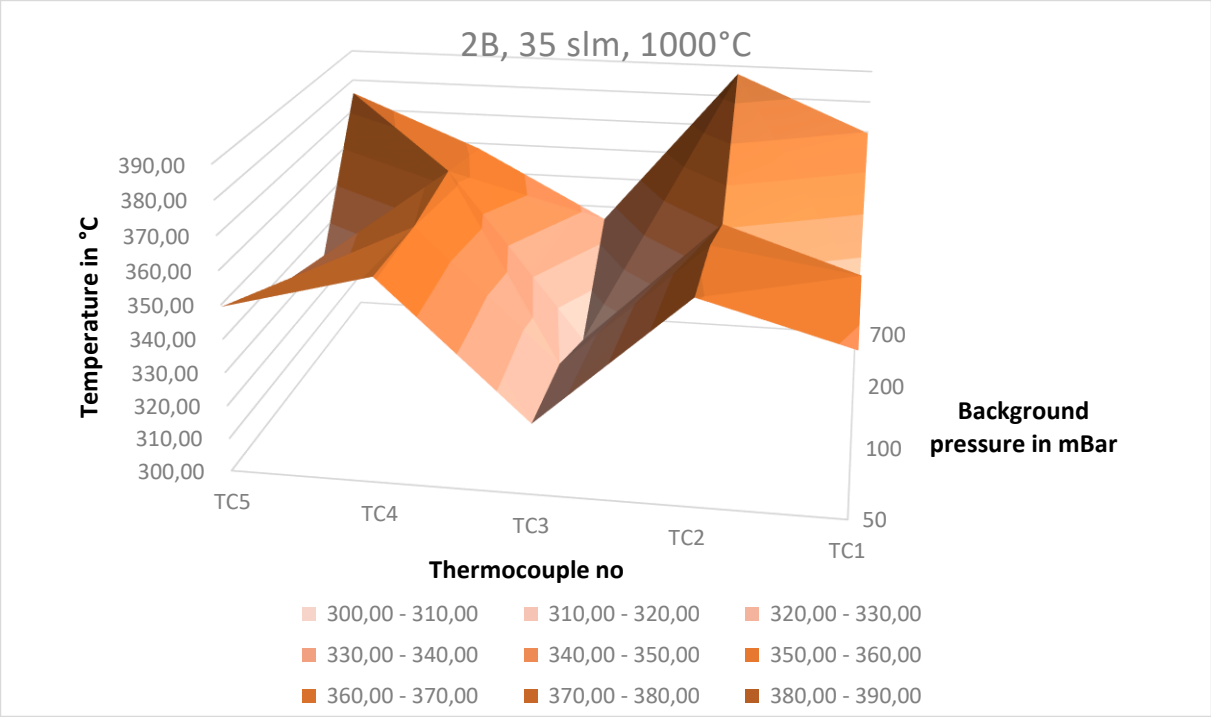

Figure 95 Position 2B at 35 SLM gas flow and at a susceptor temperature of 1000°C.

9.8.2.4 Position 2C

At 450 °C, in Figure 96 the temperature profile is a V-shaped plane with descending temperature towards the center, TC3. This profile is seen for gas flows at 15, 20, 25 and 30 SLM with background pressures at 20, 50, 100, 200 and 700 mBar and the profile look like Figure 97. The result is presented at 15, 25 and 35 SLM. The result show strong indications of laminar flow up to 700 mBar at 15 SLM, likewise at 25 SLM except for 20 mBar, and turbulent flow at all background pressures at 35 SLM in Figure 98.

At 1000 °C, in Figure 99 the temperature profile is a V-shaped plane with descending temperature towards the center, TC3. The data shows a plateau between TC4 and TC5 as with TC1 and TC2. This profile is seen for gas flows at 15, 20, 25, 30 and 35 SLM with background pressures at 20, 50, 100, 200 and 700 mBar and the profile look like in Figure 100. The result is presented at 15, 25 and 35 SLM. The result show strong indications of laminar flow up to 700 mBar at 15 SLM. Figure 100 and Figure 101 indicates a turbulent flow up to 100 mBar and a laminar flow at 200 and 700 mBar.

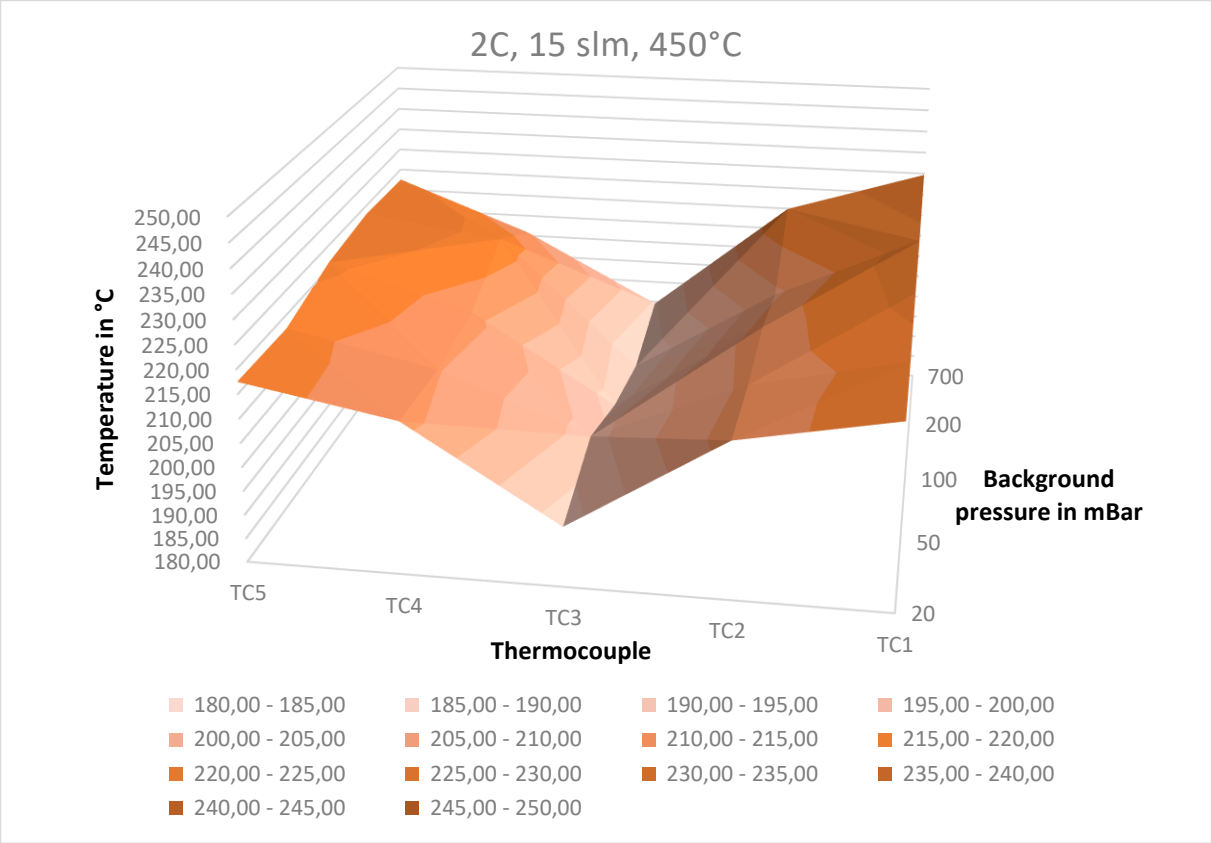

Figure 96 Position 2C at 15 SLM gas flow and at a susceptor temperature of 450°C.

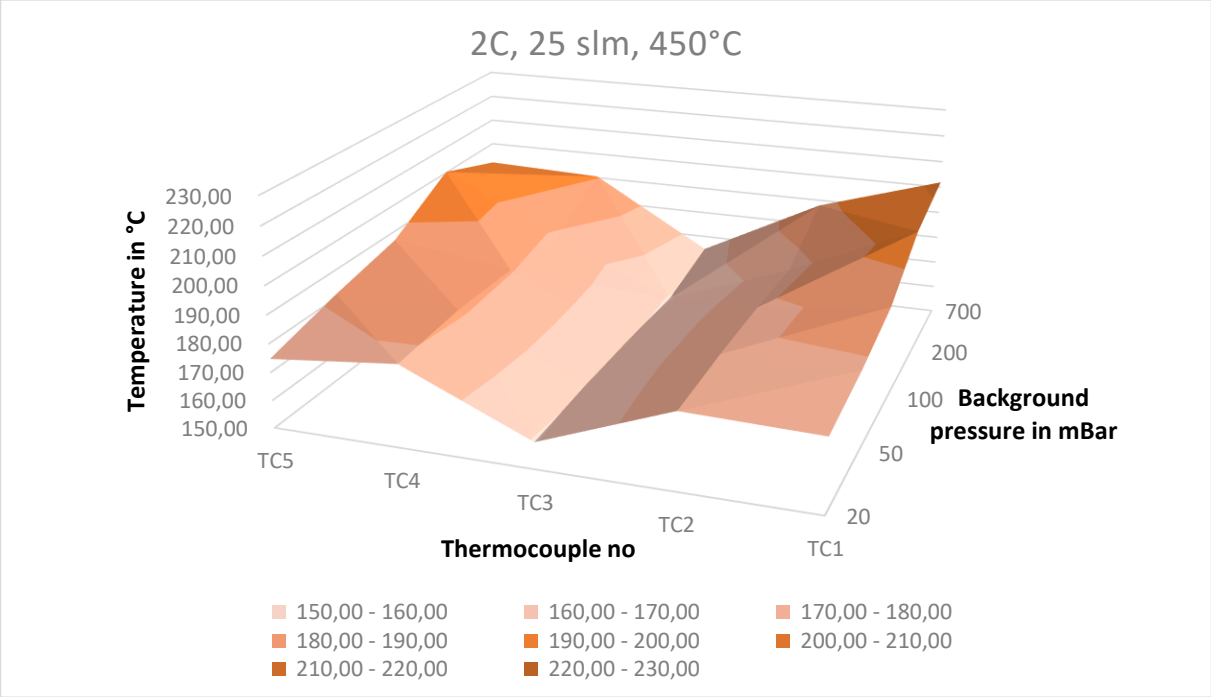

Figure 97 Position 2C at 25 SLM gas flow and at a susceptor temperature of 450°C.

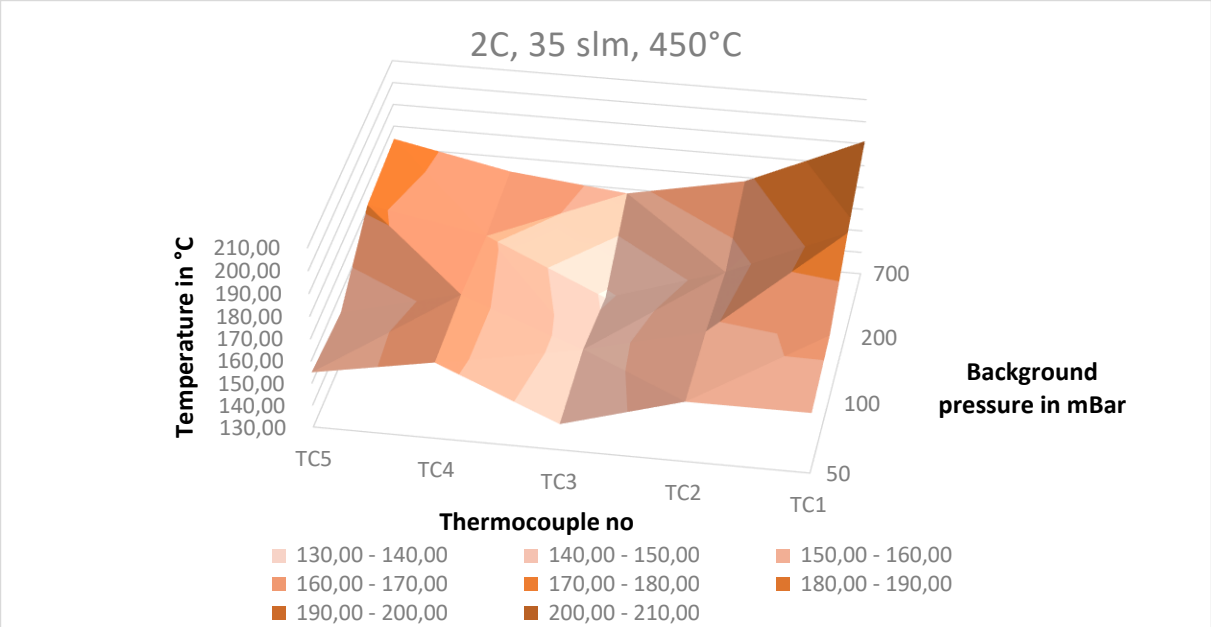

Figure 98 Position 2C at 35 SLM gas flow and at a susceptor temperature of 450°C.

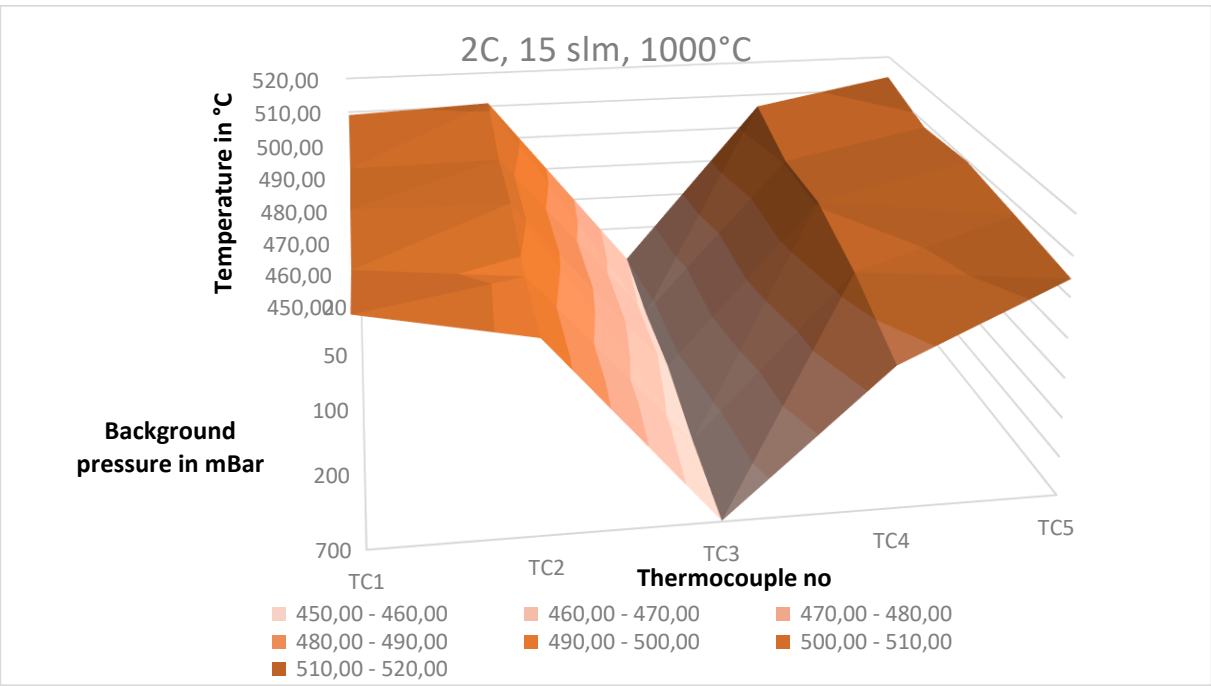

Figure 99 Position 2C at 15 SLM gas flow and at a susceptor temperature of 1000°C.

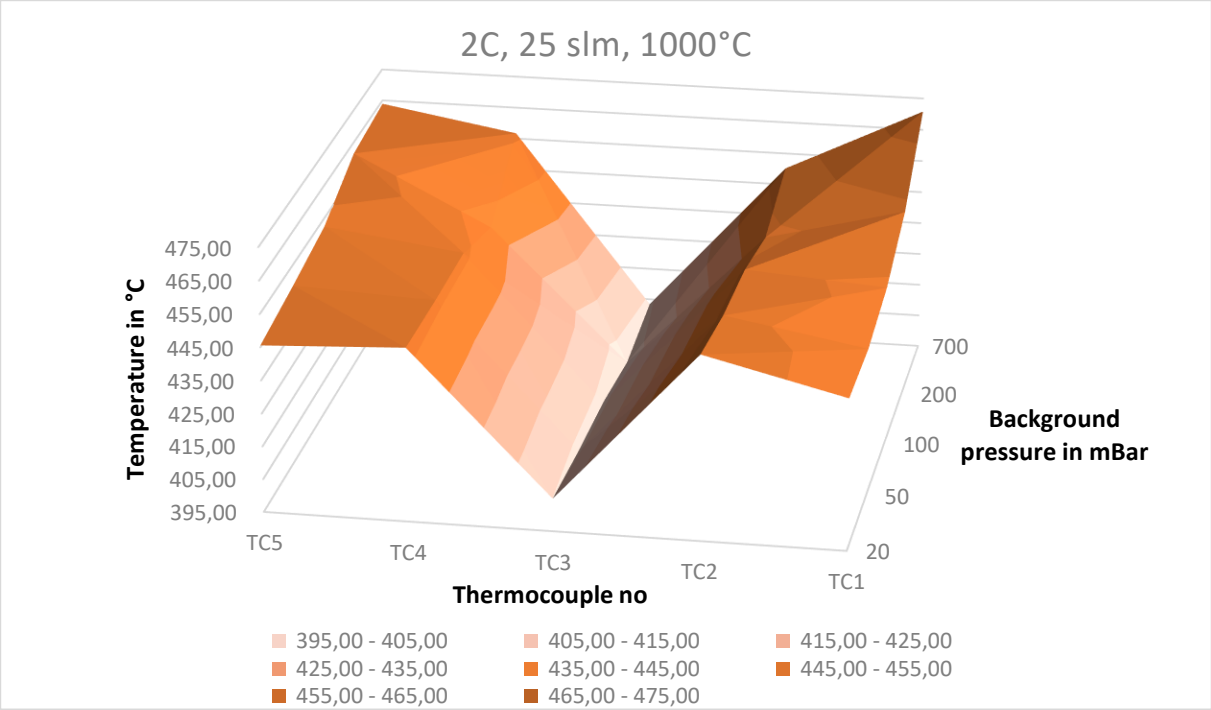

Figure 100 Position 2C at 25 SLM gas flow and at a susceptor temperature of 1000°C.

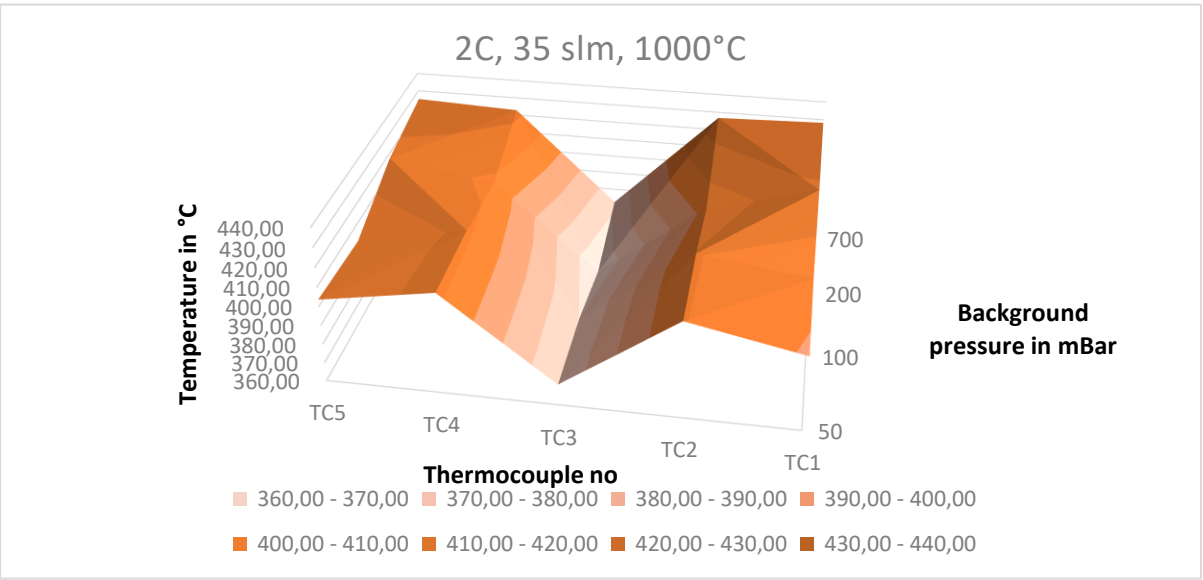

Figure 101 Position 2C at 35 SLM gas flow and at a susceptor temperature of 1000°C.

9.8.2.5 Position 3A

At 450 °C, in

Figure 102 the temperature profile is a V-shaped plane with descending temperature towards the center, TC3. This profile is seen for gas flows at 15, 20, 25, 30, 35 and 40 SLM with background pressures at 20, 50, 100, 200 and 700 mBar and the profile look like Figure 103. The result is presented at 15, 25, 35 and 40 SLM. The result show strong indications of laminar

flow up to 200 mBar at 15 and 25 SLM and 50 mBar for 35 SLM in Figure 104. Indications of laminar flow is seen at 700 mBar for 40 SLM in Figure 105, but not at the other pressures.

At 1000 °C, in Figure 106 the temperature profile is a V-shaped plane with descending temperature towards the center, TC3. The data shows a plateau between TC4 and TC5 as with TC1 and TC2. This profile is seen for gas flows at 15, 20, 25, 30, 35 and 40 SLM with background pressures at 20, 50, 100, 200 and 700 mBar and the profile look like Figure 107. The result is presented at 15, 25, 35 and 40 SLM. The result show strong indications of laminar flow up to 200 mBar at 15 and 25 SLM and 100 mBar for 35 SLM in Figure 108. Figure 109 at 40 SLM indicates turbulent flow at all background pressures.

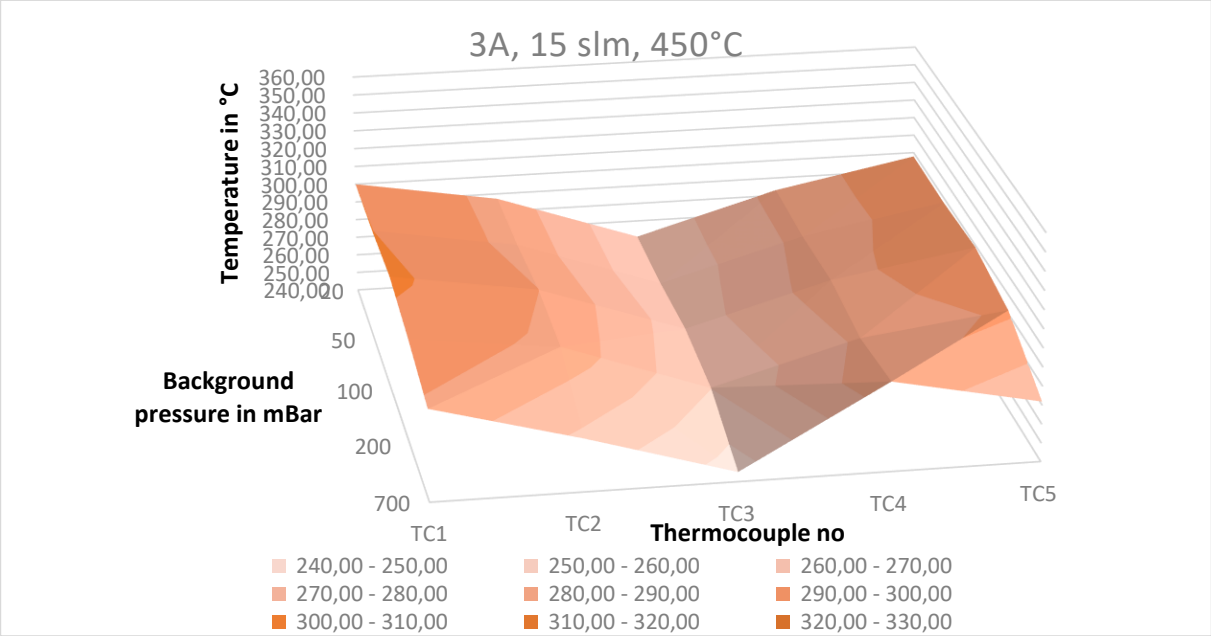

Figure 102 Position 3A at 15 SLM gas flow and at a susceptor temperature of 450°C.

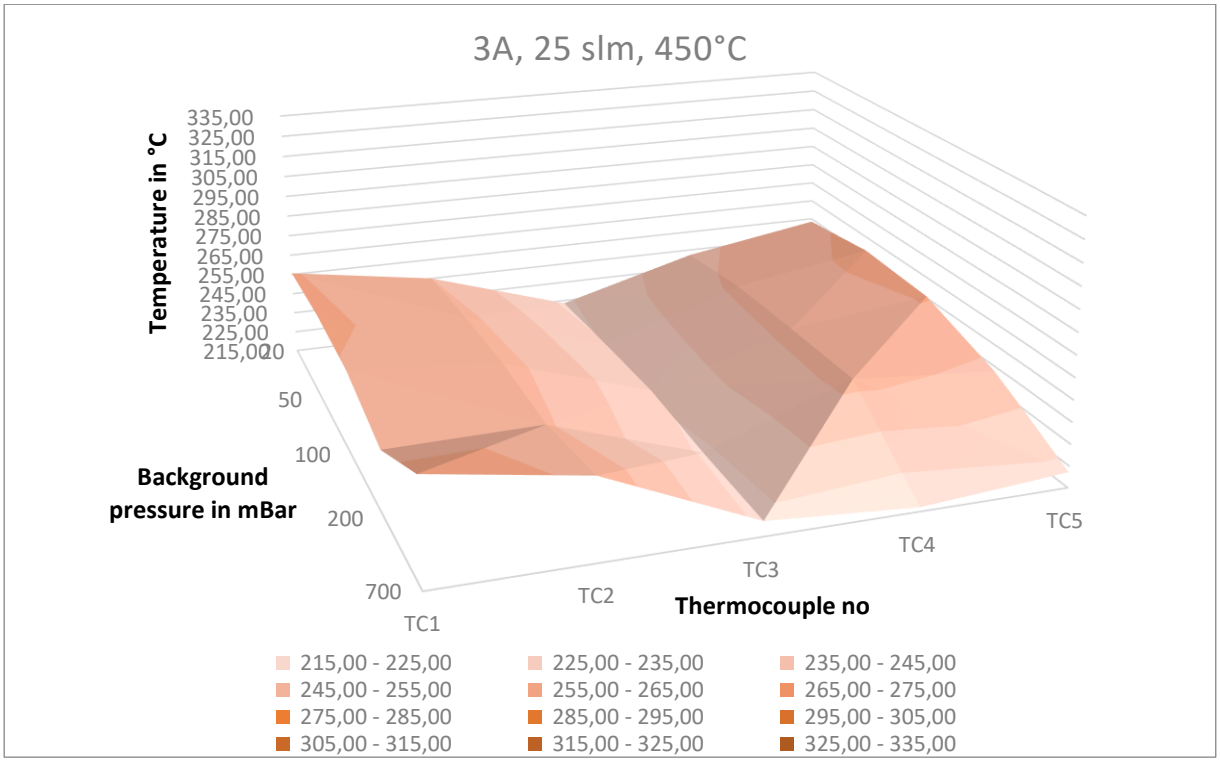

Figure 103 Position 3A at 25 SLM gas flow and at a susceptor temperature of 450°C.

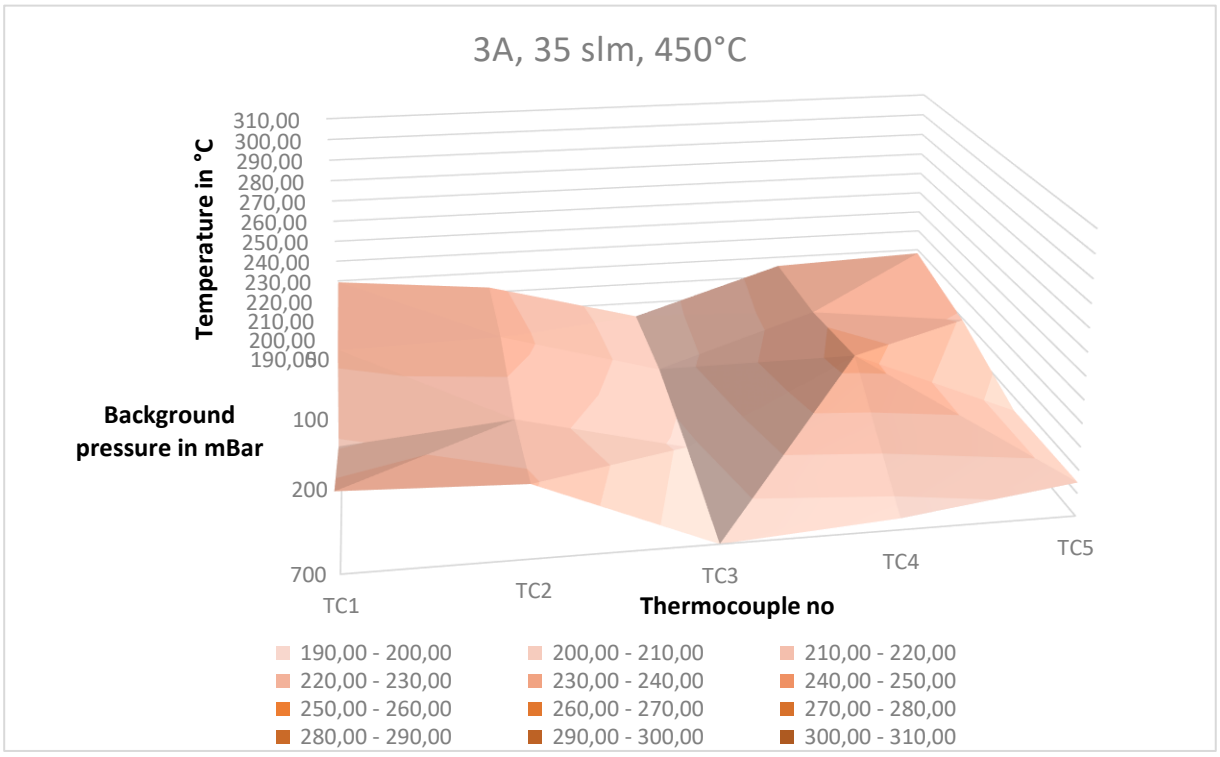

Figure 104 Position 3A at 35 SLM gas flow and at a susceptor temperature of 450°C.

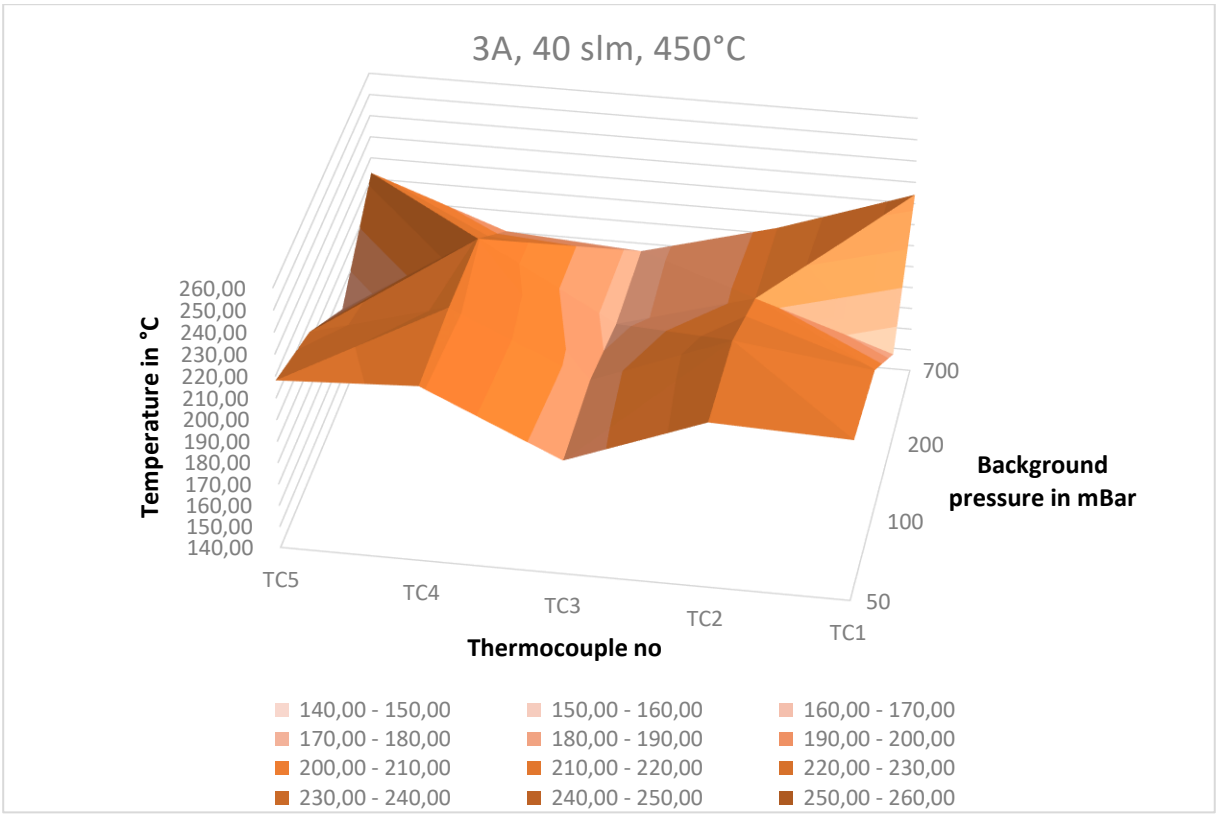

Figure 105 Position 3A at 40 SLM gas flow and at a susceptor temperature of 450°C.

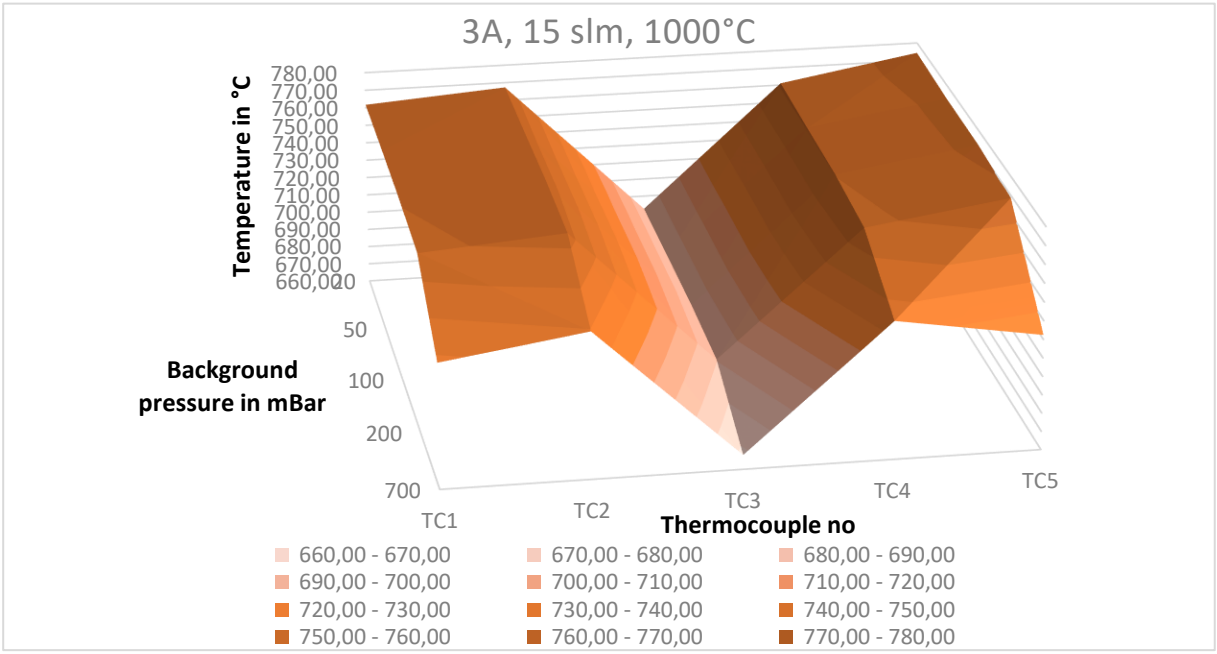

Figure 106 Position 3A at 15 SLM gas flow and at a susceptor temperature of 1000°C.

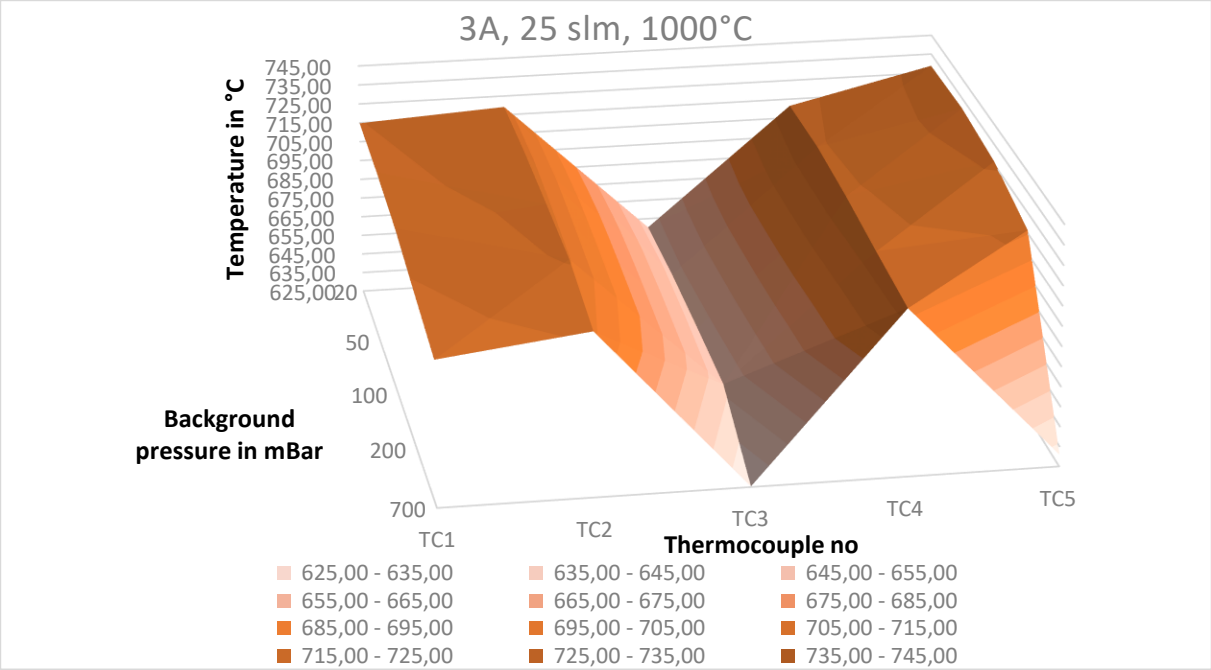

Figure 107 Position 3A at 25 SLM gas flow and at a susceptor temperature of 1000°C.

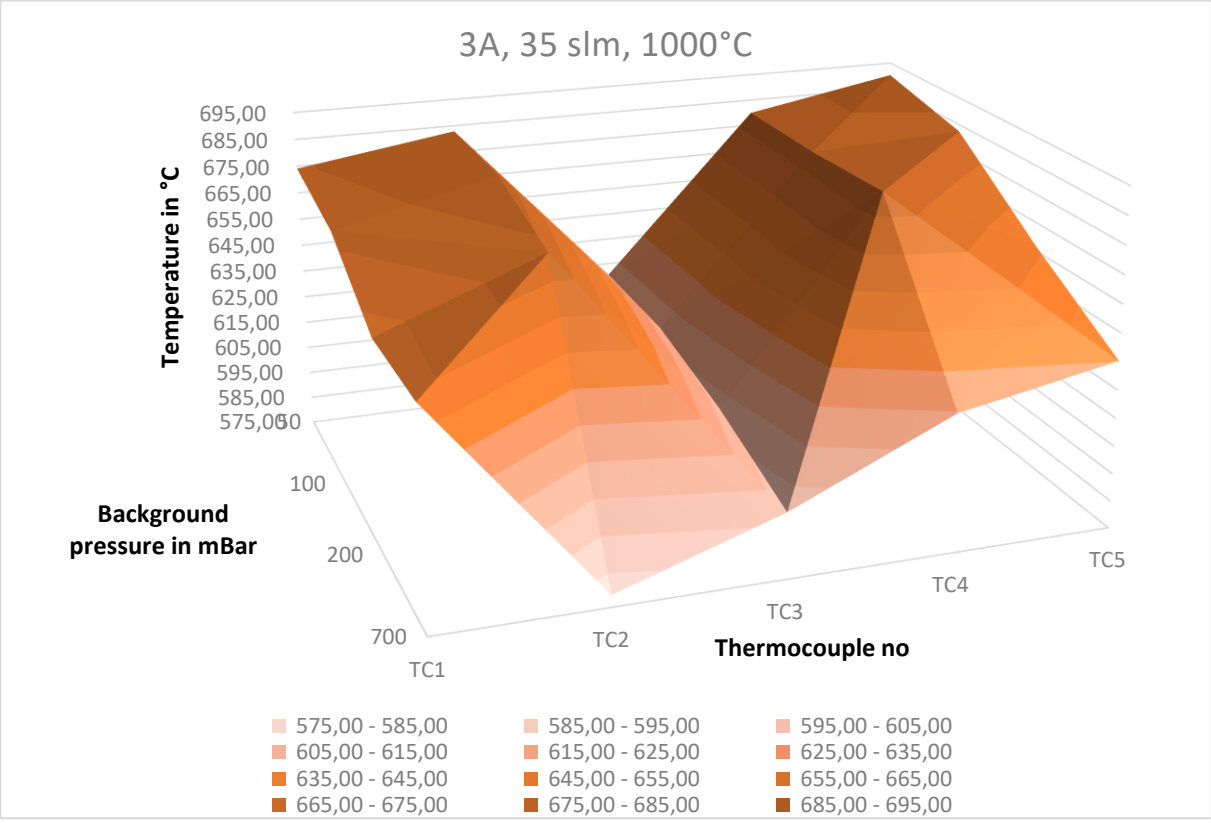

Figure 108 Position 3A at 35 SLM gas flow and at a susceptor temperature of 1000°C.

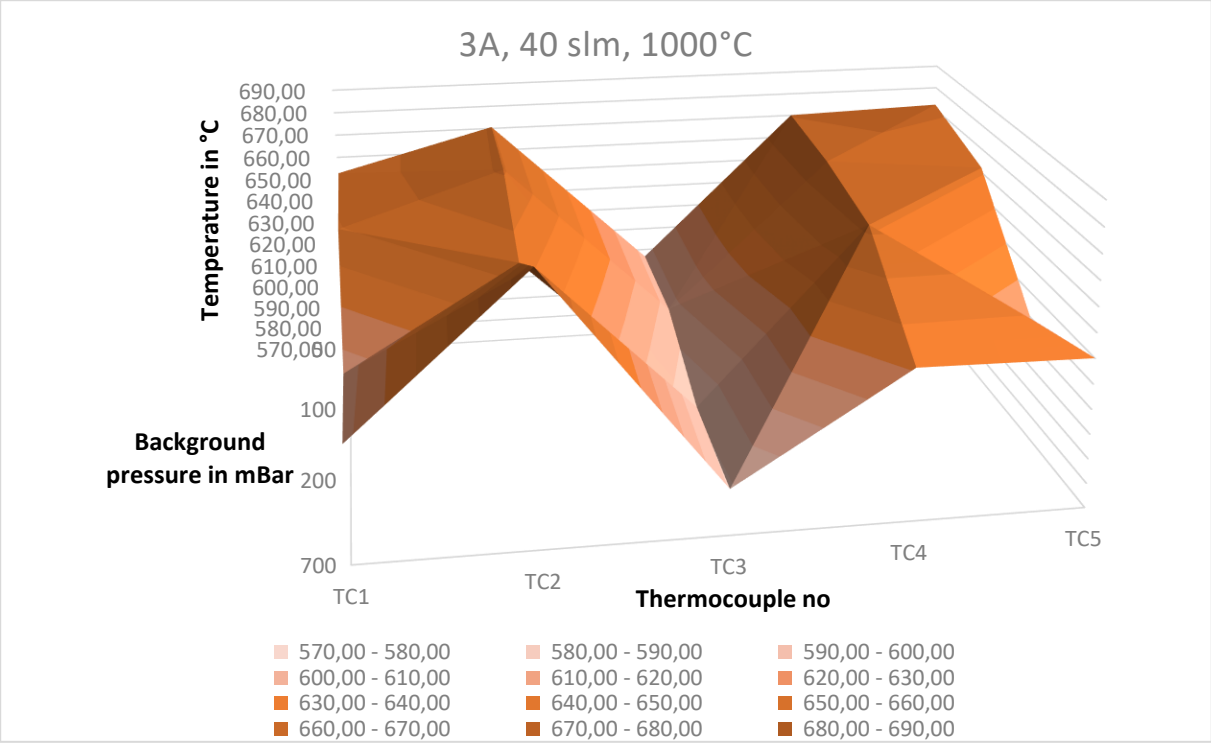

Figure 109 Position 3A at 40 SLM gas flow and at a susceptor temperature of 1000°C.

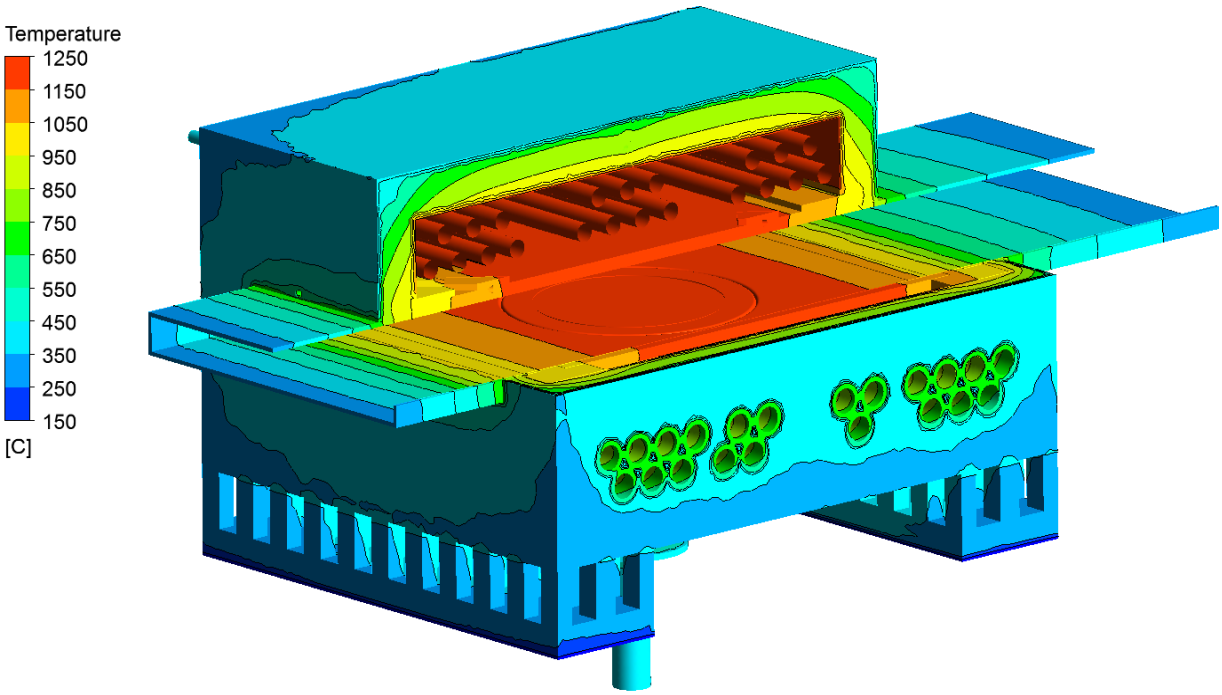

Figure 110 Temperature distribution in the MOCVD system performed with CFD at Linköping University supercomputer. Copyright Örjan Danielsson, LiU.

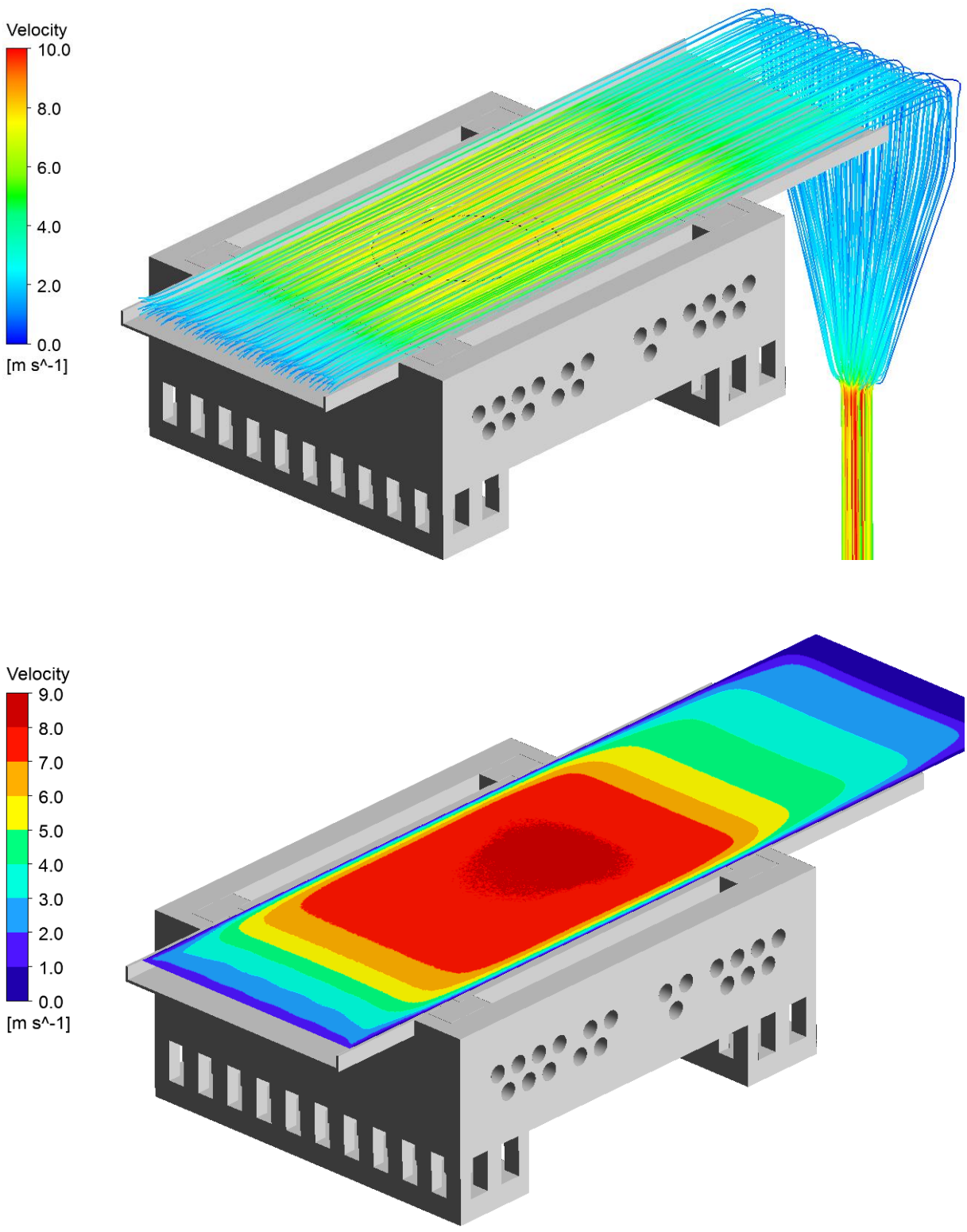

Figure 111 Gas velocity distribution in the MOCVD system performed with CFD at Linköping University supercomputer. Copyright Örjan Danielsson, LiU.